Enzymatic Function of Active Site Loop in Enolase: Preparation and Characterization of G37A and G41A Mutant Yeast Enolases

Shujun Liu

A Thesis

in

The Department

of

Biology

Presented in Partial Fulfillment of the Requirements

for the Degree of Master of Science at

Concordia University

Montreal, Quebec, Canada

November 2005

Your file Votre référence
ISBN: 0-494-14223-5
Our file Notre référence
ISBN: 0-494-14223-5

ABSTRACT

Enzymatic Function of Active Site Loop in Enolase:
Preparation and Characterization of G37A and G41A Mutant Yeast Enolases

Shujun Liu

Enolase catalyzes the reversible dehydration of 2-phosphoglyceric acid (2-PGA) to phosphoenolpyruvate (PEP) near the end of the glycolytic pathway. During enolase catalysis, three major loops undergo a large position change upon substrate and metal ion binding, especially in the active site loop (Pro35-Ala45). The hinge sites in the active site loop are Gly residues at positions 37 and 41. To gain some information about the function of active site loop movement in catalysis and subunit interactions, the Gly residues at position 37 and 41 in yeast enolase have been mutated to Ala. Recombinant wild type and two mutant enolases have been expressed in *Escherichia coli*. The purified mutant proteins are correctly folded dimers, as indicated by the 4^{th} derivative UV and near UV-CD spectra as well as the sedimentation coefficients from AUC. The G37A and G41A mutant enzymes only have 2.4% and 0.7% the activity of the wild type enzyme under the standard assay conditions. Higher [Mg^{2+}] can significantly stimulate G37A's and G41A's activity by 7 fold and 13 fold, respectively.

Two mutant enolases are more readily dissociated than wild type by $NaClO_4$. The K_d for two mutants have been increased by less than 1 order of magnitude relative to the wild type, indicating the subunit interactions in two mutants are slightly weakened. Kinetic studies indicate that two mutants are distinctly different from the wild type in the

following aspects: (1) K_m increased by 3 orders of magnitude for Mg^{2+}, and by 6-10 fold for Mn^{2+}; (2) a lower rate of catalysis (3) no inhibition is observed at high concentration of divalent cations; (4) 4 orders of magnitude lowered catalytic efficiency when assayed with Mg^{2+}. We interpret the lower rate of catalysis and depressed catalytic efficiency in two mutants as a direct result of the weak binding of the second divalent cation and other effects induced by the mutation. No inhibition may imply that the inhibitory binding site has been distorted in two mutants.

These observations confirm the active site loop movement is not only essential for correctly positioning Ser39 for coordination of the catalytic metal ion, but also plays some crucial function in maintaining the proper linkage with other loops. In turn, these precise loop conformations are essential in maintaining the correct active site structure and proper subunit interactions.

ACKNOWLEDGEMENTS

I especially thank my research supervisor Dr. Mary Judith Kornblatt for her guiding me and invaluable advice throughout my research, as well as for her spending innumerable hours to edit this manuscript. I would like thank my committee members Dr. Justin Powlowski and Dr. William Zerges for their excellent suggestions and valuable time.

I offer my special thanks to Dr. Ulycznyj Peter for his kindly running the AUC and to Dr. Jack Kornblatt for allowing me to use his osmometer, as well as Dr Louis A.Cuccia for allowing me to use his lyophilizer.

I also thank the following people, Songping Zhao, Bonny Choy, Heng Jiang, Yu Lei and Xuying Shan for their helpful suggestions, many assistances and wonderful friendship.

My deep appreciation is given to my family, especially, my husband Haichuan Xu. His love, understanding and encouragement are my spiritual support. It is his constant support that this thesis is able to be finished.

TABLE OF CONTENTS

List of Figures

List of Tables

Abbreviations

ADP	Adenosine diphosphate
AUC	Analytical Ultracentrifugation
BSA	Bovine serum albumin
CD	Circular Dichroism
DSC	Differential scanning calorimetry
E. coli	*Escherichia coli*
E. hira	*Enterococcus hirae*
EDTA	Ethylenediaminetetraacetic acid
EPR	Electron paramagnetic resonance
FBP-aldolase	Fructose-1,6-biophosphate aldolase
FT-IR	Fourier transform infrared spectroscopy
G37A	Gly at position 37 in yeast enolase mutated to Ala
G41A	Gly at position 41 in yeast enolase mutated to Ala
ΔG_0	Free energy
β4Gal-T1	β1,4-Galactosyltransferase-I
HI-HL	Four α–helices in N-terminal domain
HA-HG	Eight α–helices in 8-fold α/β barrels of C-terminal domain
K_d	Dissociation constant
K_m	Michaelis constant
k_{cat}	Turnover number
K_i	Inhibitory constant
KIE's	Kinetic isotope effects
Loop 1	Composed of residues Ser36-Ala45, also called active site loop
Loop 2	Comprised of residues Val153-Phe169, also named catalytic loop
Loop 3	Comprised of residues Ser250-Ser267
LDH	Lactate deydrogenase

MAL	3-methylaspartate ammonia lyase
MD	Molecular dynamics
Mes	4-morpholineethane sulfonic acid
MLE	Muconate lactonizing enzyme
MR	Mandelate racemase
$NaClO_4$	Sodium perchlorate
NaOAc	Sodium acetate
NMR	Nuclear magnetic resonance
NADH	Nicotinamide adenine dinucleotide
PCR	Polymerase chain reaction
PEP	Phosphoenolpyruvate
2-PGA	2-phospho-D-glycerate
[2-^{2}H]-2-PGA	Deuterium 2-PGA at C-2
PK	Pyruvate kinase
PhAH	Phosphonoacetohydroxamate
Q-ToF –MS	Q-ToF Mass Spectrometry
QM/MM	Quantum mechanism/molecular mechanical
S1-S8	Eight β-strands in 8-fold α/β barrels of C-terminal domain
S9-S11	Three anti-parallel β-strands in N-terminal domain
SDS-PAGE	SDS-polyacrylamide gel electrophoresis
S. pneumoniae	*Streptococcus pneumoniae*
T. brucei	*Trypanosoma.brucei*
TIM	Triose phosphate isomerase
UV	Ultraviolet
WT	Wild type

1 Introduction

1.1 Enolase

Enolase (EC 4.2.1.11) catalyzes the dehydration of 2-phospho-D-glycerate (2-PGA) to form phosphoenolpyruvate (PEP) near the end of the glycolytic pathway and the reverse reaction of hydration of PEP to 2-PGA in gluconeogenesis (Wold, 1971). All eukaryotic and many prokaryotic enolases are homodimer (Wold, 1971). In spite of this, there have been reports of octameric enolases discovered mainly from some bacteria (Singh and Setlow, 1978; Kaufmann and Bartholmes, 1992; Schurig *et al.*, 1995; Brown *et al.*, 1998; Ehinger *et al.*, 2004). The molecular mass of each enolase subunit ranges from 40,000-50,000Da (Wold, 1971). In yeast (*Saccharomyces cerevisiae*) enolase, each subunit is composed of 436 amino acid residues (Chin *et al.*, 1981b).

There are three genes that encode mammalian enolases, giving α, β, and γ subunits (Chin, 1990). α-Subunits are present ubiquitously in mammalian organisms, whereas the β-subunits and γ-bubunits are muscle specific and neuron specific, respectively. The two tissue-specific subunits may associate naturally into homodimers by themselves or with α-subunits to form heterodimers (Chin, 1990). In yeast, there are two genes, namely *ENO1* and *ENO2*, that code for enolase (Holland *et al.*, 1981). The product of *ENO1* is enolase 1, which was first isolated by Warburg *et al.* (Warburg, 1942). Then, its sequence was confirmed using chemical methods (Chin *et al.*, 1981a; Chin *et al.*, 1981b) and gene sequencing methods (Holland *et al.*, 1981). The product of *ENO2* is enolase 2. The

expression levels of the two yeast enolase isozymes are regulated by growth conditions (McAlister and Holland, 1982). To date, much of the research performed on yeast enolase has been carried out on the enolase 1.

Enolases have highly conserved amino acid sequences between isozymes, as well as different species. In yeast, enolase1 and 2 share up to 95% sequence identity (Holland *et al.*, 1981). In addition, the three mammalian enolase isozymes exhibit over 80% sequence identity (Chin, 1990). Furthermore, yeast and mammalian enolases also display at least 60% sequence identity (Chin, 1990). The details about the sequence identity among yeast, lobster, *E. coli* and *Trypanosoma brucei (T. brucei)* enolases are summarized in Table 1 (Holland *et al.*, 1981; Duquerroy *et al.*, 1995; Kuhnel and Luisi, 2001; da Silva Giotto *et al.*, 2003). The sequence alignments indicate that the largest difference between prokaryotic and eukaryotic enolase is in the loop (named as loop 3) containing the residues 248-268 of yeast enolase (Kuhnel and Luisi, 2001).

Enolase from	Yeast	Lobster	*E. coli*	*T. brucei*
Yeast	100%	64%	50%	59%
Lobster	64%	100%	50%	58%
E. coli	50%	50%	100%	51%
T. brucei	59%	58%	51%	100%

Table 1: Summary for sequence identity among yeast, lobster, *E. coli* and *T. brucei* enolases

Enolase is attributed to a group of functionally related enzymes, known as the

enolase superfamily. The members of this superfamily were previously partitioned into three different subgroups, based on the identities of the general basic residues participating in formation of the enolic intermediate (Gulick *et al.*, 2000): (1) the mandelate racemase (MR) subgroup; (2) the muconate lactonizing enzyme (MLE) subgroup; (3) the enolase subgroup. But recently, another highly diverged subgroup represented by 3-methylaspartate ammonia lyase (MAL) was also added to the enolase superfamily (Gerlt *et al.*, 2005). These subgroups share the same structural framework and functional similarity, since all these enzymes have a similar active site structure positioned at the C-terminal end of β-strands of an α /β barrel, and possess the ability to catalyze the initial abstraction of the α-proton of a carboxylic acid to form an enolic intermediate (Babbitt *et al.*, 1996).

The crystal structure of enolase was first established as the yeast apo-enzyme at 2.25 Å resolution (Lebioda *et al.*, 1989; Stec and Lebioda, 1990), followed by a series of crystal structures of enolase-Mg^{2+}-substrate or analogue complexes determined at different resolutions (Lebioda and Stec, 1991; Wedekind *et al.*, 1994; Wedekind *et al.*, 1995; Larsen *et al.*, 1996; Zhang *et al.*, 1997). At present, X-ray crystal structures of enolase are not only available from yeast, but also from lobster (Duquerroy *et al.*, 1995), *E .coli* (Kuhnel and Luisi, 2001), *Enterococcus hirae (E. hirae)* (Hosaka *et al.*, 2003), *T. brucei* (da Silva Giotto *et al.*, 2003), enolase γ from human neuron (Chai *et al.*, 2004), as well as enolase α from *Streptococcus pneumoniae* (*S. pneumoniae*) (Ehinger *et al.*, 2004). Aside from these crystal structures of enolase from different species, X-ray crystal

structures are now also available for other members of enolase superfamily, such as MR (Neidhart *et al.*, 1991), MLE (Helin *et al.*, 1995; Hasson *et al.*, 1998) and MAL (Asuncion *et al.*, 2002; Levy *et al.*, 2002). The growing number of crystal structures of members of enolase superfamily offers us considerable insight into the relationships between the structures and the functions of the superfamily. These high-resolution crystal structures of enolase from different species also provide us with a better view and understanding of the enolase active site structure, dimeric interface arrangement, and the catalytic mechanism, as well as the relationship of the loop structures and functions.

1.2 Enolase structure

1.2.1 Overall structure of enolase

Enolase is a dimer with two identical subunits. Figure 1 depicts the butterfly enzyme of the yeast enolase dimer with its natural cofactor of Mg^{2+} and the substrate 2-PGA binding sites. The structure of the yeast enolase monomer is illustrated in Figure 2. Enolase monomer contains two domains (Lebioda *et al.*, 1989; Stec and Lebioda, 1990). The N-terminal domain is an α/β barrel that extends from the residues 1-142 in yeast enolase. It consists of a three stranded amphiphilic /anti-parallel β-strands (S9-S11), followed by a long loop and four α–helices (HI-HL) (Lebioda *et al.*, 1989; Stec and Lebioda, 1990), as indicated in Figure 2. The C-terminal domain extends from residues 143-436 and is an 8-fold α/β barrel, which is composed of eight β-strands (S1-S8) surrounded by eight α–helices (HA-HH) (Lebioda *et al.*, 1989; Stec and Lebioda, 1990),

as shown in Figure 2 and Figure 3. The barrel also contains some additional β-sheet inserts. The two subunits connect between the β-strands (S9 and S10) in one subunit and the helices (HA and HH) of the other subunit forming the dimer interface (Lebioda *et al.*, 1989).

Figure 1: Yeast enolase dimer (PDB: 1ONE). α-helices and β-strands are shown in pink and orange, respectively. The Mg^{2+} is shown in purple ball, and the substrate 2-PGA is shown in green ball. The active site loop (Pro35-His43) is shown in solid blue ribbon, in which the hinge sites Gly37 and Gly41 are indicated in red. Trp56 and Glu188 are labeled in cyan and green stick, respectively. The figure is prepared using Rasmol 2.6.

In the N-terminal domain, the hydrophobic side of the β-strands makes contact with the first helix (HI) and the third helix (HK) in the same domain, but the other side of the β-strands is exposed to the solvent, with a large number of hydrophilic side-chains

protecting the peptide chain (Stec and Lebioda, 1990). In the middle of helix I (HI), there is Pro74, which can break the helix I, resulting in a bend in the helix I (Lebioda *et al.*, 1989; Stec and Lebioda, 1990). Between β-strand (S11) and helix I (HI), there is a long loop, which closes over the active site upon metal ion binding during enolase catalysis (Lebioda and Stec, 1991).

The C-terminal domain of the enolase is an 8-fold α/β barrel, with the $\beta\beta\alpha\alpha(\beta\alpha)_6$ topology (Lebioda *et al.*, 1989), as depicted in Figure 3. This $\beta\beta\alpha\alpha(\beta\alpha)_6$ topology is distinct from the classical $(\beta\alpha)_8$ topology found in Triose phosphate isomerase (TIM)(EC5.3.1.1) (Lebioda *et al.*, 1989). Figure 3 shows that in the C-terminal domain, nearly all the β-strands involved in the barrel are positioned in the interior of the barrel that is surrounded by α–helices (Lebioda *et al.*, 1989). The β-strands (S1) and (S2) are connected by another loop, which also moves closer to the active site upon substrate binding (Larsen *et al.*, 1996). Helix A (HA), the longest helix in the barrel, forms an extended entrance to the active site and is involved in forming the subunit interface (Lebioda *et al.*, 1989; Stec and Lebioda, 1990). Nearly all the helices in the barrel are located on the outside of the molecule and are amphiphilic, with the exception of Helix G (HG), which lies between the α/β barrel and the N-terminal domain interface and is fully buried (Stec and Lebioda, 1990) (Figure 2). An additional feature worth noting about the structure of enolase is Helix H (HH), which is positioned at the subunit interface. Both Helix G and Helix H shows about 63% sequence identity among yeast, lobster, *E. coli*, *T. brucei* and human enolases (da Silva Giotto *et al.*, 2003).

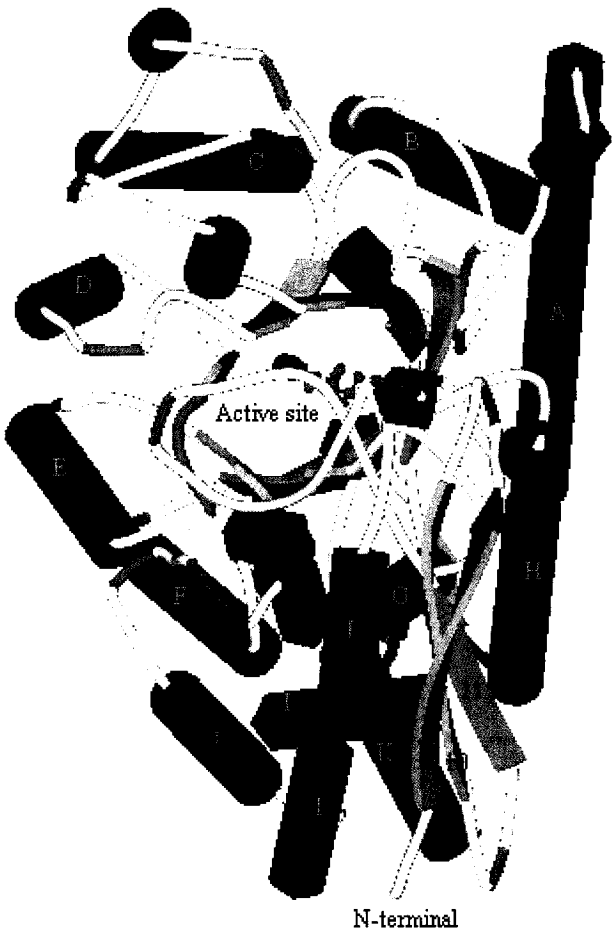

Figure 2: Yeast enolase monomer (PDB: 1ONE). α-helices are marked as red cylinders, β-strands are indicated in cyan arrows. Substrate 2-PGA is demonstrated in green ball and stick. Mg^{2+} is shown in pink ball. Figure was prepared using Weblab viewerlite 4.0.

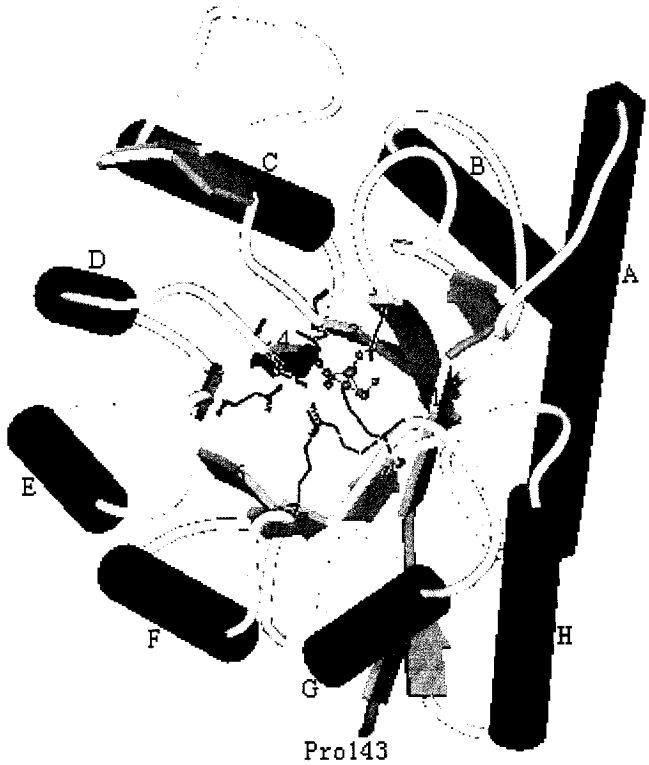

Figure 3: The $\beta\beta\alpha\alpha(\beta\alpha)6$ topology of enolase (PDB: 1ONE). The active site is positioned in a deep cavity at the C-terminal of the α/β barrel. The Mg^{2+} is shown in pink ball. The 8-α-helices are marked as red cylinders and located in the outside of the barrel; the main 8-β-strands are indicated in cyan arrows and lie in interior of the barrel. The side chains of the active site residues (E168, D246, E295, D320, K345, R374 and K396) are indicated in blue stick. The secondary structure elements are symbolized in accordance with the Lebioda *et al.*'s notation (Lebioda *et al.*, 1989), and the sequence along the peptide chain is: 1, 2, A, B, 3, C, 4, D, 5, E, 6, F, 7, G, 8, and H, -COOH. Figure was prepared using Weblab viewerlite 4.0

The residues involved in the main secondary structure features in yeast enolase are listed in Table 2 (Lebioda *et al.*, 1989)

N-terminal domain	Anti-parallel β-meander	Strand 9	5-13
		Strand 10	17-25
		Strand 11	29-35
	α-helices	Helix I	61-80
		Helic J	86-96
		Helix K	107-125
		Helix L	128-136
C-terminal domain	8-fold α/β barrel	Strand 1	150-153
		Strand 2	168-172
		Helix A	179-200
		Helix B	221-235
		Strand 3	241-247
		Helix C	275-288
		Strand 4	293-296
		Helix D	303-312
		Strand 5	316-320
		Helix E	327-336
		Strand 6	341-345
		Helix F	352-365
		Strand 7	368-373
		Helix G	382-389
		Strand 8	394-397
		Helix H	404-419

Table 2: The secondary structure components in yeast enolase (Lebioda *et al.*, 1989)

1.2.2 Active site structure of enolase

The location of the active site is illustrated in Figure 1 and Figure 3. The active site of enolase is positioned in the deep cavity of the C-terminal of the 8 fold α/β-barrel domain (Stec and Lebioda, 1990). Similar active site structures are found in some other enzymes with an 8-fold α/β-barrel structure (Lebioda *et al.*, 1982). The active sites of enolase from yeast, lobster, *E. coli* and *T. brucei* are very similar in structure, and all the residues participating in enzyme catalysis are highly conserved (Lebioda *et al.*, 1989; Duquerroy *et*

al., 1995; Kuhnel and Luisi, 2001). These residues are all situated on the β-strands of the α/β-barrel with the exception of the first β-strand (S1) (Lebioda and Stec, 1991), and are all ionizable amino acids (E168, D246, E295, D320, K345, R374 and K396), as shown in Figure 3. The positions of several important active site residues and the active site loop (Pro35-His43) are illustrated in Figure 4.

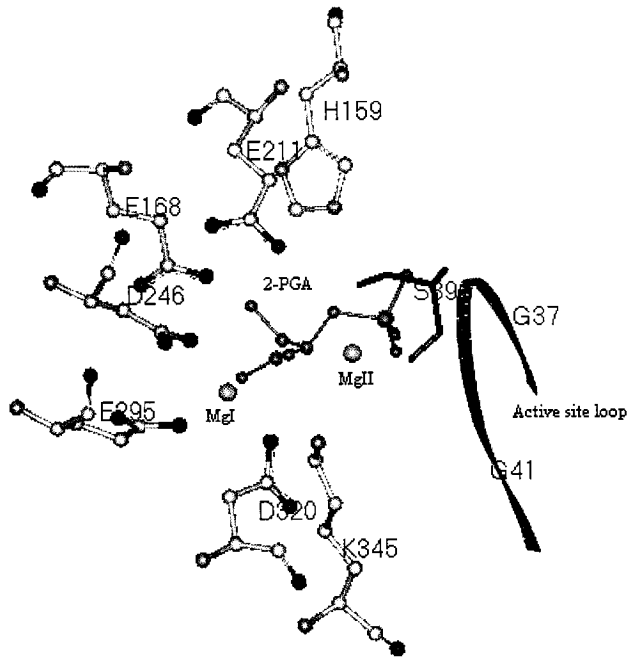

Figure 4: Active site structure of yeast enolase and the active site loop position (PDB: 1ONE). Substrate 2-PGA is indicated in green ball and stick. Mg I and Mg II are shown in cyan ball. The backbone of active site loop Pro35-His43 (closed) is shown in blue line ribbon, in which the loop hinge sites Gly37 and Gly41 are shown in red. Ser 39 is indicated in purple stick. Figure was prepared using Weblab viewerlite 4.0.

1.3 Loops in enolase

Close to 50% of the polypeptide chain of enolase participates in the formation of loops and turns between the β-strands and α–helices (Stec and Lebioda, 1990). It is therefore very intriguing to study the loop structures and their functions in enolase. The following

paragraphs will provide some detailed description of the three major loops present in enolase.

1.3.1 Three major loop conformations in enolase

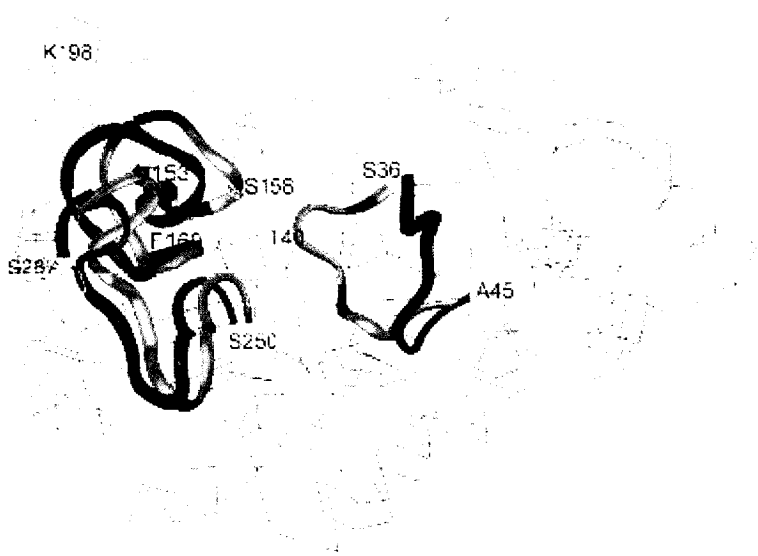

Figure 5: Superposition of the open (apo: blue) and closed (holo: cyan) conformations of yeast enolase. Three loops show structural variations, whereas loop 1 (Ser36-Ala45) demonstrates large positional variation. The positions of Gly residues in these loops are shown in blue color in holo-yeast enolase structure (Gunasekaran *et al.*, 2003).

The substrate bound (Lebioda and Stec, 1991) and unbound crystal structures of yeast enolase (Lebioda *et al.*, 1989) reveal that the binding of metal ions and substrate are associated significantly with structural variations in three regions. More specifically, they are associated with the movements of 3 major loops, namely loops 1, 2, and 3 (Lebioda *et al.*, 1989; Lebioda and Stec, 1991; Wedekind *et al.*, 1994). Loop 1 is composed of residues Ser36-Ala45, which will be discussed in detail in my project. Loop 2 and loop 3 are comprised of residues Val153-Phe169 and Ser250-Ser267, respectively. Figure 5 is a

diagram by Gunasekaran *et al.* (2003), which demonstrates the conformation of three loops varies upon ligand binding.

In the apo-enolase structure (PDB code: 3ENL (Stec and Lebioda, 1990)), the three loops are characterized as "open" conformations (see Figure 5), and the active site is largely exposed to solvent. On the other hand, in the holo-enolase structure, with two metal ions and the substrate, 2-PGA, bound (PDB code: 1ONE (Larsen *et al.*, 1996)), the three loops are characterized as "closed" conformations. This is because as the metal ions and substrate bind, loop 1 moves over to the active site in order to position Ser39 to chelate the second divalent cation, and loop 2 also moves closer to the active site, so that His159 in loop 2 may interact with the phosphoryl oxygen of the substrate 2-PGA. The crystal structure of asymmetric dimer yeast enolase with an equilibrium of mixture of PGA and PEP (PDB code: 2ONE (Zhang *et al.*, 1997)) clearly shows that the three loop conformations are different between the PGA-bound subunit and the PEP-bound subunit. The anticipated "closed" loop conformation is present in the PGA-bound subunit. Whereas in the PEP-bound subunit, loop 1 resembles the "closed" conformation, but loop 2 and loop 3 adopt conformation similar to the "open" conformation (Zhang *et al.*, 1997).

1.3.2 Loop movements in other proteins

Loop 1 is also termed the "active site loop" in enolase, since it moves about 8 Å closer to the active site upon cofactor and substrate binding and is accompanied by an open-to-closed conformational change (Lebioda and Stec, 1991; Zhang *et al.*, 1997).

Similar loop movements are also observed in TIM (Lolis and Petsko, 1990), β1,4-Galactosyltransferase-I (β4Gal-T1) (Ramakrishnan and Qasba, 2001) and Class II Fructose-1,6-biophosphate aldolase (FBP-aldolase) (Hall *et al.*, 1999), when substrate is bound to these enzymes.

TIM is typically considered as a model system to study the relationship of loop movement upon the enzyme activity. Crystallographic studies indicate that a mobile loop in TIM (residues 166-176) leaves the active site open to solvent in the unliganded form (Lolis *et al.*, 1990), and closes down the substrate analogous in the liganded form (Lolis and Petsko, 1990). Subsequent mutagenesis experiments (Sampson and Knowles, 1992b; Sampson and Knowles, 1992a) have found those mutations that destabilized the interactions contributing to the "closed" form of enzyme significantly affected the catalytic properties. These studies further confirmed the crucial role of loop closure upon the catalytic function. Then, a number of different NMR investigations have been performed to examine the dynamics of the flexible loop. NMR investigations demonstrate that the loop motion and product release seem to be partially rate limiting for chemistry (Rozovsky *et al.*, 2001; Rozovsky and McDermott, 2001). These detailed studies on the loop motion in TIM through different approaches provide us with a clear demonstration of the role of protein dynamics in promoting and controlling chemical reactivity.

In the case of β4Gal-T1, a large long loop (residues 345-365) undergoes a significant conformational change upon substrate binding; the conformational change is necessary to create a binding site for the substrate (Ramakrishnan and Qasba, 2001). In

addition, the conformational change of this long loop is accompanied by a short loop conformational change (residues 313-316), which brings Trp314 to the catalytic pocket (Ramakrishnan and Qasba, 2001). In order to further understand the loop movement in β4Gal-T1, Trp314 was mutated to Ala by site-directed mutagenesis (Ramasamy *et al.*, 2003). Then, substrate binding, limited-proteolysis and crystal structure studies were employed to examine the differences between WT and W314A mutant (Ramasamy *et al.*, 2003). W314A mutant has only 1% the activity of the WT and binds substrate poorly. The long loop in W314A mutant is cleaved at a faster rate than that in the WT, indicating that there is conformational difference in the long loop between the two proteins. These studies finally determined the essential function of Trp314 involved in the long loop conformational state and in binding the substrate, as well as in enzyme catalysis. The impact of the short loop containing Trp314 upon the conformational changes of the long loop was also substantiated by molecular dynamics (MD) simulations (Gunasekaran *et al.*, 2003). During the MD simulation, if the short loop is restrained, or the Gly residues in the short loop are mutated to Ala, both changes significantly reduce the movement of the long loop.

As for FBP-aldolase, crystallographic studies (Hall *et al.*, 1999) demonstrate that substrate binding leads to a conformational change in the β5-α7 loop (residues 177-198), which, in turn, further causes the repositioning Glu181 and Glu182 to approach the active site (Zgiby *et al.*, 2002). Since there are four Gly residues (Gly176, Gly179, Gly180, Gly184) located in the same loop and in the vicinity of the Glu182, a quadruple mutant

(each Gly was changed to Ala) was subsequently prepared by Zgiby *et al.* (2002). They utilized the steady state kinetic and kinetic isotope effects (KIE's) to study this mutant, and conclusively proved that the flexibility of this loop was important for correctly positioning Glu182 for enzyme catalysis.

1.3.3 Crucial function of loops in enolase

In yeast enolase, the "active site loop" is the most mobile part of a long loop that is comprised of Pro35-Gly60, which extends from the smaller domain and connects the third β-strand (S11) and the first helix (HI) in the N-terminal domain (Lebioda *et al.*, 1989; Lebioda and Stec, 1991; Wedekind *et al.*, 1994). The entire loop extends directly from the active site to subunit interface. The backbone N of Trp56 in one subunit forms a hydrogen bond with the carboxyl oxygen of Glu188 in the other subunit across the subunit interface (Stec and Lebioda, 1990), as illustrated in Figure 6. According to the crystal structure of yeast enolase, a very important residue, Ser39, is located in the "active site loop" and coordinates metal II with its carbonyl and hydroxyl oxygens (Wedekind *et al.*, 1994). Replacement of Ser39 with Ala has resulted in a reduction of enzyme activity by 4 orders of magnitude and incomplete closure of the active site loop (Brewer *et al.*, 1998; Poyner *et al.*, 2002). It seems that Ser39 has a crucial function in fixing the closed conformation of the active site loop (Poyner *et al.*, 2002). In addition to Ser39, residues Ala38 and Glu44 located on loop 1 are thought to be important for enzyme catalysis based on quantum mechanism/molecular mechanical (QM/MM)

analysis of the active site of enolase (Liu, 2000). The hinge sites in the active site loop are Gly residues at positions 37 and 41. The positions of Gly37 and Gly41 in the active site loop are indicated in Figure 1, Figure 4 and Figure 5. These Gly residues, which are in the vicinity of Ser39, probably provide Ser39 with enough space to rotate into a position where its carbonyl and hydroxyl oxygena can correctly coordinate with metal II, and/or presumably facilitate the maximal loop movement (Wedekind *et al.*, 1994). The importance of the function of the two Gly residues at position 37 and 41 will be investigated in this project.

Unlike loop 1, both loop 2 and loop 3 extend from the large C-terminal domain (Lebioda *et al.*, 1989; Lebioda and Stec, 1991; Wedekind *et al.*, 1994). Loop 2 connects β-strand S1 and S2, and is termed the "catalytic loop" (Gunasekaran *et al.*, 2003), because an important active site residue, His159, is located in this loop. H159A prepared by Vinarov and Nowak (1999) displayed 4 orders of magnitude reduced catalytic rate, and lost the capacity to ionize the C-2 proton of 2-PGA investigated by examining the H/D exchange of C-2 proton with solvent D_2O. Metal binding studies on H159A demonstrated that His mutation to Ala at position 159 has no effect on the Mn^{2+} binding at site I and II, but causes a factor of 3 decrease in binding at site III (Vinarov and Nowak, 1999). Thus, His159 has been suggested to be involved in catalysis by protonating the phosphate of the substrate 2-PGA and could also serve as one of the "inhibitory" metal ion binding ligands (Vinarov and Nowak, 1999). Additionally, the crystal structure of asymmetric dimer yeast enolase with an equilibrium mixture of PGA and PEP (Zhang *et*

al., 1997) confirmed that, in addition to the loop conformational differences between PGA-bound and PEP-bound subunits, the side chain of His159 is also in touch with the phosphate group of the substrate/product molecule in PGA-bound subunit, while in the PEP-bound subunit, there are water molecules that separate His159 from the substrate. The content of this research provides direct evidence that the loop conformations have a crucial relationship with the enzyme catalytic function.

Loop 3 connects β-strand (S3) and helix C (HC) and has one Trp, one Tyr and three Phe residues located within the loop (Kornblatt *et al.*, 1996). Loop 3 is situated far away from the active site (Lebioda *et al.*, 1989) (Figure 5). The residues 247-284 (including loop 3) were found to undertake the biggest movement of any continuous parts of the chain when the strong inhibitor PhAH was bound to enolase (Wedekind *et al.*, 1994). Duquerroy *et al.* (1995) also observed a large movement of loop 3 while studying lobster enolase, but the contribution of loop 3 to the metal ion or inhibitor binding was not identified. Although there are contacts between loop 3 and loop 2 and the movement of loop 3 seems to be associated with that of loop 2 (Zhang *et al.*, 1997), loop 3 does not seem to contain any residues that are directly involved in the active site structure. On the other hand, the results of sequence alignments of enolase indicates that loop 3 in plant enolase is 2 residues longer than that in animal enolase, and four residues shorter than that of bacterial enolase (Zhang *et al.*, 1997).

In addition to the commonly used methods to study protein structures such as site-directed mutagenesis and X-crystallography, enolase loop functions were also

determined by other theoretical methods. Gunasekaran *et al.* (2003) have utilized MD simulations to study the function of loops movement in three different enzymes, β4Gal-T1, enolase and lipase. In enolase, they first started with the holo crystal structure of enolase to perform the simulations, and found that there were strong interactions between loop 1 and loop 2 during simulation. If they restrained the movement of loop 2, loop 1 was observed to move away from the other two loops during the simulation. If the Gly residues (Gly156, Gly157, Gly161, Gly162) in the vicinity of His159 (in loop 2) were mutated to Ala, the same result was obtained as when restraining the motion of loop 2. Moreover, they also started with the apo structure of enolase to carry out the simulations. These results show during the simulation, if loop 2 is not restrained, loop 1 moves closer to loop 2, but if loop 2 is restrained, loop 1 doesn't (Gunasekaran *et al.*, 2003). The loop movements in β4Gal-T1 and lipase were also examined by the MD simulations and a similar mechanism of loop movements was acquired, though these proteins have different folds and functions (Gunasekaran *et al.*, 2003). Hence, they conclude that: (1) there is a triggering loop that initiates and controls the movement of the functional loop in these enzymes and loop movement is apparently coordinated; (2) the triggering loop seems to play the role of decreasing the energy barrier for the functional loop to overcome through the loop-loop interaction; (3) in enolase, it is loop 2 that controls the movement of loop 1 (Gunasekaran *et al.*, 2003). Another theoretical approach, QM/MM analysis, was also employed to analyze the active site of enolase (Liu, 2000). The QM/MM analysis results emphasized the key roles of some residues located

on these loops. For example, Ala38 (loop 1), His159 and Gln167 (both in loop 2) favorably contribute to lowering the energy barrier for proton abstraction, whereas Glu44 (loop 1) and Glu168 (loop 2) favor the β–hydroxyl group leaving step in the forward reaction catalyzed by enolase.

Figure 6: Demonstration of one hydrogen-bond between Trp56 and Glu188 located near subunit interface. The whole loop of Pro35-Gly60 is shown in solid blue ribbon, in which the hinge sites Gly37 and Gly41 are shown in red. Trp56 and Glu188 are labeled in cyan and red ball and stick, respectively.

All in all, these loops not only include about half of the aromatic amino acid residues in yeast enolase, but also comprise some of the residues involved in the active site structure and subunit interactions. For example, the respective movement of loop 1 and loop 2 causes the functional Ser39 and His159 into correct position for catalysis; His373, Arg374 and Lys396, all of which are in contact with the substrate (Zhang *et al.*, 1997) (Figure 10), are located on different loops (Kornblatt *et al.*, 1996); residues 402

and 403, which participate in subunit interactions, are positioned in the 398-403 loop (Kornblatt *et al.*, 1996). Specific movements of these loops are associated with metal ion and substrate bindings. At the same time, some parts of the loops are apparently brought near to the active site due to the movement of these loops. Therefore, it has been suggested that precise loop conformations are essential for maintaining the correct active site structure and proper subunit interactions; disrupting the correct loop conformation would not only impair the stability of the enolase dimer, but would break the active site structure as well (Kornblatt *et al.*, 1996). In the present study, our purpose is to directly introduce a small disturbance on loop 1 and study this disrupting effect on enzyme catalysis and subunit interactions.

1.4 Catalytic mechanism of enolase reaction

1.4.1 General reaction catalyzed by enolase

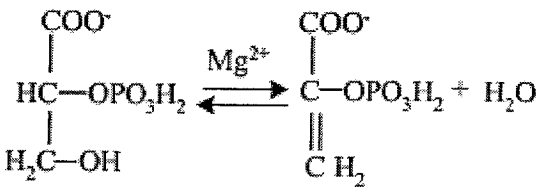

Figure 7: General reaction catalyzed by enolase (Wold, 1971)

Enolase catalyzes the reversible dehydration of 2-phosphoglyceric acid (2-PGA) to phosphoenolpyruvate (PEP) near the end of the glycolytic pathway (Figure 7). The removal of H_2O from 2-PGA was confirmed to be specifically anti in stereochemistry,

which meant that H^+ and OH^- departed from the opposite sides of 2-PGA (Cohn *et al.*, 1970). In the anti removal of H_2O from 2-PGA, two bonds are required to be broken. One is the carbon-hydrogen bond at C-2, which is a relatively non-acidic proton (pKa ~28-32) (Wedekind *et al.*, 1994). The other is the carbon-oxygen bond at C-3, where OH is a poor leaving group (Stubbe and Abeles, 1980; Anderson *et al.*, 1994). This elimination reaction was originally considered as a two-step process (Dinovo, 1971; Shen and Westhead, 1973). Shortly after, evidence from KIE's (Anderson *et al.*, 1994) and site-directed mutagenesis (Poyner *et al.*, 1996) further demonstrated that the enolase catalyzed reaction proceeded in a stepwise mechanism, which involves primarily the abstraction of the α-proton from C-2 of 2-PGA to form the carbanion intermediate, followed by the removal the β-hydroxyl group to form H_2O. Although this stepwise mechanism of enolase catalyzed reaction has been widely accepted among investigators, the question of how a relatively non-acidic α-proton and a poor leaving β-hydroxyl group can be removed from enzyme in two different reaction directions still remains an issue, and has not been completely defined only considering the metal cations and catalytic acid/base groups. Liu *et al.* (2000), using a QM/MM approach, have presented a clear answer to this interesting question. They concluded that the first step of this reaction was supported by the electrostatic interactions between the two divalent cations and substrate (Liu, 2000). The second step, although disfavored by the two oppositely charged divalent cations, may still take place. As the enzyme reorganizes the polar and charged groups in the active site, some negatively charged residues contribute significantly to

transition-state stabilizing effect on the second step, counterbalancing the transition-state destabilizing effect of the same divalent cations (Liu, 2000). The charge reorganization results in a decrease in the negative charge on the carboxylate group of 2-PGA, from which the negative charge is transferred to Glu211. Finally the carboxylate group of 2-PGA is probably not charged (Liu, 2000).

The rate limiting step in the enolase catalyzed reaction was also investigated by several research groups. KIE's was firstly used to study the mechanism of enolase from yeast (Shen and Westhead, 1973; Anderson *et al.*, 1994) or from rabbit muscle enolase (Shen and Westhead, 1973). Both of these studies concluded that, with Mg^{2+} as the cation, the removal of H^+ and OH^- from 2-PGA as well as the product release were the rate limiting steps to the overall reaction. However, Kornblatt (1996), using steady state and non steady state techniques, has studied the mechanism of ββ-enolase (from rabbit muscle) with Mn^{2+} as the cation, and provided the evidence that the rate limiting steps are the conformational changes and the dissociation of the PEP (Kornblatt, 1996). The two incompletely identical conclusions about the rate limiting step could be due to the difference in divalent cation, and also could be due to the difference in investigation methods, as well as the difference in the isozyme of enolase studied.

1.4.2 Proposed catalytic mechanism

Several proposals have been presented to confirm the enolase catalysis mechanism. The most widely recognized catalytic base/acid pair is Lys345-Glu211.

Lys345 as the catalytic base was primarily suggested by Wedekind *et al.*'s (1994) study on the crystal structure of enolase-$(Mg^{2+})_2$-PhAH complex, and was later supported by Poyner *et al.*'s (1996) research work. E168Q, E211Q and K345A mutant enolases prepared by Poyner *et al.* (1996), demonstrated greatly reduced activity (~10^5 fold reduction), indicating that the three residues are all crucial for catalysis. The capability of these three mutants to perform the first partial reaction was investigated by assaying the exchange rate of C-2 proton of 2-PGA with deuterons in D_2O (Poyner *et al.*, 1996). K345A demonstrated complete loss of H/D exchange activity, whereas E168Q and E211Q showed relatively normal H/D exchange activity. H/D exchange experiments evidently suggest that Lys345 is the catalytic base in the first step of enolase catalyzed reaction (Poyner *et al.*, 1996). The ability of three mutants to perform the second partial reaction was also investigated by assaying the hydrolysis of (Z)-3-Cl-P-enolpyruvate (Poyner *et al.*, 1996). This reaction is similar to the reverse reaction of enolase by adding the OH^- to the C-3 of PEP. Although all three mutants demonstrated depressed activity in the hydrolysis of (Z)-3-Cl-P-enolpyruvate compared with wild type, the E211Q showed the slowest hydrolysis activity among three mutants (Poyner *et al.*, 1996). Therefore, the Lys345-Glu211 as the catalytic base/acid was widely accepted by most investigators. In addition, this catalytic base/acid pair is in agreement with the stereochemical requirements for the anti-elimination of H_2O from 2-PGA, since the Lys345 and Glu211 are positioned on the opposite side of 2-PGA in the active site (Figure 8). Details about the catalytic mechanism is also illustrated in Figure 9, which has been supported by

stereochemical requirements (Cohn *et al.*, 1970), isotope exchange data (Dinovo, 1971) and X-ray crystallography (Larsen *et al.*, 1996; Zhang *et al.*, 1997).

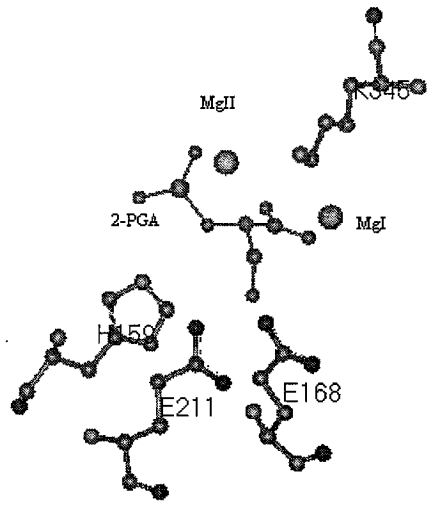

Figure 8: Position of Glu211, Glu168, His159 and Lys345 in relation to Mg^{2+} and substrate 2-PGA in the active site of yeast enolase (PDB: 1ONE). Mg^{2+} is indicated in ball, 2-PGA is shown in ball and stick. Figure was prepared using Weblab viewer 4.0.

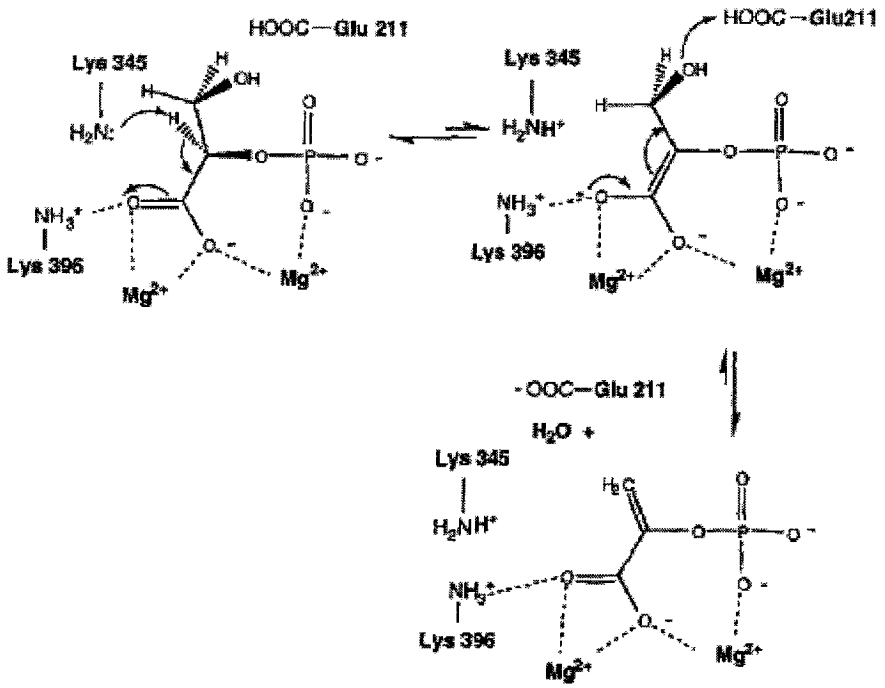

Figure 9: Proposed catalytic mechanism of enolase (Sims *et al.*, 2003)

Other than the widely accepted catalytic mechanism as shown above, there are two other proposed mechanisms which also received some attention. One of the mechanisms is based on the structure of enolase-Mg^{2+}-PGA/PEP complex, crystallized by Lebioda and Stec (1991). They proposed that a water molecule, which is near the C-2 of 2-PGA, serves as the catalytic base. Here, the proton is first passed to the water molecule, then to Glu168, and finally to the hydroxyl of 2-PGA to form H_2O (Lebioda and Stec, 1991). The other mechanism is based on the structure of lobster enolase-Mn^{2+}-phosphoglycolate complex, which indicates that the imidazole group of His 157 (His 159 in yeast enolase) is in Van der Waals contact (4.5 Å) with C-2 of the inhibitor (Duquerroy *et al.*, 1995). The pH dependence of the reaction catalyzed by yeast–Mg^{2+} enolase indicated that an unprotonated residue with the pK_A of 5.9 (presumably His) was crucial

for substrate binding and catalysis (Vinarov and Nowak, 1998). Later, H159A mutant yeast enolase was shown to possess 4 orders of magnitude reduced activity relative to wild type and to have lost the capability to ionize the C-2 of 2-PGA (Vinarov and Nowak, 1999). Therefore, these investigators suggested that His159 may serve as the catalytic base. However, His159 as the catalytic base was debated by the investigation of Brewer *et al.* (2000). They confirmed that H159A mutant yeast enolase held substantial activity and therefore may not be the catalytic base of the enzyme. With regard to the activity of H159A mutant, it is not clear which group's investigation result is correct.

1.5 Metal ion binding sites and activating, non-activating metal ion

1.5.1 Metal ion binding sites

Enolase is a "metal-activated metalloenzyme" (Brewer, 1981) and absolutely requires certain divalent cations (Me^{2+}) for activity (Wold and Ballou, 1957). Mg^{2+} is the natural cofactor of enolase and produces the highest activity (Wold and Ballou, 1957; Brewer, 1985). Each monomer of apo-enolase has one metal ion binding site, whereas in the presence of substrate, there are three metal ion binding sites per monomer.

Metal binding at site I and site II are required for enzyme activity and two binding sites have been formally confirmed using the crystal crystallographic method (Wedekind *et al.*, 1994) and through binding studies (Hanlon and Westhead, 1969a; Faller *et al.*, 1977; Lee and Nowak, 1992). However, metal ion binding at site III can lead to inhibition. The metal ion binding at site I is traditionally named as the "conformational" metal ion,

because it causes a conformation change in the overall structure of the protein, as proved by the fluorescence, absorption and near CD spectrum changes upon addition of divalent cations (Brewer and Weber, 1966; Brewer and Collins, 1980; Collins and Brewer, 1982). This conformation changes make it possible for the substrate and substrate analogues to bind (Hanlon and Westhead, 1969a; Faller and Johnson, 1974). Following binding of the substrate or the substrate analogue, the second metal ion, named as the "catalytic", may bind at site II, and the catalytic metal ion is an essential requirement for enzymatic activity to occur (Faller *et al.*, 1977). At higher metal ion concentration, the third metal ion, named the "inhibitory" ion, can bind to the enzyme, resulting in inhibition of enzyme activity (Faller *et al.*, 1977; Elliott and Brewer, 1980; Brewer and Ellis, 1983). As cited, the "conformational" metal ion has a tighter binding affinity than that of the "catalytic" and "inhibitory" metal ions, since there is about 1 order of magnitude difference in each of the dissociation constants for these sites with Mg^{2+} as the Me^{2+} (Hanlon and Westhead, 1969a; Faller and Johnson, 1974; Faller *et al.*, 1977).

The detailed schematic diagram of the active site residue interactions with Mg^{2+}-PGA complex is illustrated in Figure 10, which is taken from Larsen *et al.* (1996). The metal binding at site I is formed by carboxylate oxygens from three side chains of Asp246, Glu295 and Asp320, as well as a water molecule and two carboxylate oxygens of the substrate 2-PGA (Wedekind *et al.*, 1994). The metal binding at site II binds to a phosphoryl oxygen of substrate 2-PGA, the carbonyl and hydroxyl oxygens of Ser39 from the active site loop and two water molecules, as well as one carboxylate oxygen of

2-PGA (Wedekind *et al.*, 1994). It is obvious, as shown in the structure above, that metal II is very close to the phosphoryl oxygen of 2-PGA, which probably suggests its participation in catalysis.

As far as the inhibition of the enzyme activity at excess Me^{2+} is concerned, two different hypothesis exist. One proposed that Me^{2+} inhibition was due to product inhibition (Poyner *et al.*, 2001). In this model, higher Me^{2+} concentration prohibits the release of metal ion from site II, which is necessary for further release of the product. The other hypothesis suggests that enolase has a third "inhibitory" binding site. At higher Me^{2+} concentration, the metal binding to this site would inhibit enzyme activity (Faller *et al.*, 1977; Elliott and Brewer, 1980; Brewer and Ellis, 1983). Support for this hypothesis was obtained by Lee and Nowak's (1992) work. They demonstrated that there were 3 Mn^{2+} binding sites per monomer in the presence of 2-PGA. The dissociation constant for the third Mn^{2+} measured by EPR was almost identical to the kinetically determined K_i (Lee and Nowak, 1992). To date, although this site has not yet been determined in the crystal structures of enolase from yeast, lobster and *E. coli*, it has been shown in that of *T. brucei*. The crystal structure of *T. brucei* enolase is the first to provide direct visual evidence of the inhibitory metal binding at site III, which confirmed that the side chain of His156 in *T. brucei* enolase (His159 in yeast enolase) was one of the ligands of metal binding at site III (da Silva Giotto *et al.*, 2003). Furthermore, the Me^{2+} binding at this site made it impossible for the loop 2 to adopt the closed conformation. The inhibitory metal binding ligand determined by *T. brucei* enolase crystal structure was in good agreement

with results obtained through Mn^{2+} binding studies of the H159A mutant yeast enolase (Vinarov and Nowak, 1999), since H159A mutant demonstrated the same level of metal binding affinity as the wild type at site I and site II, but weaker (one third) metal binding affinity at site III than wild type. Wrapping up, we have good reason to believe that a third inhibitory metal ion binding site is present in enolase.

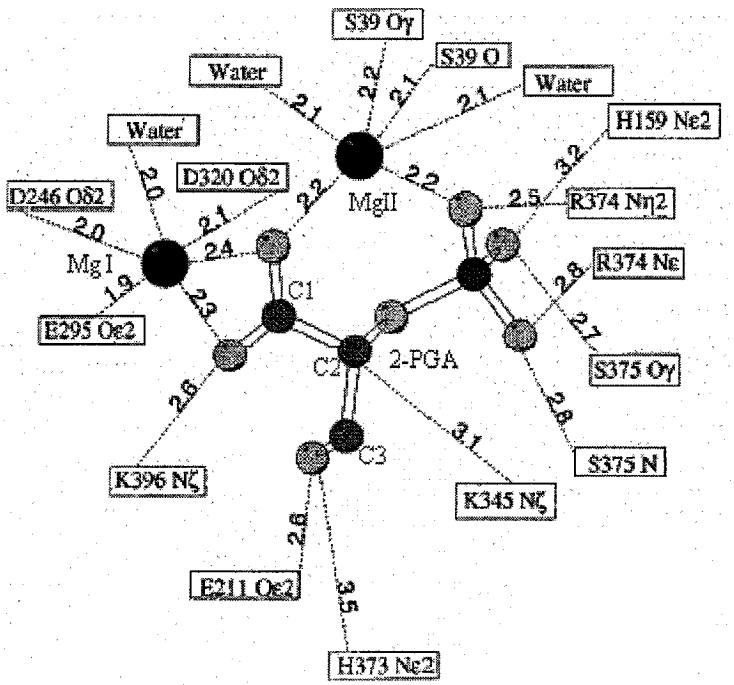

Figure 10: Schematic diagram of the enolase active site residue interactions with the Mg^{2+}-substrate complex. The hydrogen bonds are depicted in dashed line from 2-PGA to amino acids. The coordination of Mg I and Mg II are also demonstrated in dashed line from magnesium ions. The distances in angstroms are given on the dashed lines (Larsen *et al.*, 1996).

1.5.2 Activating and non-activating metal ions

Yeast enolase can bind different species of metal ions at its "conformational" site, other than the natural cofactor Mg^{2+} (Wold, 1971; Brewer, 1981). Some other divalent cations, such as Mn^{2+}, Zn^{2+}, Co^{2+}, Ni^{2+}, Cd^{2+}, Fe^{2+} (Wold and Ballou, 1957) and Cu^{2+} (Sinha and Brewer, 1984), which can substitute the natural cofactor Mg^{2+}, produce lower enzymatic activity. These are called as "activating" metal ions, which have been well studied and were ranked according to the level of activity they produced when bound to enolase: $Mg^{2+}>Zn^{2+}>Mn^{2+}>Fe^{2+}>Co^{2+}>Cu^{2+}>Cd^{2+}>Ni^{2+}$ (Wold and Ballou, 1957; Elliott and Brewer, 1980; Sinha and Brewer, 1984), though recently Mn^{2+} was proved as the second activating divalent cation by Poyner *et al.*'s (2002) studies. Several other metal ions, such as Tb^{3+}, Sm^{3+} and Ca^{2+} (Elliott and Brewer, 1980; Brewer *et al.*, 1983), can also bind at the "conformational" site, but don't produce enzyme activity. These are termed as "non-activating" metal ions. However, it has been found that "non-activating" metal ions Sm^{3+}, $Ca^{2+}$and Tb^{3+} can bind to the enzyme in the conformation site more strongly than does the natural cofactor Mg^{2+} (Elliott and Brewer, 1980). Such results clearly indicate that higher metal binding affinity does not mean higher enzyme activity.

In addition to above trivalent and divalent cations, Kornblatt *et al.* has reported some monovalent cations, such as Na^+, Li^+, K^+, NH_4^+, Cs^+, and Rb^+, which can also affect the activity of enolase (Kornblatt and Klugerman, 1989; Kornblatt and Musil, 1990). The rabbit and yeast enolase were well studied; both types of enolase can be inhibited by Na^+

and Li^+, however, only the rabbit enolase, not yeast enolase, can be activated by K^+, NH_4^+, Cs^+, and Rb^+ (Kornblatt and Klugerman, 1989). Based on the kinetic differences between rabbit and yeast enolases, they concluded that there were probably some differences in the detailed active site structure between mammalian and yeast enolases, though the overall catalytic mechanism was most likely the same (Kornblatt and Klugerman, 1989).

1.6 Dimer interface and dissociation studies

1.6.1 Dimer interface

The yeast enolase dimer structure is shown in Figure 1. It has been found that yeast, lobster and *E. coli* enolases have analogous dimer interfaces, with the same contact shapes, charge distributions, as well as the same amount of buried surface area (Kuhnel and Luisi, 2001). Thus it is very interesting that this region is highly conserved between the prokaryotic and eukaryotic enolases, since no allosteric functions are known for enolase (Kuhnel and Luisi, 2001). The subunit contacts in dimer only account for 13% and 12% of the solvent accessible surface in yeast (Stec and Lebioda, 1990) and Lobster enolases (Duquerroy *et al.*, 1995), respectively. Hence, the subunit interface is relatively small, as confirmed by the subunit contacts burying areas of 3320Å^2 and 3370Å^2 for *E. coli* (Kuhnel and Luisi, 2001) and lobster (Duquerroy *et al.*, 1995) enolases, respectively.

Most of the subunit contacts are between the β-strands (S9, S10) in the N-terminal domain of one subunit and the first helix (HA) and last helix (HH) in the C-terminal domain of the other subunit (Lebioda *et al.*, 1989). There are a large number of

hydrophilic interactions across the subunit interface (Stec and Lebioda, 1990). In yeast enolase, the two ion pairs, Arg8-Glu417 and Glu20-Arg414 as well as several hydrogen bonds between the subunits are listed in Table 3. In order to study the effect of disrupting salt bridges on the subunit interactions, Glu414 in ββ-enolase from rabbit muscle (Glu417 in yeast enolase) was mutated to Leu by Kornblatt *et al.* (2002). They confirmed that E414L mutant was less stable than the wild type by a factor of 20, but had no distinct difference in kinetic properties from the wild type. The lower stability of the E414L mutant supports the idea that the relatively small interactions area through ionic and hydrogen bonds is responsible for the major contribution to the dimer stability. Moreover, it has been reported that the ratio of charged/hydrophobic interface residues is 1.5 for enolase (Kuhnel and Luisi, 2001), which is more than twice the average of 0.7 for oligomeric proteins, thus the dimer interface is more polar in enolase than in other oligomeric proteins (Janin *et al.*, 1988). This presents a good explanation for the salt dependence for dimerization in enolase (Brewer and Weber, 1968; Kuhnel and Luisi, 2001), as well as the reason to why the enolase dimer is readily dissociated into monomers in the absence of the natural cofactor Mg^{2+} (Stec and Lebioda, 1990).

Bond	Residue 1	Residue 2	R1(-)....R2(+)	R1(-)...H...R2(+)
Ionic bond	E20	R414	OE1...NE	-
	E20	R414	OE2...NH2	-
	E417	R8	OE1...NH2	-
	E417	R8	OE2...NE	-
Hydrogen bond	N410	E379	-	ND2...OE1
	N410	Y11	-	ND2...O
	N410	Y11	-	OD1...N
	E404	S403	-	OE1...N
	E188	W56	-	OE1...N
	H191	R14	-	NE2...O
	S13	R402	-	O...N
	V208	V208	-	O...N

Table 3: Ionic and hydrogen bonds between subunits in yeast enolase (Stec and Lebioda, 1990). The atoms involved in ionic interactions and hydrogen-bonding are shown in forth and fifth row, respectively. R1: residue 1, R2: residue 2.

The crystal structure of apo-yeast enolase (Stec and Lebioda, 1990) displayed 353 water molecules that were present in the solvent structure of enolase; 11 water molecules were considered to be in the interior of enolase. Most ordered water structure was observed in the active site cavity and in the deep cleft formed between the dimer subunits (Stec and Lebioda, 1990). These water molecules in the active site are associated with ligand coordination (section 1.5.1) and are proposed to participate in catalysis (section 1.4.2).

1.6.2 Dissociation studies

Except for octameric enolase from some bacteria, most enolases are dimeric and have two active sites per dimer. Each of the active sites is completely contained within the monomer and exists separately from that of the other monomer (Kornblatt *et al.*,

1998). Since the active site of each monomer is neither a result of two monomers dimerization, nor dependent on the dimer interface, it remains a query as to why most monomers produced through different dissociation methods seem catalytically inactive? Are there any conformational differences between the monomer and dimer, or is the quaternary structure indispensable for the activity to occur? In order to understand these interesting questions, many investigators have tried to dissociate the dimeric enolase into monomers using different methods.

1.6.2.1 Dissociation methods

Salts (Brewer and Weber, 1968; Trepanier *et al.*, 1990; Kornblatt *et al.*, 1996; Kornblatt *et al.*, 2002) and hydrostatic pressure (Paladini and Weber, 1981; Kornblatt and Hui Bon Hoa, 1982; Kornblatt *et al.*, 1993; Kornblatt *et al.*, 1998; Kornblatt *et al.*, 2004) were the two main methods used in many studies to dissociate enolase. However, most of these methods yielded inactive monomers. Although these inactive monomers lose catalytic activity, they are correctly folded and maintain native secondary structure. Nonetheless, there have been reports of successful production of active monomers (Trepanier *et al.*, 1990; Kornblatt *et al.*, 2004).

Brewer and Weber (1968) have successfully dissociated enolase dimer into monomers using excess EDTA (2-3 mM) at high concentrations of KCl (1 M) without the presence of Mg^{2+}. The monomers formed by this approach are inactive. As it is well known, EDTA is a cation chelator, which may remove the metal ion from the protein, and

KCl favors a more "open" protein structure through exposure of the hydrophobic regions (Brewer, 1969). Another kind of salt widely used to dissociate enolase is $NaClO_4$, a more effective chaotropic salt. Kornblatt *et al.* utilized $NaClO_4$ to dissociate different isozymes of mammalian enolase and produced inactive monomers (Kornblatt *et al.*, 1996; Kornblatt *et al.*, 2002) or active monomers (Trepanier *et al.*, 1990). $NaClO_4$ is a chatropic salt, which is believed to disrupt the structure of water, thereby making protein structures less stable through lowering the hydrophobic interactions and facilitating the hydration of the buried surface area (Collins and Washabaugh, 1985), or contributing to the formation of a larger surface area through directly binding to the protein (Arakawa and Timasheff, 1982). Additionally, Jensen *et al.* (1995) conclude "the capability of the salts containing chaotropic anions, in particular, to interact with the polypeptide backbone and side chain amide dipoles of the protein results in the destabilization of the enzyme".

Hydrostatic pressure was considered as another relatively gentle method to dissociate enolase. Dissociation effects induced by hydrostatic pressure were partially ascribed to hydration of the buried protein surface (Kornblatt *et al.*, 1993). Paladini and Weber (1981) first utilized hydrostatic pressure to dissociate yeast enolase and the dissociation was confirmed to be reversible. Extensive studies on dissociation of enolase through hydrostatic pressure were carried out by Kornblatt *et al.* They confirmed that this dissociation process was also fully reversible and the monomers formed by this method were either inactive (Kornblatt and Hui Bon Hoa, 1982; Kornblatt *et al.*, 1993; Kornblatt *et al.*, 1995) or active (Kornblatt *et al.*, 2004) depending on the different enzyme forms

used. These dissociation studies were performed using the following enzyme forms: apo-enolase, Mg^{2+}-enolase and Mn^{2+}-enolase. From this investigation, it was concluded that inactive monomers produced from Mg^{2+}-enolase are the result of the Mg^{2+} release from the enolase during dissociation (Kornblatt *et al.*, 1998; Kornblatt *et al.*, 2004). However, the monomers produced from Mn^{2+}-enolase using the same method were active, which may be due to the fact that Mn^{2+} is still bound to the enolase even in the monomeric form (Kornblatt *et al.*, 2004). Therefore the presence of divalent cations seems to be necessary for allowing enolase monomer to have activity under these conditions (Kornblatt *et al.*, 2004).

In addition to above two widely used methods, it has been confirmed that enolase could be dissociated into active monomers through increasing temperature (above 40 °C) and decreasing the protein concentration (below 0.7 ug/ml) in the presence Mg^{2+} and substrate (Keresztes-Nagy and Orman, 1971; Holleman, 1973).

1.6.2.2 Proposed mechanism of forming active or inactive monomer through dissociation

Why are some monomers active, but others inactive? What is the conformational difference between these monomers? Kornblatt *et al.* (1998) has presented a detailed proposal to the differences between the monomers. They have also provided reasonable arguments to these questions. They proposed that the correct loop conformation and metal ion bindings are essential for keeping the monomers active. Details about the loop

conformations and function, as well as ligand bindings in the active site have been described in section 1.3 and section 1.5, respectively. In the active site of enolase, certain residues that directly chelate the Mg^{2+} can also have interactions with other residues, which are mostly located near the loop regions (Kornblatt *et al.*, 1998). For example, Asp246 can form hydrogen bonds to the backbone N of Asp248; Glu295 and Asp320 can form electrostatic interactions with Lys396 and Lys345, respectively. All of these residues are near the beginning of a loop. In addition, residues 402 and 403, which participate in subunit interactions, are positioned in the 398-403 loop. Such facts suggest that the precise conformation of these loops is crucial both for the subunit interactions and for the active site structure (Kornblatt *et al.*, 1998). Thus the presence of divalent cation can maintain the correct active site structure and the loop conformation, which further allow the monomeric enolase to have activity.

Now, it is not difficult to understand why the monomer produced through increasing the temperature and lower protein concentration is active, whereas monomers produced through salts are inactive. The main reason is that the former is able to maintain the divalent cation, whereas the latter loses it. Hydrostatic pressure can produce both active and inactive monomers, which is also dependent on whether the divalent cation is bound to the monomeric enolase or not.

1.7 Thesis objectives

During enolase catalysis, the loop movement is a significant and remarkable

characteristic. These specific loop movements are evidently related to metal ions and substrate binding as well as subunit interactions. The disturbance on the loop conformation would probably not only cause changes in the precise position of these active site residues for correct coordination the cofactors, but also result in weakened subunit interactions.

In the active site loop (Pro35-His43), there is a very important residue Ser39 located, which directly coordinates metal II with its carbonyl and hydroxyl oxygens, and is the only ligand coming from enzyme polypeptide that participates in metal II binding. The Gly residues in the vicinity of Ser39 probably provide Ser39 with enough space to rotate into a position to correctly coordinate metal II, and/or presumably contribute to maximal loop movement. Moreover, this active site loop is also the most mobile part of a whole loop (Pro35 –Gly60), which extends directly from active site to subunit interface. It seems that the active site loop would not only be directly involved in cofactor binding, but also indirectly has some relationship with the subunit interactions. Therefore, it is hypothesized that the movement of the active site loop has a crucial function for enolase catalysis to occur and in maintaining subunit interactions.

In order to confirm this hypothesis, the hinge sites at position Gly37 and Gly41 in the active site loop in yeast enolase were mutated to Ala residues through site-directed mutagenesis. This is based on the previous work performed by Kornblatt (Kornblatt, 2005). They prepared the same mutants from ββ-enolase (rabbit muscle) and confirmed that the perturbation on the flexibility of the active site loop had subtle effects on catalytic

activity, but no evidence about the effect on subunit interactions. Therefore, we are still interested in investigating the same mutation in yeast enolase in terms of enzymatic activity and subunit interactions. The replacement of Gly by Ala was conservative and was not expected to significantly disrupt the overall secondary and tertiary structure of protein. After the mutation Gly to Ala, the active site loop would be hinged with a slightly larger residue and the movement of the active site loop is expected to be inhibited more or less in two mutants.

Enolase in the present project is coming from yeast. G37A and G41A mutant enolases were constructed through site-directed mutagensis and over expressed in *E. coli*. These purified proteins were subjected to steady state kinetic and dissociation studies.

2 Materials and Methods

2.1 Materials

2.1.1 Bacterial growth media

M9 salt composed of Na_2HPO_4, KH_2PO_4, NH_4Cl and NaCl, was prepared as 5×concentration stock and autoclaved as sterile (Maniatis, 1989). Ampicillin (sodium salt, Biotech grade) was from Fisher Scientific. Solutions of ampicillin (100 mg/ml) were sterilized by filtration through a 0.45 μm Nalgene syringe filter and stored at -20 °C until use.

2.1.2 Bacterial strains

XL1-Blue *E. coli* was used to store pET-3a vector containing wild type and mutant yeast enolase gene insert at -80 °C for long time. Site-directed mutagenesis was carried out on the pET-3a vector, into which the yeast enolase gene was inserted. BL21(DE3) *E. coli* was employed to express recombinant wild type, G37A and G41A mutant yeast enolases.

2.1.3 Extraction of plasmid DNA

RNAse A (from bovine pancreas) was purchased from Boehringer Mannheim. RNAse A was prepared as a 10 mg/ml stock solution and heat inactivated (Maniatis, 1989). PEG 6000 and PEG 8000 were from Fisher Scientific and prepared as 30% stock

solutions. Both stock solutions were kept at 4 °C. TE buffer (10 mM Tris-HCl, 1 mM EDTA, pH 8.0) used to dissolve DNA was prepared as described by Maniatis (1989). Sucrose was A.C.S. grade and from Fisher Scientific. Lysozyme (from chicken egg white) was from Sigma.

2.1.4 Site-directed mutagenesis

Cloned *Pfu* DNA polymerase (2.5 U/μl), 10× cloned *Pfu* buffer And a 10 mM dNTPs mixture were all purchased from Fermentas. Oligonucleotides were synthesized by BioCorp Inc (Montreal).

2.1.5 Restriction enzyme digestion

BamHI (10 U/μl), *NdeI* (10 U/μl), and *DpnI* (10 U/μl) were purchased from Fermentas. *BsawI* (5000 U/μl) was purchased from New England Biolabs. Digest buffers corresponding to each restriction enzyme were provided by each supplier with the purchased enzymes.

2.1.6 Agarose gels

TAE buffer (40 mM Tris-Acetic acid, 1 mM EDTA) was prepared as 50×stock solution and stored at 4 °C (Maniatis, 1989). Agarose (genetic technology grade) was from MP Biomedicals and dissolved in TAE buffer as 1% before preparing agarose gels. λ-DNA marker (*EcoRI/HindIII* digest, 500 μg/ml) was purchased from Promega. λ-DNA

marker was normally mixed with 6×loading dye and stored at -20 °C until use.

2.1.7 Glycerol stocks

Glycerol (A.C.S. grade) was from Fisher Scientific and sterilized by autoclaving in order to store XL-Blue *E. coli* containing pET-3a vector, into which the wild type and mutant yeast enolase DNA were inserted. This was used in order to prepare glycerol stocks and give a final 15% glycerol.

2.1.8 Purification of proteins and determination of protein concentration

DNAse 1 (from bovine pancreas, grade II) and RNAse (from bovine pancreas) were from Boehringer Mannheim. Phospho-glycolic acid (tri(monocyclohexyl -ammonium) salt dessicate, >99%) was purchased from Sigma, prepared as a 100 mM stock solution and stored at -20 °C. Q-Sepharose Fast Flow resin was from Amersham Biosciences AB. $(NH_4)_2SO_4$ (Ultra pure grade) was from ICN.

The Bio-Rad protein assay reagent was from Bio-Rad. BSA used for standard curves was from Sigma.

2.1.9 SDS-PAGE

Acrylamide (>99.9%), Bio-acrylamide(>97%), low range SDS-PAGE standards (MW from 14.4-97.4 kD), Coomassie brilliant blue R, TEMED, 2-mercaptoethanol and APS were all electrophoresis purity grade and purchased from Bio-Rad. Acrylamide was

prepared as a 30% solution and stored at 4 °C, and APS was prepared as 10% stock solution and stored at -20 °C. Both Gly (>99%, A.C.S grade) and SDS were purchased from Fluka. SDS was prepared as 10% solution and stored at room temperature.

2.1.10 Synthesis of 2-PGA and coupling determination of 2-PGA concentration

PEP (Tricyclohexylamonium salt, A.C.S grade) was purchased from Roche. Mes (>99.0%) and TMA-hydroxide (purum) were from Fluka. Both $MgSO_4$ and HCl were A.C.S grade and from Fisher Scientific. Dowex 1×2-400 ion-exchange resin was from Sigma.

NADH (HPLC grade, >97%, disodium salt hydrate) was from Fluka. PK/LDH (from rabbit muscle) was purchased from Roche. ADP (sodium salt, HPLC grade) was from Sigma. 3.6 mg/ml NADH and 17.3 mg/ml ADP solutions were freshly prepared before using every time.

2.1.11 Proteins dialysis, $NaClO_4$ incubation and chelating reagents

Dialysis tubing (6.4 mm or 15.5 mm wet diameter) was from Bio Design Inc. Both $NaClO_4$ (99%, A.C.S grade) and NaOAc (99.5%, A.C.S grade) were from Fluka. Both solutions were typically prepared in Buffer A (pH 7.4) as a 2 M stock and stored at 4 °C. Chelex 100 resin (sodium form, ACS grade) was purchased from Bio-Rad. Nitric acid was trace metal grade and from Fisher Scientific

2.2 Methods

2.2.1 Oligonucleotides design and synthesis

Mutagenic oligonucleotides were designed using the WEBCUTTER tool (http://www.firstmarket.com/cutter/cut2). In order to screen for mutants, the mutagenic oligonucleotides were designed such that a specific restriction site was removed when introducing the amino acid substitution from Gly to Ala at positions 37 and 41. Silent mutations and amino acid substitutions were introduced keeping *E. coli* codon usage in mind. The mutagenic oligonucleotides used to construct two mutants are shown in Table 4.

Mutants	Mutagenic oligonucleotides
G37A	5'-C-ATT-GTC-CCA-TCT-**GCG**-GCT-TCT-ACG-GGT-GTC-CAC-GAA-GC-3
	3'-G-TAA-CAG-GGT-AGA-**CGC**-CGA-AGA-TGC-CCA-CAG-GTG-CTT-CG-5'
G41A	5'-GGT-GCT-TCT-ACC-**GCG**-GTC-CAC-GAA-GCT-TTG-3'
	3'-CCA-CGA-AGA-TGG-**CGC**-CAG-GTG-CTT-CGA-AAC-5'

Table 4: Oligonucleotides used to construct G37A and G41A mutant yeast enolase. The bold regions indicate the mutagenic codon, while the underlined regions indicate the silent mutation.

The oligonucleotides were synthesized by BioCorp Inc, Montreal. Each of the oligonucleotides in lyophilized form was dissolved in 250 µl of sterile dH_2O. The concentration of each oligonucleotide was determined by measuring OD_{260nm}: one OD_{260nm} unit equals 33 µg of oligonucleotides ml^{-1} (Brown, 1991).

2.2.2 Extraction of plasmid DNA

Mini scale (5 ml bacterial cultures) preparation of plasmid DNA was performed with the alkaline lysis method (Good, 1997). Plasmid DNA obtained from mini scale was utilized to screen mutants. Large scale (100 ml bacterial cultures) isolation of plasmid DNA was performed using the lysozyme plus alkaline lysis method (Kreiq, 1991). Plasmid DNA obtained from large scale isolations was used for DNA sequencing. Plasmid DNA concentration and quality were measured on the basis of OD_{260} and OD_{280} (Brown, 1991). TE buffer was routinely used to dissolve the purified DNA.

2.2.3 Site-directed mutagenesis

Site-directed mutagenesis in yeast enolase was carried out using the Stratagene Instruction Manual. Briefly, PCR reactions were prepared as following (total volume of 100 µl): 400 ng of parental DNA, 450 ng of each complimentary oligonucleotide strand, 2 µl of 10 mM of dNTPs mixture, 10 µl of 10× *Pfu* buffer, and sterile dH_2O. Reactions were covered with 120 µl of mineral oil and heated to 95 °C, then 5 U of cloned *Pfu* polymerase was added to the system. PCR was started and carried out in the following thermal cycle parameters, see Table 5.

Thermal cycles	Denaturation		Annealing		Extension	
	Time (min)	Temperature (°C)	Time (min)	Temperature (°C)	Time (min)	Temperature (°C)
First cycle	2	95	1	54	14	72
2-16 cycles	0.5	95	1	54	14	72

Table 5: Thermal cycle parameters of PCR reaction

2.2.4 Transformation

PCR products were digested with 10 U of *DpnI* at 37 °C for 1 hour. After *DpnI* digestion, the PCR products were transformed into competent XL1-Blue *E. coli* cells, which were plated on LB medium containing 0.01% ampicillin. The following day, 3 colonies were normally picked and inoculated into 5 ml of LB broth containing 0.01% ampicillin. The liquid cultures were grown overnight at 37 °C, 225 RPM. The small scale isolation of plasmid DNA was performed the next day as described in section 2.2.2.

2.2.5 Screen of the G37A and G41A mutants using restriction enzyme digestion

In order to screen for introduction of mutations, DNA was digested with 5 U of *BsawI*. At the same time, parental DNA was also digested with the same amount of *BsawI* for the purpose of comparison. All digestions were carried out at 60 °C for 1 hour. After *BsawI* digestion, the samples were mixed with 6×loading dye and run on 1% agarose gels. Gels containing ethidium bromide were routinely prepared in 1×TAE buffer. Agarose gel electrophoresis was always run at 80 volts for 1 hour (small gel) or 100 volts for 2 hours (big gel).

In the case of G37A mutation, the codon for **Gly** at position 37 was changed to one codon for **Ala**, while a silent mutation near the mutation amino acid was also introduced to remove the restriction site recognized by the *BsawI*. In the case of the G41A mutation, the codon for **Gly** at position 41 was changed to one codon for **Ala**, at same time introducing a silent mutation and removing one restriction site recognized by the *BsawI*. G37A and G41A mutants were all screened on the basis of loss of a *BsawI* restriction site. Parental template DNA was digested by *BsawI* producing 7 fragments of the following size: **1321 bp**, 1084 bp, 1017 bp, 971 bp, 831 bp, **540 bp**, and 147 bp. DNA from plasmids encoding G37A and G41A mutants digested by *BsawI* would yield only 6 fragments of the following sizes: **1861 bp**, 1084 bp, 1017 bp, 971 bp, 831 bp, 147 bp.

2.2.6 Yeast enolase mutant sequencing

DNA sequencing was performed by Bio S&T Inc (Montreal, Quebec). In order to make sure that the desired mutations had been introduced and no other unwanted mutations present, DNA sequencing results were aligned with wild type yeast enolase gene (#J01322) using the BLAST server at the National Center for Biotechnology Information (accessed from the web http://www.ncbi.nlm.nih.gov/).

2.2.7 Preparation of glycerol stock of wild type and mutants

Wild type, G37A and G41A mutant plasmids were re-transformed into

competent XL1-Blue *E. coli* cells. LB liquid cultures (5 ml) of each mutant were grown by inoculating one colony from the respective plates. The following day, the cultures were diluted 100 times with fresh LB broth and grown for 2-3 hours until the OD_{600}=0.5. Three glycerol stocks of each mutant were prepared in sterile cryogenic vials by mixing 1.7 ml of each growth culture with 0.3 ml of sterile glycerol (final glycerol concentration =15%).

2.2.8 Recombinant protein expression

Wild type and mutant proteins were over-expressed by the method recommended by Poyner *et al.* (1996). Plasmid DNA containing wild type, G37A and G41A mutant gene inserts were transformed into competent BL21(DE3) *E. coli* cells. The cells from LB plates were re-suspended in 5 ml LB broth. The suspension of bacteria were inoculated into 100 ml medium (1% tryptone, 0.5% yeast extract, 0.04% ampicillin, M9 salts (Maniatis, 1989)) using 0.5% inoculating amount. Cells were grown at 37 °C, 225 RPM until an OD_{600} about 0.5. Then 10ml of these cell cultures were immediately inoculated into 1 liter of medium, which was composed of 1% tryptone, 0.5% yeast extract, M9 salts and 0.04% ampicillin, as well as 1.6% lactose (which was used to induce yeast enolase expression). Cells were grown in above medium for 14 hr at 37 °C, 225 RPM, and were harvested by centrifugation at 4 °C, 7000 RPM, 10 minutes in a Beckman J2-HS centrifuge (JA-10 rotor) in the following day. Normally, 4 liters of bacterial culture were prepared and the wet cell pellet obtained were weighed each time,

and stored at -20 °C.

2.2.9 Purification of proteins

Buffer A (50 mM Tris (pH 7.4)/0.1 mM EDTA/1 mM Mg^{2+}) was used throughout all the purification steps and the subsequent spectroscopy experiments. All purification steps were performed at 4 °C.

2.2.9.1 Preparation of crude extract

The cell pellet obtained from 1 liter cultures was suspended in 20 ml of buffer A and treated with 0.003 g DNAse 1 and RNAse. Phospho-glycolic acid (substrate analogue) was added to the cell suspension to a 0.5 mM final concentration. Cells were sonicated on ice with a Branson 250 Sonifier. For every 10 g of wet cell pellet, six 30-seconds bursts were routinely performed with 1 minute cooling time between two bursts. The pH of the cell lysate was adjusted to 7.4 with 1 M Tris stock, and the cell lysate was centrifuged at 4°C, 14000 RPM, 30 minutes. After centrifugation, the supernatant was considered as the crude extract.

2.2.9.2 $(NH_4)_2SO_4$ fractionation and Fast-Flow Q-Sepharose chromatography

The crude extract was brought to 40% $(NH_4)_2SO_4$ saturation and then centrifuged at 4 °C, 14000 RPM, 30 minutes. The supernatant was brought to 85% $(NH_4)_2SO_4$ saturation. The final pellet from 40-85% $(NH_4)_2SO_4$ precipitation was

dissolved in 6-8 ml of buffer A and $(NH_4)_2SO_4$ was removed through dialysis of the protein overnight against two 100 fold volume changes of buffer A. Following dialysis, the protein mixture was centrifuged in the same way as above to remove the precipitated particles and loaded on a 200 ml Q-Sepharose Fast Flow anion exchange column equilibrated with buffer A. Fractions were collected for 6 minutes at a flow rate of about 1 ml/min. Every fifth fraction was analyzed by measuring the absorbance at 280 nm and 260 nm and assaying the enzyme activity. Fractions with high enolase activity and ratio of OD_{280nm}/OD_{260nm} above 1.7 were pooled and brought to 4.23 M $(NH_4)_2SO_4$. The precipitated protein pool was normally stored at 4 °C. At the same time, an aliquot from each purification step was saved for assaying enzyme activity and protein content. Each of the aliquots was also run on 12% SDS-PAGE to check the purity from each purification step.

2.2.10 Protein concentration determination

For purification experiments, protein concentration was either determined by the absorbance at 280 nm using an extinction coefficient of 0.895 ml mg^{-1} cm^{-1} (Warburg, 1942), or by the method with Bio-Rad reagent using the BSA as the standard (Engel, 1996). For spectroscopic studies, protein concentration was measured by the absorbance at 215 and 225 nm (Murphy, 1960). For enzyme kinetic studies, protein concentration was measured by the absorbance at 280nm.

2.2.11 Proteins molecular weight determination

The molecular weight of recombinant wild type, G37A and G41A mutant yeast enolase were determined by Alain Tessier at the Concordia University, Center for Biological Applications of Mass Spectrometry (Montreal, Quebec). Stock proteins were dialyzed at 4 °C overnight against two 100 fold volume changes of Buffer A, and then typically diluted to 2-6 μM final concentration with the same buffer. These diluted samples were then passed through a HPLC column before recording the signal through Q-ToF 2 Micromass Spectroscopy.

2.2.12 SDS-PAGE

The purity of the protein from each purification step was checked by SDS-PAGE. Normally, 4% stacking gel and 12% resolving gel were prepared and run according to methods as described by Lammli (Laemmli, 1970).

2.2.13 Proteins dialysis

For spectroscopy experiments, recombinant wild type and mutant proteins were routinely dialyzed at 4 °C against two 100 fold volume changes of buffer A. For kinetic studies, the dialysis buffer was 25 mM Mes and 25 mM Tris, pH 7.1, containing 1 mM Mg^{2+} or 0.1 mM Mn^{2+} depending on the experiment.

2.2.14 Synthesis of 2-PGA and determination of 2-PGA concentration

2-PGA was enzymatically prepared from PEP as described by Shen and Westhead (Shen and Westhead, 1973) with slight changes (Kornblatt and Klugerman, 1989).

The concentration of the solution of 2-PGA was determined by connecting 2-PGA to lactate using enolase, PK and LDH. In this coupled assay, 9.5 ml of enolase assay buffer containing 250 μM NADH and 250 μM ADP were prepared, then 15 μl LDH/PK, 2 μl 2-PGA solution and 5 μl concentrated yeast enolase were added in 2.5 ml above enolase assay buffer; the disappearance of NADH at 340nm was monitored due to the conversion of PEP to pyruvate, which was then converted to lactate. The concentration of 2-PGA was calculated using the ε_{340nm}= 6.22 mM^{-1} cm^{-1}.

2.2.15 $NaClO_4$ dissociation

Wild type and mutant enolases were incubated at various concentrations of $NaClO_4$ in buffer A at 15 °C overnight. In order to maintain constant ionic strength as $NaClO_4$ concentration was varied, NaOAc concentration was added such that all samples had the same [Na^+] and the same ionic strength. $NaClO_4$ concentration was increased from 0 mM to 340 mM for dissociation wild type enolase. For G37A and G41A enolase, $NaClO_4$ concentration was increased from 0 mM to 270 mM. After incubation, the samples were assayed for enzyme activity, scanned from 260-305 nm for UV absorption spectra and from 250-350 nm for near CD spectroscopy. For dissociation studies

monitored by spectra, protein concentration was 1 mg/ml (10.6 μM) for all three proteins. For dissociation studies monitoring enzyme activity, protein concentrations were 0.1 mg/ml for wild type and G37A, and 0.5 mg/ml for G41A.

2.2.16 Enzyme activity assays

The enzyme activity was assayed on the Cary UV-Visible spectrophotometer in 10mm quartz cuvette at room temperature. For purification experiments, assays were carried out in enolase assay buffer (50 mM imidazole (pH 7.1)/1 mM Mg^{2+}/0.1 mM EDTA /250 mM KCl) plus 2 mM PEP by monitoring the disappearance of PEP at 244 nm (since 2-PGA is unavailable commercially). For $NaClO_4$ dissociation experiments, the activities were assayed by measuring the appearance of PEP at 240 nm under different conditions for wild type and two mutants. For wild type, assays were performed in enolase assay buffer plus 0.5 mM 2-PGA, while for two mutants, assays were performed in same assay buffer containing additional Mg^{2+}. Based on the kinetic studies of the effect of [Mg^{2+}] on enzyme activity, 50 mM Mg^{2+} for G37A and 100 mM $Mg^{2+}$for G41A were used in the assay buffer. Assays were initiated by adding enzyme to above assay mixture. The amount of each enzyme which would produce an optimal reaction velocity was determined empirically. Only the first 30 s of the assay was chosen to calculate the velocity of reactions, because the enzyme inactivated by $NaClO_4$ was slowly reactivated under the enzyme assay condition.

2.2.17 Circular Dichroism (CD) spectroscopy

All CD spectra in the peptide bond and aromatic region were recorded in a Jasco 710 spectrometer under continuous N_2 gas flow (flow rate ≈3 L/min).

Far CD-spectra were collected in the region of 200-260 nm with the following parameters: scan speed was 20 nm/min with a response time of 1 second, 0.5 nm bandwidth, 5 accumulations, temperature was 15 °C. Protein concentration was 0.5 mg/ml (5.3 μM) and 1 mm path rectangular quartz cuvette was used. Near CD spectra were recorded in the region of 250-350 nm in the same instrument with the same parameters as in the Far CD spectra. Protein concentration was 1.0 mg/ml (10.6 μM) and 10 mm rectangular quartz cuvette was used. The buffer spectrum was subtracted from the spectra of the proteins, and the obtained spectra were smoothed using the Jasco standard analysis software.

2.2.18 4^{th} derivative UV spectroscopy

Absorption spectra of yeast enolase and mutant proteins were recorded on a Cary UV-Visible Spectrophotometer with the following parameters: scan range from 260 to 305 nm, 0.1 nm data interval, 1.0 second average time, spectra bandwidth of 1.0 nm, with a scan rate of 6.0 nm/min and step width of 0.1 nm, 1 accumulation, temperature was 15 °C. Protein concentration was 1.0 mg/ml (10.6 μM) and 10 mm path rectangular quartz cuvette was used. Buffer solution was scanned in the same condition as samples, and the buffer spectrum was subtracted from the spectra of proteins. 4^{th} derivative UV spectra

were calculated as described by Lange *et al.* (1996).

2.2.19 Calculation of dissociation constants

K_d values were calculated at each [$NaClO_4$] with the following equation (Kornblatt *et al.*, 1998):

$$K_d = 4(f_M)^2[\text{enolase}]/(f_D)$$

Where f_M and f_D are the fractions of monomeric and dimeric enolase, respectively, and [enolase] is the molar concentration of enzyme. Calculations were done using activity, 4th derivative UV and near UV-CD data. By plotting K_d as a function of [$NaClO_4$], dissociation constants for each protein at 0 M $NaClO_4$ were obtained. ΔG_0 was also determined for each protein according to the equation: $\Delta G_0 = -RT \ln K_d$ (Stephen, 1997).

2.2.20 Temperature denaturation

Loss of protein secondary structure was monitored at 222 nm on the Jasco 710 spectrometer using the following parameters: temperature range from 30-75 °C, heating rate of 15 °C/hour, 0.2 °C step resolution, with a response time of 0.25 second, 1.0nm bandwidth, and a wait time of 2 minutes. Protein concentration was 1 mg/ml (10.6 μM) and 1mm circular quartz cuvette was used. 300 μl sample were prepared in buffer A. Temperature denaturations were typically performed in duplicate.

2.2.21 Sedimentation velocity analytical ultracentrifugation

Beckman XL-I analytical ultracentrifuge was used to determine the sedimentation velocity of wild type and mutant enolases. Wild type and mutant protein samples were prepared as described in section 2.2.15. Samples were centrifuged in 60-Ti rotor at a speed of 42,000 RPM at 15 °C for 14 hours. Data were collected at 230 nm, 250 nm or 280 nm depending on the protein concentrations.

Sedimentation velocity data were analyzed and fit to one species model using the dc/dt$^+$ software (version 1.14). The final $S_{20,w}$ were corrected for buffer viscosity and density. Generally, buffer density and viscosity used in the AUC experiment can be determined using SEDNTERP software (version 1.07, 2002). Due to the $NaClO_4$ and NaOAc used in the experiment, buffer density and viscosity were calculated from a standard curve obtained through experimental measurement by Dr. Kornblatt (personal communication).

2.2.22 Removal of contaminating divalent cations

When measuring enzyme activity as a function of divalent cation concentration, metal-free conditions were required. Buffer B (25 mM Mes and 25 mM Tris, pH 7.1) and 2-PGA were passed through a 1×10 cm and a 1×1 cm Chelex 100 column to remove metal ions, respectively. In order to decrease the amount of other contaminating divalent cations, both were stored in plastic bottles rather than in glass. These bottles need to be soaked in 20% nitric acid for at least 1 hour and cuvettes were properly soaked in the

same solution for overnight, then rinsed exhaustively in deionized H_2O.

2.2.23 Enzyme kinetics studies

The dehydration of 2-PGA for wild type and two mutant enolases has been determined using the steady state kinetic assay. Enzyme activities were measured at 25 °C in buffer B by following the production of PEP at 240 nm. All kinetic studies were carried out in duplicate.

For studies of the activation or inhibition by divalent cations Mg^{2+} and Mn^{2+}, the K_m and K_i for the two divalent cations were determined using buffer B plus 0.5 mM 2-PGA by varying the concentration of Mg^{2+} and Mn^{2+}. Michaelis constant (K_m) for 2-PGA was determined using buffer B plus constant Mg^{2+} by varying the concentration of 2-PGA. Mg^{2+} used to determine the K_m for 2-PGA varied due to the preliminary experiment results and the kinetic studies on the enzyme activity as a function of $[Mg^{2+}]$. Thus, the following constant Mg^{2+}concentrations were used: 1 mM, 50 mM and 100 mM Mg^{2+} for wild type, G37A and G41A, respectively. ENZFITTER (Biosoft, 2004) was used to fit the kinetic data to the Michaelis-Menten equation when measuring K_m for 2-PGA, or to either of the following equations when inhibition was observed by high concentrations of divalent cations (Kornblatt, 2005).

$$v = (V_{max} \times [S])/(K_m+[S]+([S]^2/K_i)) \qquad \text{Eq (1)}$$

$$v = (V_{max} \times [S]+V_2[S]^2/ K_i)/(K_m+[S]+([S]^2/K_i)) \qquad \text{Eq (2)}$$

where S is the metal ion concentration. Eq(1) is the substrate inhibition equation which

represents binding excess S that leads to complete inactivation of the enzyme; Eq(2) is the modified substrate inhibition equation, in which the enzyme can be partially inhibited by excess S, V_2 is the residual activity (Kornblatt, 2005).

Kinetic constants for divalent cations were normally obtained from the best fit to either of above two equations. k_{cat} can be obtained by dividing V_{max} with protein concentration using the following equation:

$$k_{cat} = V_{max} / ([protein]_{total} \times 2)$$

where 2 symbolizes the number of active site per mole of enzyme, ε_{240nm} for PEP in the presence of Mg^{2+} and Mn^{2+} are 1.376 $mM^{-1}.cm^{-1}$ and 1.308 $mM^{-1}.cm^{-1}$ (Kornblatt, 2005), respectively.

3 Results

3.1 Purification of WT and mutant proteins

3.1.1 Identification of G37A and G41A mutants

Recombinant native yeast enolase gene has been formerly ligated into pET-3a vector polycloning site, between the *NdeI* and *BamHI* restriction site by Isabelle Rajotte (Padovani, 2003). This plasmid has a size of 4.7 kb, and contains the yeast enolase gene insert, which has a size of 1.3kb. Thus, the complete plasmid DNA containing the yeast enolase gene insert is 6.0 kb. Plasmids containing the G37A and G41A mutation were identified on the basis of loss of one *BsawI* restriction site, because a silent mutation near or at the mutation site was designed in order to remove one *BsawI* restriction site. Thus, a positive G37A or G41A mutant is identified by the appearance of a new fragment of **1860 bp** and the disappearance of the fragments of **1321 bp** and **540 bp** in the agarose gel (Figure 11). DNA sequencing results further confirmed that the desired mutation was introduced and no other unwanted mutations were found in G37A and G41A mutants.

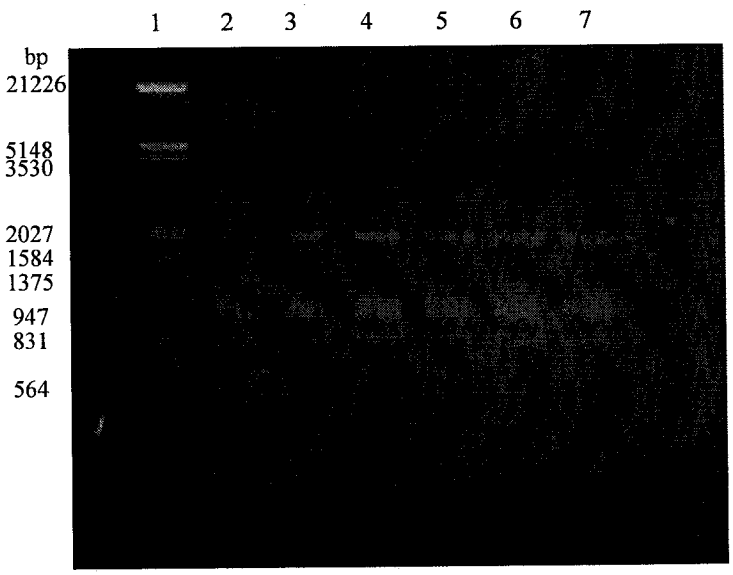

Screen of G37A mutant using *BsawI* digestion

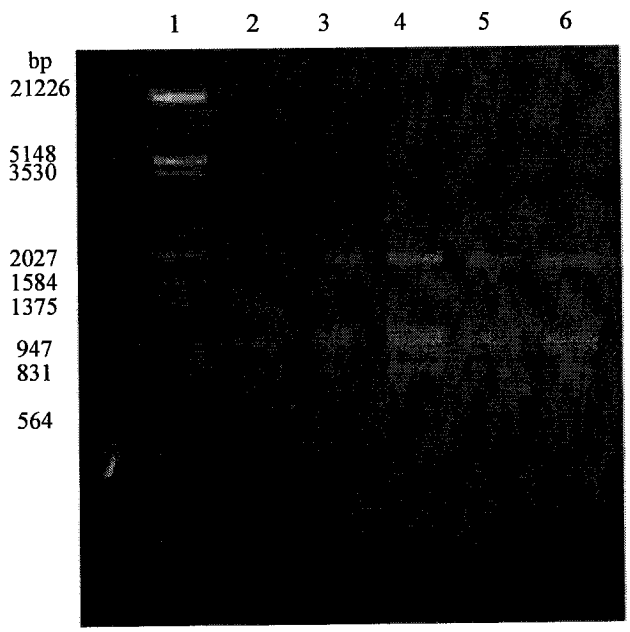

Screen of G41A mutant using *BsawI* digestion

Figure 11: Agarose gel indicating the results of screening G37A and G41A mutant with *BsawI* digestion. Lane 1: λ-DNA marker digested with *EcoRI-HindIII*; lane 2: Plasmid DNA containing the WT yeast enolase gene digested with ***BsawI***; other lanes: screening yeast enolase mutants with ***BsawI*** digestion.

3.1.2 Purification of recombinant wild type yeast enolase

Recombinant wild type yeast enolase was expressed and purified using the methods as described in section 2.2.8 and 2.2.9, respectively. Following two steps of $(NH_4)_2SO_4$ precipitation, the final pellet containing the enolase was re-suspended in buffer A and $(NH_4)_2SO_4$ was routinely removed through dialysis as described in section 2.2.9.2. Then, the protein mixture was further purified through a Q-Sepharose anion exchange column. Bound protein was eluted using the buffer A, and the fractions were collected on the basis of monitoring the enzyme activity and absorbance at 280 nm and 260 nm. A characteristic wild type elution profile from Q-Sepharose column is indicated in Figure 12. It is obvious that the protein content and enzyme activity have the same varying tendency, and fractions with high activities are comparatively concentrated in a few fractions, which is ideal for acquiring the best possible purification. Finally, fractions with high activity and ratio of OD_{280nm}/OD_{260nm} above 1.7 were pooled as the Q-Sepharose pool. Table 6 shows the summary for purification of wild type from each step in terms of protein content and specific activity. The specific activity of wild type is markedly increased as the progress of purification due to the removal of unwanted protein. At the same time, the Q-pool showed as one single band in the SDS-PAGE (Figure 13), indicating that the recombinant wild type is highly purified. The final yields of protein were normally determined by the absorbance at 280 nm and by the method with Bio-Rad reagent, as described in section 2.2.10. Generally, about 300 mg protein

(determined by the absorbance at 280 nm) from 4 L cultures was obtained for wild type yeast enolase.

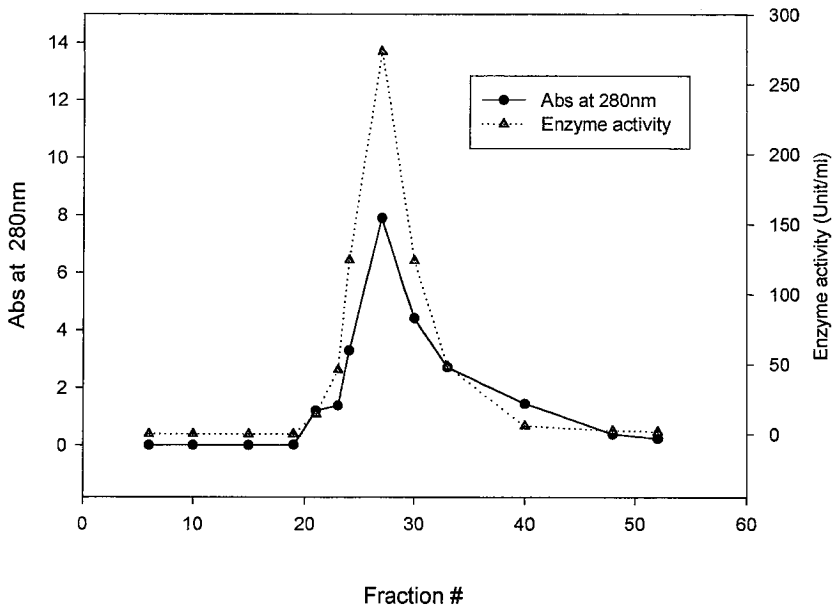

Figure 12: Elution profile of WT enolase from Q-Sepharose column in terms of protein content and enzyme activity.

Purification step	Volume (ml)	Total activity (ΔOD 244/min)	Total Protein (mg)	Specific activity (ΔOD 244/min/mg)	% Recovery activity
Crude Extract	35	20953	2184	9.6	100
Supernatant of 0-40% $(NH_4)_2SO_4$Cut	34	18496	1689	10.9	88.2
40-85% $(NH_4)_2SO_4$Cut	15	13920	1590	8.7	66.4
Dialysis	24	13392	1437	9.3	63.9
Q-Sepharose Pool	44	9328	372 298 [a]	25.1	44.5

Table 6: Summary for purification of wild type yeast enolase. Specific activity equals the total activities divided by total proteins. Activity assays were conducted in enolase assay buffer (pH 7.1) plus 2 mM PEP by monitoring the disappearance of PEP at 244 nm. [a]: Protein concentration was determined by the absorbance at 280 nm; other protein concentrations were determined by the method with Bio-Rad reagent using BSA as the standard (section 2.2.10).

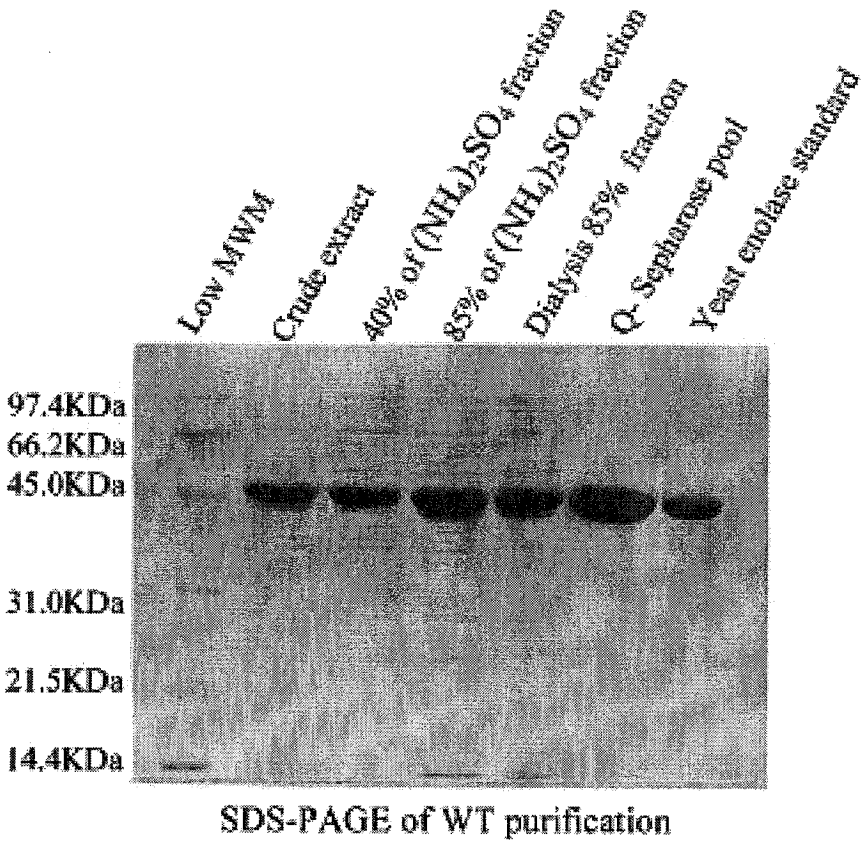

Figure 13: SDS-PAGE demonstration of the results of purification of wild type enolase. About 20 μg protein from each purification steps was loaded to different lanes, while 5 μg yeast enolase standard was loaded in the last lane.

3.1.3 Purification of G37A and G41A mutant proteins

3.1.3.1 Determination of mutant's activity peak

G37A and G41A mutants were expressed and purified using the same protocols as for purification of the wild type. Elution profile from the Q-Sepharose column for G37A and G41A mutants compared with that of the wild type is shown in Figure 14. It should be noted that there was one notable difference between two mutants and the wild type with regard to the elution profiles, because two activity peaks are observed in the mutant's elution profiles. One position of the activity peak is almost similar to that of the wild type, the other elutes much later than the wild type activity peak. As this is the case,

two different activity peaks were pooled separately in order to determine the true mutant activity peak. For the purpose of convenient comparison, the former and the latter activity peaks in the mutant elution profiles are named as Q-pool I and Q-pool II, respectively.

SDS-PAGE was first utilized to examine the purity of the two Q-pools, and several fractions from the former activity peak, as shown in Figure 15 (A) and (B), respectively. Here, only G41A is presented, since the two mutants behave similarly. From SDS-PAGE, it clearly indicates both the fractions from Q-pool I and Q-pool I migrate as a single dark band at the same position as yeast enolase standard, whereas the Q-pool II contains many bands, including one faint band at the same position as yeast enolase standard.

Although Q-pool I occurred as one single dark band in the SDS-PAGE, we still could not conclude that the former activity peak is from the mutants only based on the SDS-PAGE. Thus, samples from Q-pool I for two mutants and the final Q-pool for the wild type were examined using Q-ToF mass spectrometry. The results obtained by using mass spectroscopy are shown in Figure 16. There is a 14 Da difference for two mutants (samples from Q-pool I) from the molecular weight of wild type, which is in consistent with theoretically changing from a Gly to Ala residue (Table 7). The results from Q-ToF mass determination have provided us with the definite evidence that the Q-pool I contains the desired mutant protein, while the later peak may represent *E. coli* enolase. Since both the recombinant wild type and two mutants were all over expressed in *E. coli* host cells, it

was reasonable to find the presence of *E. coli* enolase. In order to further identify the latter activity peak, a control experiment was performed in untransformed BL21(DE3) *E. coli* cells. Cell growth and protein purification experiments were performed as for *E. coli* expressing recombinant enolase. It was found that the total enzyme activities and its elution position from the Q-Sepharose column were almost comparable to the Q-pool II fraction observed in the mutant elution profile (Figure 14). This observation supports our suggestion that the later activity peak contains *E. coli* enolase, though the exact position of *E. coli* enolase's activity peak (Figure 14) is not completely identical with these of two mutants, which is probably due to the difference in the starting point for collecting fractions.

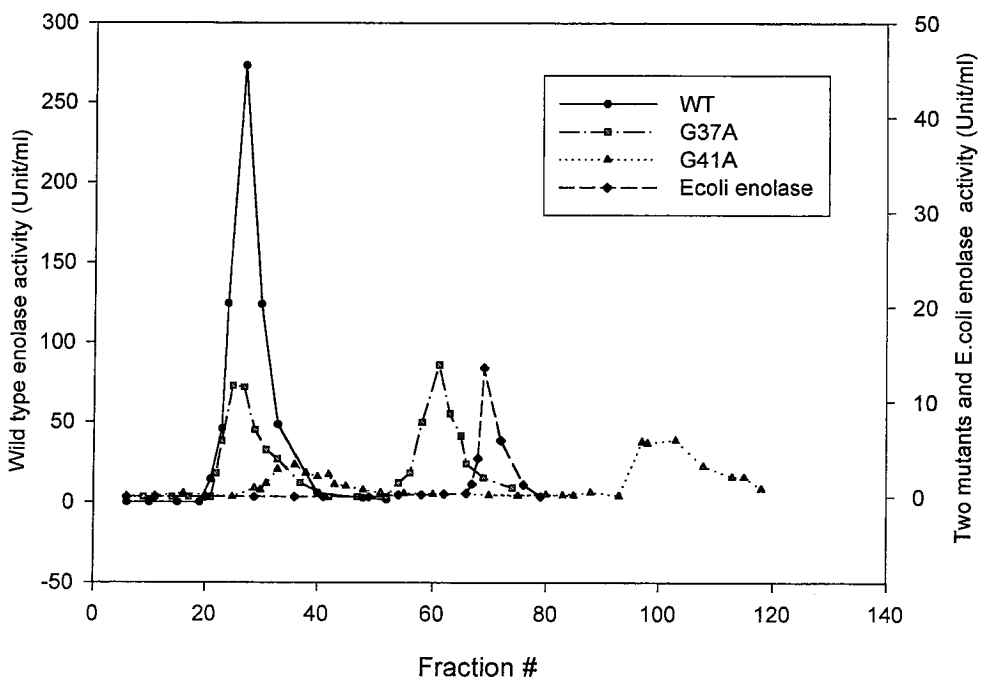

Figure 14: Comparing WT, two mutants and *E. coli* enolase elution profiles from the Q-Sepharose column in terms of activity

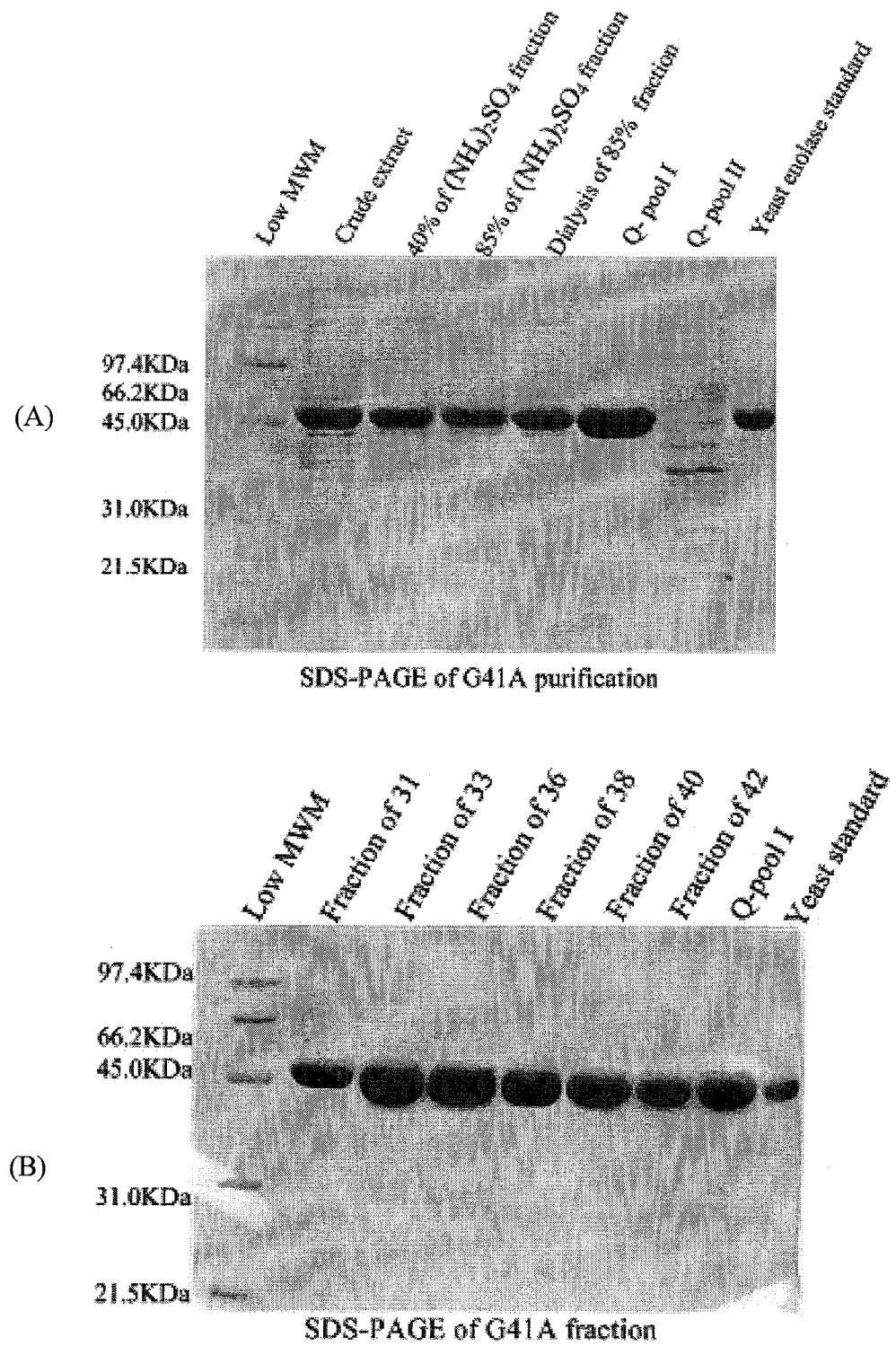

Figure 15: SDS-PAGE demonstration of the results of purification of the G41A mutant. (A) Samples from each purification steps. About 20 µg protein from each purification step was loaded in different lanes, while 5 µg yeast enolase standard was loaded in the last lane. (B) Fractions # 31-42 from the early activity peak in the elution profile from Q-Sepharose column. Aliquots (10 µl) from each fraction (1:3 dilutions) were loaded

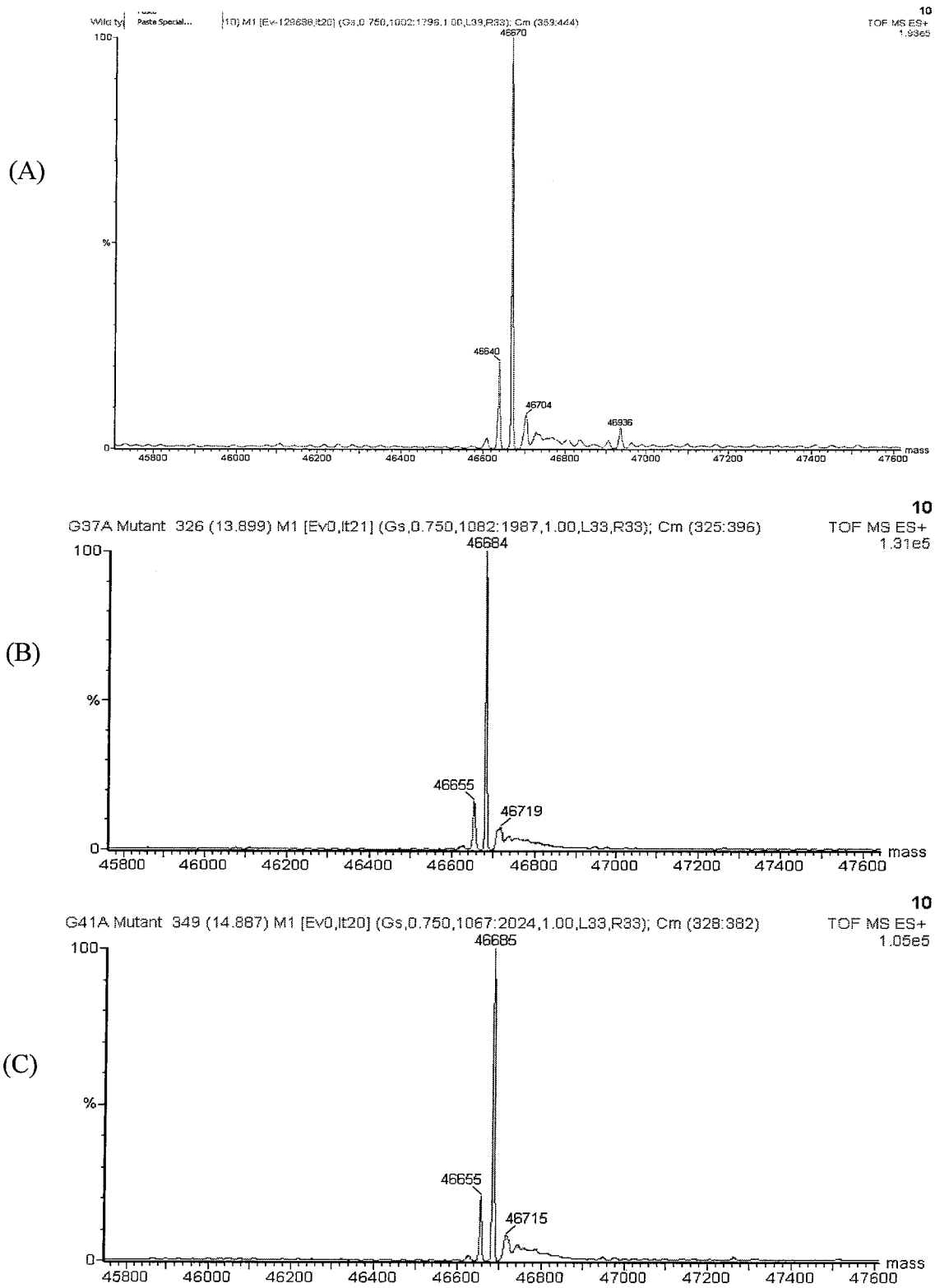

Figure 16: Q-ToF mass spectral determination of the molecular weights of recombinant proteins. (A) WT (B) G37A (C) G41A. For G37A and G41A, samples were coming from the Q-Sepharose pool I.

Yeast enolase	Molecular weight(Da)[a]	Theoretical value(Da)[b]
WT	46670.0	46670.0
G37A	46684.0	46684.0
G41A	46685.0	46684.0

Table 7: Comparison the molecular weight of recombinant WT, G37A and G41A . [a]: determined by Q-ToF Micro mass spectra [b]: determined by amino acid content.

As the molecular weights determined by mass spectra for the wild type and two mutants are in excellent agreement with the theoretical value established by amino acid content (Table 7), it can be concluded that the correct G37A and G41A mutants were successfully obtained through site-directed mutagenesis.

3.1.3.2 Summary for purification of G37A and G41A

Summary for purification G37A and G41A mutants from each step are displayed in Table 8(A) and 8(B), respectively. As can be seen in Table 8, the specific activity for two mutants is not greatly increased during the purification, since in the last step of purification of the two mutants, a significant amount of activity attributed to *E. coli* enolase (Q-pool II) were separated from the mutant activity peak (Q-pool I). This is probably the main reason that no significant increase in mutant specific activity was observed during the purification.

The specific activity of purified wild type yeast enolase is 25.1 Unit/mg. The corresponding of G37A and G41A show 4.3 % and 1.35% of the specific activity of

wild type under the same assay conditions, as indicated in Table 6 and Table 8. From Figure 14, it is clear that the two mutants demonstrate markedly lowered activity relative to wild type, and G41A possesses less activity than G37A. The yields of two mutant proteins are also quite high, which indicated that the expression of the two mutant proteins was normal. Final protein products obtained from purification of G41A and G37A were also in high purity, as shown in Figure 15 and Figure 17, respectively.

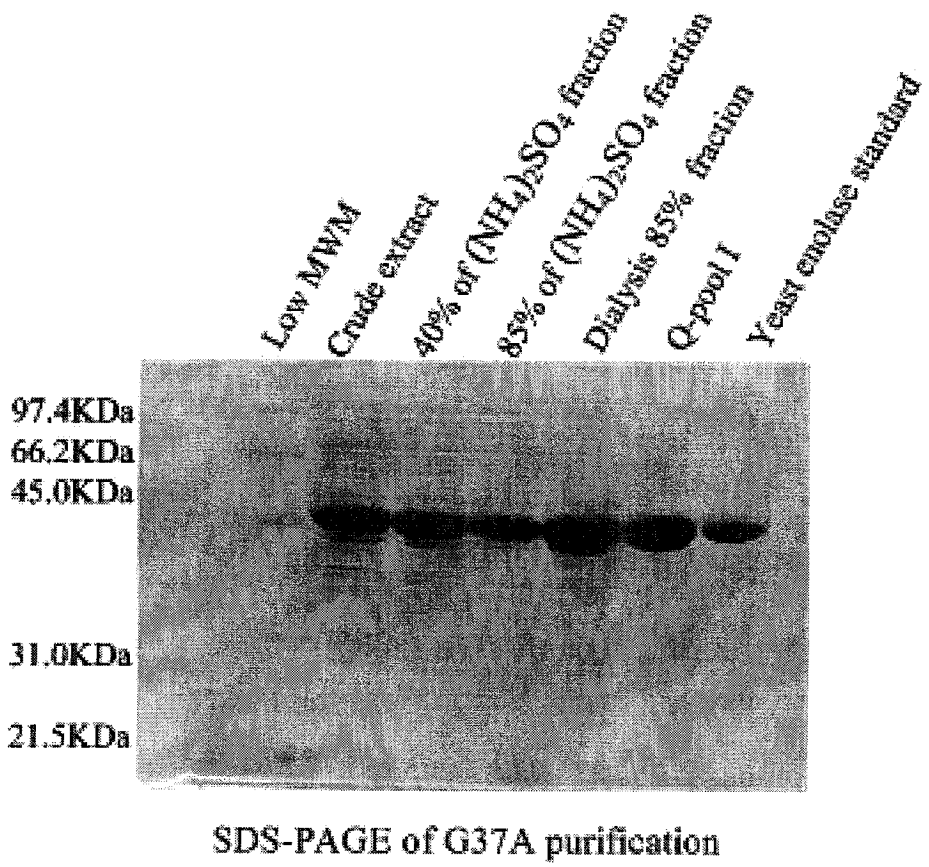

Figure 17: SDS-PAGE demonstration of the results of purification of the G37A mutant. About 20 μg protein from each purification step was loaded to different lanes, while 5 μg yeast enolase standard was loaded in the last lane.

(A)

Purification step	Volume (ml)	Total activity (ΔOD 244/min)	Total Protein (mg)	Specific activity (ΔOD 244/min/mg)	% Recovery activity
Crude extract	40	1619	2531	0.63	100
Supernatant of 0-40% $(NH_4)_2SO_4$Cut	37	1339	1810	0.74	82.7
40-85% $(NH_4)_2SO_4$Cut	17	1275	1924	0.66	78.7
Dialysis	27	1317	2305	0.57	81.3
Q- Pool (I)	55	524	476 352 [a]	1.10	32.3
Q- Pool (II)	52	556	132	4.21	34.3

(B)

Purification Step	Volume (ml)	Total activity (ΔOD 244/min)	Total Protein (mg)	Specific Activity (ΔOD 244/min/mg)	% Recovery Activity
Crude extract	35	783	2363	0.33	100
Supernatant of 0-40% $(NH_4)_2SO_4$Cut	30	611	1473	0.41	78.0
40-85% $(NH_4)_2SO_4$Cut	15	607	1331	0.45	77.5
Dialysis	29	610	1476	0.44	77.9
Q- Pool (I)	58	156	455 324 [a]	0.34	19.9
Q- Pool (II)	101	446	170	2.62	56.9

Table 8: Summary for purification of G37A and G41A mutant yeast enolases. (A) G37A (B) G41A, Specific activity equals total activities divided by total amount of proteins. Activity assays were conducted in enolase assay buffer (pH 7.1) plus 2 mM PEP by monitoring the disappearance of PEP at 244 nm. [a]: Protein concentration was determined by the absorbance at 280 nm; other protein concentrations were determined by the method with Bio-Rad reagent using BSA as the standard (section 2.2.10).

3.2 Dependence of mutant activities on [Mg^{2+}]

We measured the activity as a function of Mg^{2+} for the three enzymes using the buffer B; [Mg^{2+}] ranged from 5 μM to 70 mM for wild type, and from 2 to 100 mM or to 180 mM for G37A and G41A, respectively (Figure 18, details refer to section 3.5.1). The effect of [Mg^{2+}] upon two mutant's activities is in striking contrast to that effect upon the wild type. Significant stimulation rather than inhibition was observed in two mutants at higher [Mg^{2+}] (Figure 18). As this is the case, we compared the maximum specific activity of three enzymes obtained at above assay conditions with that obtained under standard assay conditions, and the results are summarized in Table 9. Under the standard assay conditions ([Mg^{2+}] is 1 mM), the specific activity of wild type is 116 Units/mg; G37A and G41A have 2.43% and 0.71% the specific activity of the wild type, respectively. Thus, compared with the activity obtained under the standard assay conditions, the stimulation range of Mg^{2+} upon two mutants activity is about 7 fold and 13 fold for G37A and G41A, respectively. But under both assay conditions, the wild type maintains the same level of maximum specific activity. Therefore, these comparison results, at least supply us with some information that the mutation at the active site loop has changed the enzyme's kinetic behavior.

Here, it should be pointed out that the enzyme activity was determined using 2-PGA as substrate rather than the PEP, which was previously used to measure the enzyme activity during purification proteins. Thus, for three enzymes, the specific

activity obtained here is certainly different from those obtained before (section 3.1).

Protein	Specific activity [a]		Maximum specific activity [b]	
	Specific activity (ΔOD 240/min/mg)	% of WT	Maximum specific activity (ΔOD 240/min/mg)	% of WT
WT	116	100	109.1	100%
G37A	2.82	2.43	19.3	17.7%
G41A	0.82	0.71	12.2	11.2%

Table 9: Relative activities of two mutants compared with WT. [a]: Activities were measured under standard assay condition (enolase assay buffer plus 0.5 mM 2-PGA) at room temperature. [b]: Maximum specific activity values were obtained in buffer B plus 0.5 mM 2-PGA, varying Mg^{2+} from 5 μM to 70 mM for WT and from 2-100 mM or 180 mM for mutants (details refer to kinetic studies on binding Mg^{2+}); in order to get the maximum specific activity, data were fit to modified substrate inhibition equation and Michaelis-Menten equation using ENZFITTER (Biosoft, 2004) for WT and mutants, respectively. The specific activity was determined by the changes at absorbance at 240 nm/min divided by the amount of enzyme used.

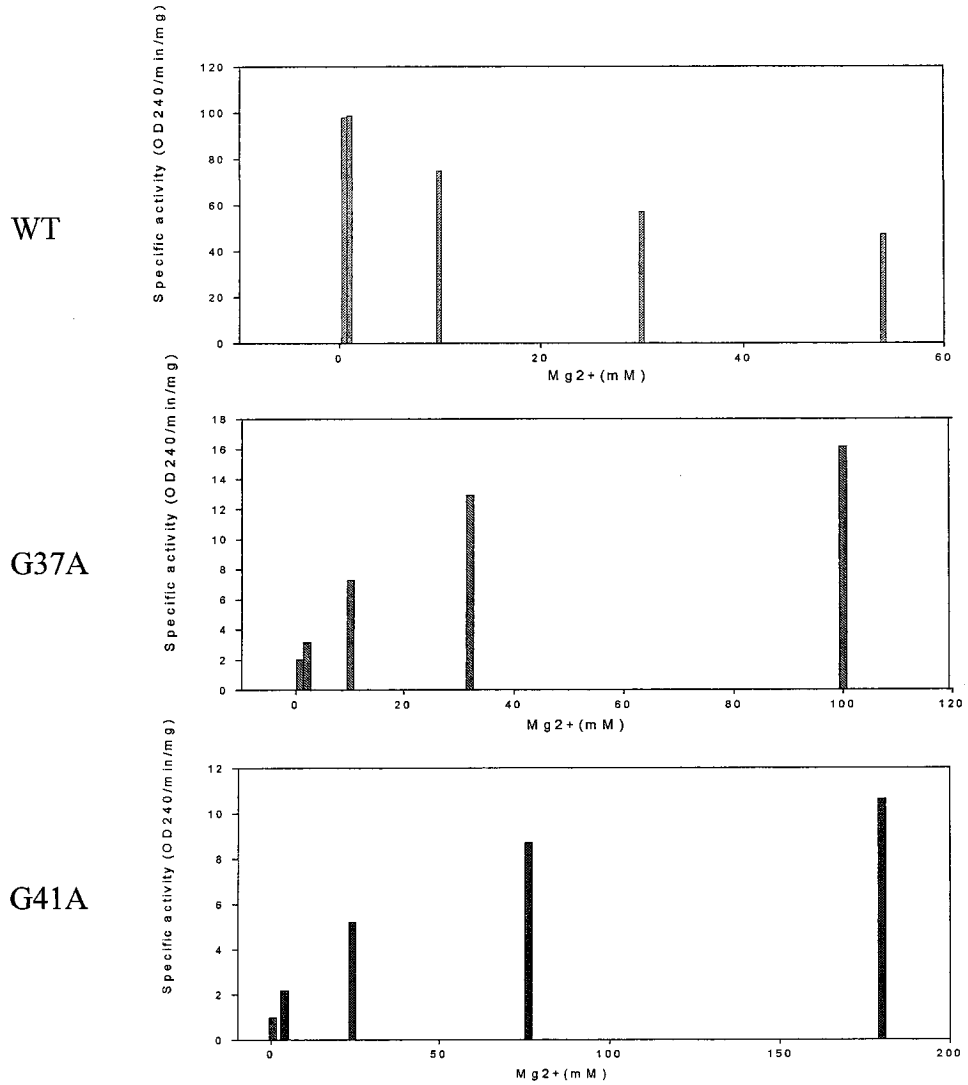

Figure 18: Comparison of the [Mg^{2+}] effect on the activities of WT, G37A and G41A. Specific activity was obtained in buffer B plus 0.5 mM 2-PGA by varying Mg^{2+}, and assays were performed at 25 °C in duplicate and the average result was shown in graph.

3.3 Structural studies of wild type and two mutants

3.3.1 Secondary structure characterization

In order to examine whether the mutations have disrupted the overall secondary structure of the protein, far UV-CD spectroscopy was performed for wild type and two mutants. Absorption in this region reflects the protein peptide backbone environment.

These far UV-CD spectra of wild type and two mutants all demonstrate the characteristic double minima at 208 nm and 222 nm, which is the typical characteristic of protein with high α-helix contents (see Figure 19). This result agrees with the reports that yeast enolase has about 37.3% α-helix contents from the known X-ray crystallographic analysis (Stec and Lebioda, 1990).

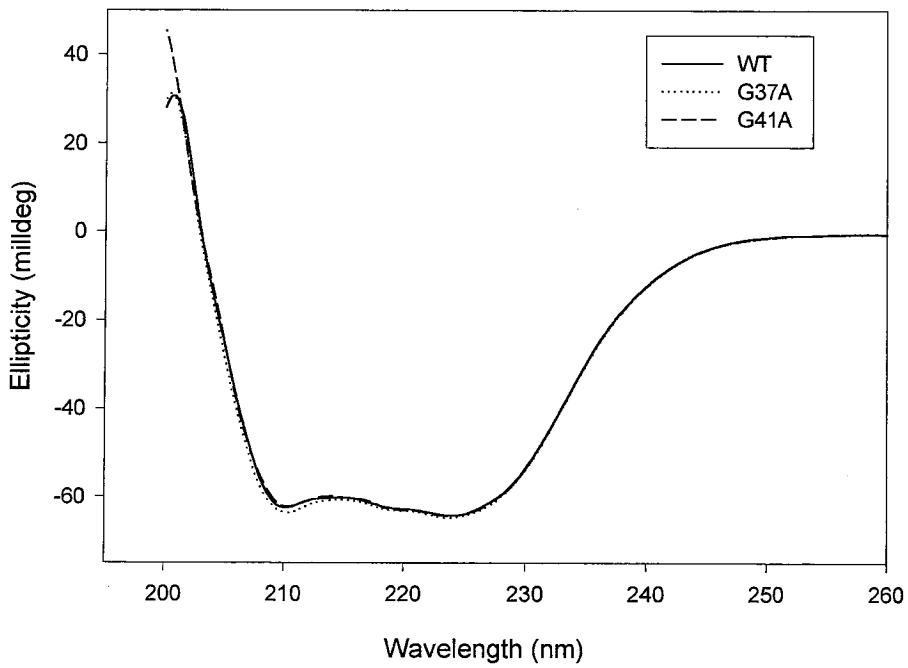

Figure 19: Far UV-CD spectra of WT, G37A and G41A yeast enolases. Protein concentration was 0.5 mg/ml (5.3 uM) in buffer A. Each scan was recorded in 1mm rectangular cell, 5 accumulations were averaged. The spectrum of the buffer was subtracted from all the protein spectra.

The far UV-CD spectra of G37A and G41A are almost superimposed on that of the wild type (Figure 19), indicating that the mutated site at the active site loop did not cause an overall secondary structure change in protein.

3.3.2 Tertiary structure characterization: 4th derivative UV and near UV-CD spectra

UV absorbance spectra for the wild type and two mutants were recorded and were converted to 4th derivative UV spectra (Lange, 1996). Since a 4th derivative UV spectrum can provide information about the local environment around aromatic residues (Lange, 1996; Kornblatt *et al.*, 1998), it should be a good probe to detect tertiary structure changes in a protein. 4th derivative UV spectra for two mutants were compared with that of the wild type, as shown in Figure 20. It appears that the 4th derivative UV spectra for two mutants are indistinguishable with that of wild type, indicating the environment around aromatic residues in protein has not undergone major alteration. In addition to 4th derivative UV spectrum, the near UV-CD spectrum is another good probe to assess the tertiary structure changes of the protein. Absorption in the near UV-CD region (250-350 nm) is principally attributed to the aromatic residues: tryptophan, tyrosine and phenylalanine. Near UV-CD spectra for two mutants were compared with that of wild type, as shown in Figure 21. These characteristic absorption bands in G41A do not produce visible alteration both in intensity and in peak positions. However, a slight overall increase in CD signal intensity is observed in the spectrum of G37A, but no peak shift is detected.

Through comparing the 4th derivative UV and near UV-CD spectra of three proteins, it could be concluded that the overall tertiary structure in G41A has no

significant alteration as a result of Gly mutation to Ala. However, with respect to G37A, though 4th derivative UV spectrum could also be superimposed on the spectrum of wild type, the near UV-CD spectra showed slightly increased intensity in aromatic region. Does it indicate there is a little dissociation in G37A, or only small conformational variation induced by mutation? Since it has been reported that dissociated native yeast enolase demonstrates a more positive CD spectrum in aromatic region (Kornblatt *et al.*, 1998), we were unable to give an unambiguous interpretation to the difference observed in the near UV-CD spectrum. Hence, the subsequent sedimentation velocity analytical ultracentrifugation (AUC) experiments seem to be necessary, such that this question could be further addressed. Moreover, in order to make sure that the present spectra experiments are comparable with the subsequent AUC experiments, the three proteins incubated in buffer A containing 0.3 M NaOAc were also scanned in the same manner as described in section 2.2.17. The experiment result (data not shown) proves that the presence of NaOAc doesn't have any observable effect on the near UV-CD spectra shown in Figure 21, though acetate salt has been reported to have a stabilizing effect on the enolase dimer (Brewer, 1969).

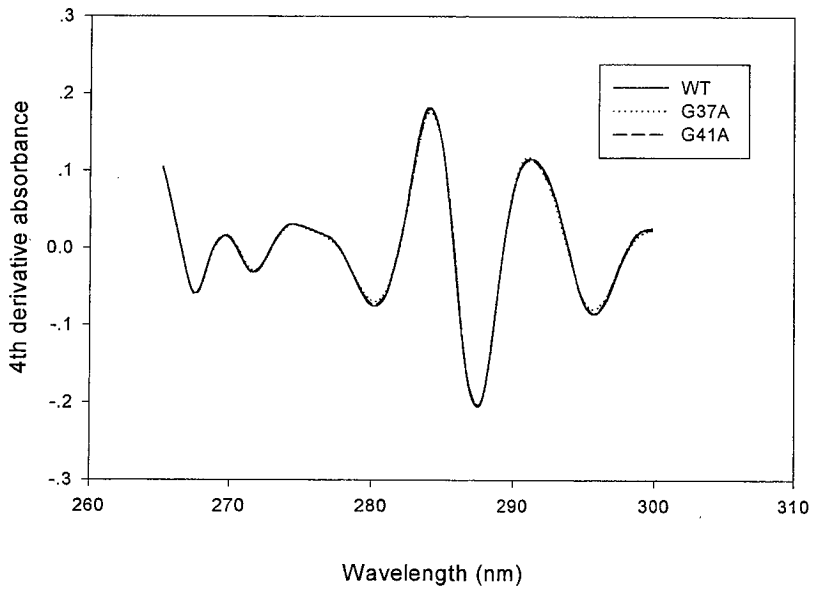

Figure 20: 4th derivative UV spectra of WT, G37A and G41A yeast enolases. Protein concentration was 1 mg/ml 10.6 uM) in buffer A. Each scan was recorded in 10 mm rectangular cell, 1 accumulation. The spectrum of the buffer was subtracted from all the protein spectra.

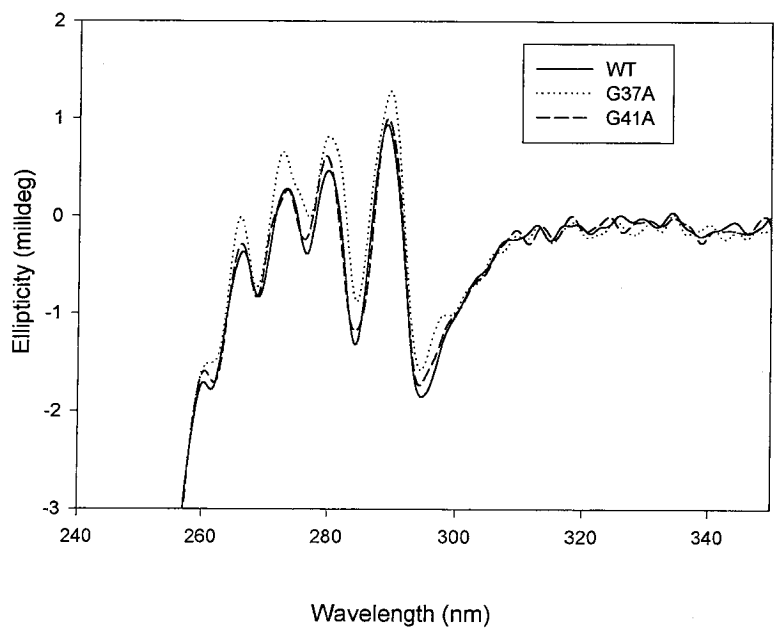

Figure 21: Near UV-CD spectra of WT, G37A and G41A yeast enolases. Protein concentration was 1 mg/ml (10.6 uM) in buffer A. Each scan was recorded in 10 mm rectangular cell, 5 accumulations were averaged. The spectrum of the buffer was subtracted from all the protein spectra.

3.3.3 Sedimentation velocity analytical ultracentrifugation determination of the quaternary structures of two mutants

Sedimentation velocity studies for wild type and the two mutants were performed at two different protein concentrations. All three samples with equal molar concentrations (1.06 μM or 10.6 μM) were prepared in buffer A containing 0.3 M NaOAc, and centrifuged under the same conditions as described in section 2.2.21. The addition of salt is required, so that the primary charge effects, which can slow down the sedimentation of a protein, can be precluded (Ralston.G, 1993). Figure 22 showed the moving boundary for each protein recorded at one specific time during running the three samples at 1.06 μM. Generally, the position of each boundary indicates how far down each protein in the respective cell has sedimentated (Ralston.G, 1993). If dissociation occurred in two mutants, the sedimenting boundary in the same scan should be sedimented more slowly than that of the wild type. The experimental results indicate that three proteins all sedimentate mainly as one single boundary, and the sedimenting boundary for two mutants is nearly overlaid on the wild type (Figure 22). AUC data was analyzed and fit to one species model using the dc/dt^{+} software (version 1.14). Values for sedimentation coefficient were corrected to $S_{20,w}$ due to the effects of solvent density and viscosity, and summarized in Table 10. As can be seen in Table 10, when protein concentration is 1.06 μM or 10.6 μM, two mutants demonstrate an almost identical $S_{20,w}$ to the wild type. As the two mutants do not display notable decreases in $S_{20,w}$, this provides definitive

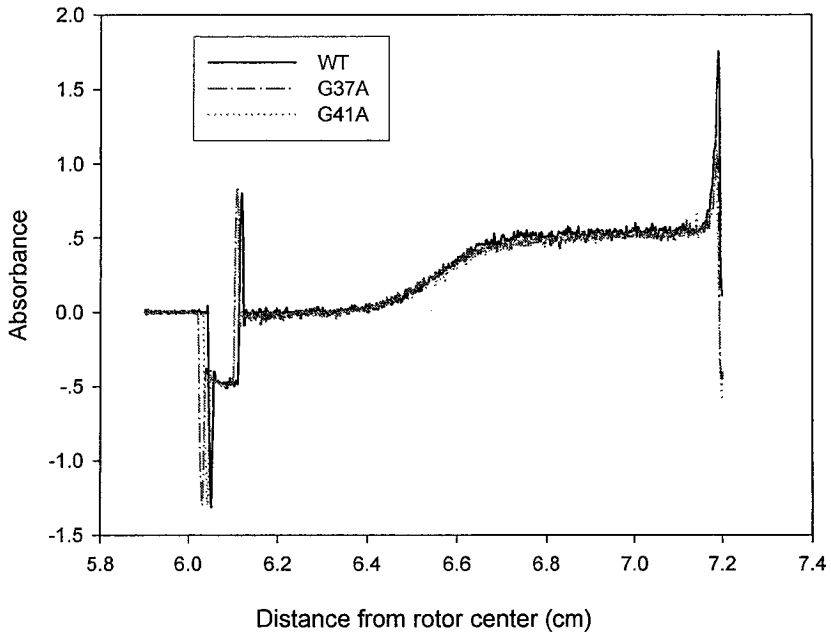

Figure 22: Sedimentation velocity studies of WT and two mutants. Data were analyzed with the dc/dt$^+$ software (version 1.14). Protein concentrations were 1.06 uM prepared in buffer A plus 0.3 M NaOAc. Graph shows the scan# 30 in the same time of running AUC.

[Protein] uM	Yeast enolase	$S_{20,w\,(S)}$
10.6	WT	5.505±0.003
	G41A	5.455±0.005
	G37A	5.447±0.005
1.06	WT	5.493±0.011
	G41A	5.459±0.011
	G37A	5.337±0.010

Table 10: Summary for the sedimentation coefficients of WT and two mutants. Data were analyzed with the dc/dt$^+$ software (version 1.14). Protein was prepared in buffer A plus 0.3 M NaOAc. Absorbance scans for [protein] at 1.06 uM and 10.6 uM were monitored at 230 nm and 280 nm, respectively.

evidence that two mutants are not appreciably dissociated. The slightly increased CD signal in the aromatic region in G37A, previously detected through near UV-CD spectra,

is therefore ascribed to conformational variation caused by mutation.

3.3.4 Temperature denaturation

Temperature induced denaturation of wild type and two mutants were performed by monitoring the peptide bond signal at 222 nm as a function of temperature. Thus, the thermal denaturation curves of the three proteins in buffer A are presented in Figure 23. It is evident that only two states, native dimer and denatured protein, exist and no intermediate occurs during the course of denaturation. This is consistent with the results from thermal denaturation of native yeast enolase followed by differential scanning calorimetric (DSC) (Brewer and Wampler, 2001). Loss of secondary structure is observed above 47 °C and 50 °C for two mutants and wild type, respectively. The melting temperature (T_m), at which half of the protein is denatured, was calculated for each protein from the denaturation curve. The T_m for wild type is 55.9 °C, which is comparable to the value of 58 °C reported for thermal denaturation of yeast enolase monitored by Fourier transform infrared spectroscopy (FT-IR)(Huang, 2003). T_m for G37A and G41A are 52.8 °C and 53.6 °C respectively. Therefore, it is apparent that the two mutants are denatured at lower temperature than wild type, which is a sign of that the two mutants are less stable than the wild type.

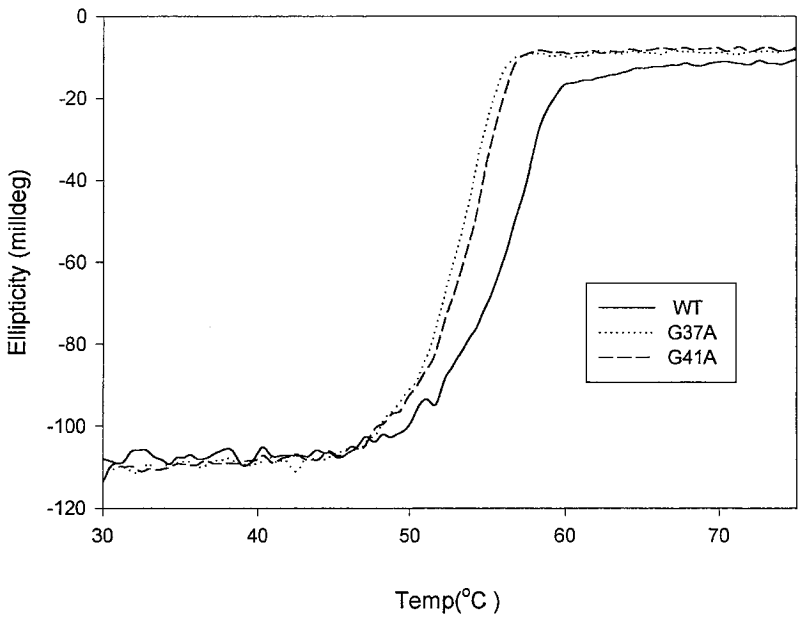

Figure 23: Temperature denaturation of WT and two mutants. Protein concentration was 1mg/ml (10.6 uM) in buffer A heated from 30 to 75 °C, scan rate was 15 °C /hour.

3.4 Dissociation of yeast enolase with $NaClO_4$

$NaClO_4$ is a chaotropic salt, which has been widely employed to study mammalian enolase dissociation (Trepanier *et al.*, 1990; Kornblatt *et al.*, 1996; Kornblatt *et al.*, 2002). The monomers yielded using this method possess native secondary structure, but the immediate environment around aromatic residues is changed and the monomers lose enzyme activity (Kornblatt *et al.*, 1996). Recently, unpublished data from Dr. Kornblatt's lab (personal communication) has confirmed that $NaClO_4$ was able to dissociate yeast enolase and the dissociation effect could be followed by the decrease in enzyme activity, 4^{th} derivative UV and near UV-CD spectra. Therefore, in the present study, dissociation of wild type and two mutant yeast enolases were performed using

$NaClO_4$, and monitored by above three probes. The effects of $NaClO_4$ on activity and spectra were the same for all 3 proteins.

In order to determine the proper range of [$NaClO_4$] used and the incubation time required for equilibrium to be reached, preliminary experiments for dissociation of wild type and two mutants were carried out. It was found that incubation of samples for at least 5 hours was necessary to ensure that all samples have reached equilibrium; near UV-CD spectra at 5 hr and at 16 hr were the same within experimental error (data not shown). Thus, all protein samples were normally incubated at 15 °C overnight in experiments. Moreover, all samples were maintained at the same [Na^+] and ionic strength as described in section 2.2.15, because Na^+ inhibits enolase activity, and ionic strength has an effect on enolase dimerization (Kuhnel and Luisi, 2001). Additionally, all samples were incubated at low [$NaClO_4$], since it has been reported that an equilibrium mixture of monomers and dimers could be formed without loss of any secondary structure under low [$NaClO_4$] (Kornblatt *et al.*, 1996).

3.4.1 Different probes used to monitor $NaClO_4$ dissociation of yeast enolase

3.4.1.1 Dissociation monitored by enzyme activity

For wild type, the enzyme activity was assayed under the standard assay conditions (enolase assay buffer plus 0.5 mM 2-PGA) by following of the production of PEP at 240 nm. For G37A and G41A, assays were performed in the same assay buffer, but containing some excess Mg^{2+} (50 mM and 100 mM Mg^{2+} for assaying G37A and

G41A, respectively). Measurement of the fraction of dimeric enolase using activity is based on the assumption that the monomeric enolase has no activity, since it has been reported that $NaClO_4$ produces inactive monomer (Kornblatt *et al.*, 1996; Kornblatt *et al.*, 2002). Protein incubated in 0 M $NaClO_4$ is considered as having 100% activity and 100% dimer. Fraction activity equals the enzyme activity after incubation in $NaClO_4$ divided by the enzyme activity after incubation in 0 M $NaClO_4$. Fraction of dimeric enolase at different of [$NaClO_4$] equals fraction activity. A typical wild type dissociation curve monitored by fraction activity is illustrated in Figure 24. It is clear that increasing $NaClO_4$ concentration results in the progressive loss of enzyme activity. But, it should also be noted that due to the relatively quick reactivation of enzyme activity under the assay conditions, especially at the higher [$NaClO_4$], it is almost impossible to observe zero activity.

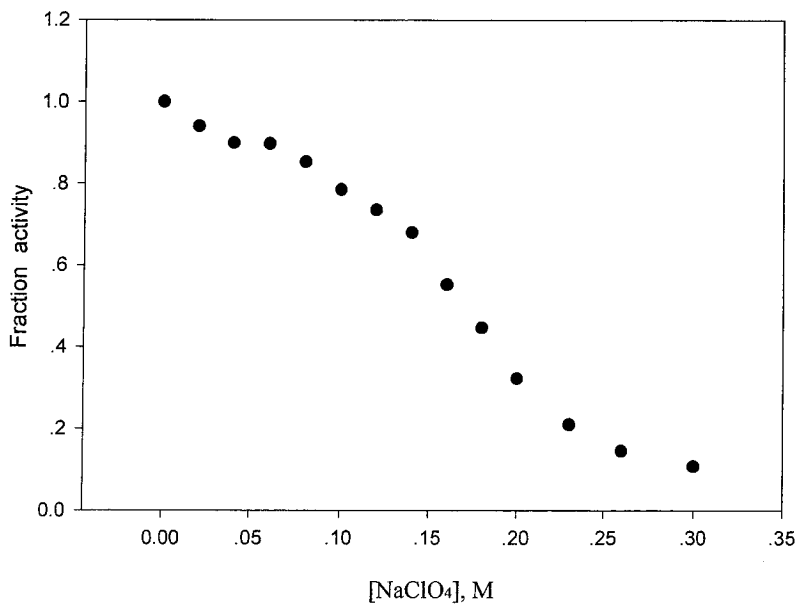

Figure 24: Effect of $NaClO_4$ on the WT dissociation monitored by fractional activity. Protein concentration was 0.1 mg/ml prepared in buffer A with varying concentration of $NaClO_4$ and NaOAc. Enzyme activity was measured in enolase assay buffer by following the production of PEP at 240 nm at room temperature.

3.4.1.2 Dissociation monitored by 4th derivative UV spectrum

After finishing $NaClO_4$ incubation, zero-order UV absorption spectra were recorded and converted to 4th derivative UV spectra (Lange, 1996). Zero-order UV spectra and 4th derivative UV spectra of wild type enolase at 0 M, 0.2 M and 0.3 M $NaClO_4$ are shown in Figure 25. The small absorbance variation occurring in the UV spectra was amplified by transforming to 4th derivative UV spectra. In the experiments, the spectra changes were analyzed using the following parameters and equation:

$$R = \Delta 1/\Delta 2$$

* $\Delta 1$= (maximum value of the 4th derivative at 284 nm) - (minimum value of the 4th derivative at 280 nm)
* $\Delta 2$= (maximum value of the 4th derivative at 291 nm) - (minimum value of the 4th derivative at 287 nm).

$NaClO_4$ dissociation yeast enolase leads to a decrease in $\Delta 1$, and at same time an increase in $\Delta 2$. As a whole, dissociation of enolase results in a decrease in R. The 4th derivative UV spectra changes as a function of [$NaClO_4$] (Figure 25), indicating that dissociation of yeast enolase is accompanied by changes in the environment of some aromatic residues. Therefore, the 4th derivative UV spectra were utilized to monitor yeast enolase dissociation.

In order to determine the fraction of dimer or monomer of enolase when incubated at different concentration of $NaClO_4$, the 4th derivative UV spectrum needs to be simulated. The spectrum of enolase at 0 M $NaClO_4$ is considered as 100% dimeric enolase, while the average spectrum of wild type incubated at 0.30 M, 0.32 M and 0.34

M $NaClO_4$ (average spectrum of mutant enolase incubated at 0.24 M and 0.27 M $NaClO_4$) is used as 100% monomeric enolase. The fully dimeric and monomeric enolase spectra from experiment data were combined at different proportion, and the parameter R was calculated for each of the theoretical spectra (Kornblatt *et al.*, 1996). Thus, a standard curve of R versus fraction of monomer was established in order to determine the fraction of monomeric enolase for the experimental data. Figure 25(B) illustrates that wild type incubation in $NaClO_4$ resulted in decrease in R as the [$NaClO_4$] is increased.

(A)

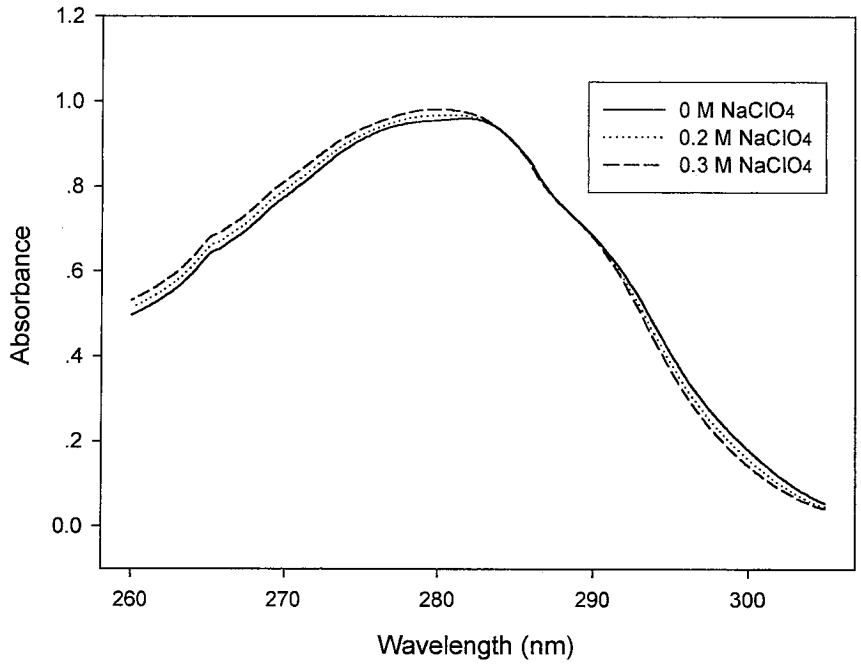

(B)

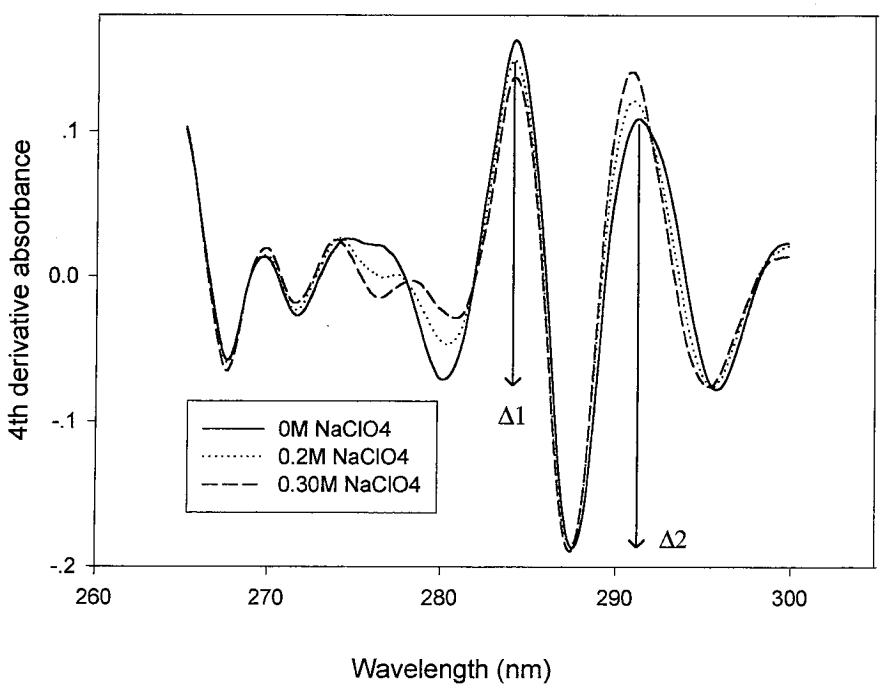

Figure 25: Comparison of the UV and 4th derivative UV spectra of WT yeast enolase at 0, 0.2 M and 0.3 M $NaClO_4$. (A) Zero order of UV absorbance spectra (B) 4th derivative UV spectra of shown in (A). Protein concentration was 1 mg/ml in buffer A with varying concentration of $NaClO_4$ and NaOAc.

3.4.1.3 Dissociation monitored by near UV-CD spectra

Generally, the near UV-CD spectrum provides information about the protein tertiary structure due to aromatic residue absorption in the near UV region. Since it has been reported that about half of the tyrosine and tryptophan residues are located on the loops (Kornblatt *et al.*, 1996), and one Trp 56 (Stec and Lebioda, 1990) and three Tyr residues are near the dimer interface in yeast enolase (Kornblatt *et al.*, 1995), dissociation of enolase may be accompanied by changed environments around these aromatic residues. Thus, the near UV-CD spectrum should be a good probe to detect enolase dissociation. This is further confirmed by the near UV-CD spectral changes of wild type yeast enolase upon dissociation, as demonstrated in Figure 26(A). It is obvious that dissociation of yeast enolase results in a noticeable increased intensity in the near UV-CD spectrum, a more positive spectrum in aromatic region, which is also fairly consistent with previously reported spectral changes (Kornblatt *et al.*, 1998).

By subtracting the near UV-CD spectrum of protein incubated at 0 M $NaClO_4$ (100% dimer) from these of protein incubated at different [$NaClO_4$], the corresponding induced spectra changes are shown in Figure 26(B). It is clear that there are three major peaks around 277 nm, 284 nm and 293 nm in the difference spectra with obvious changes as a function of [$NaClO_4$]. Although using these three peaks as probes to detect dissociation produces similar results (data not shown), the major peak at 284 nm in difference spectra was normally chosen as probe to calculate the fraction of monomeric

(A)

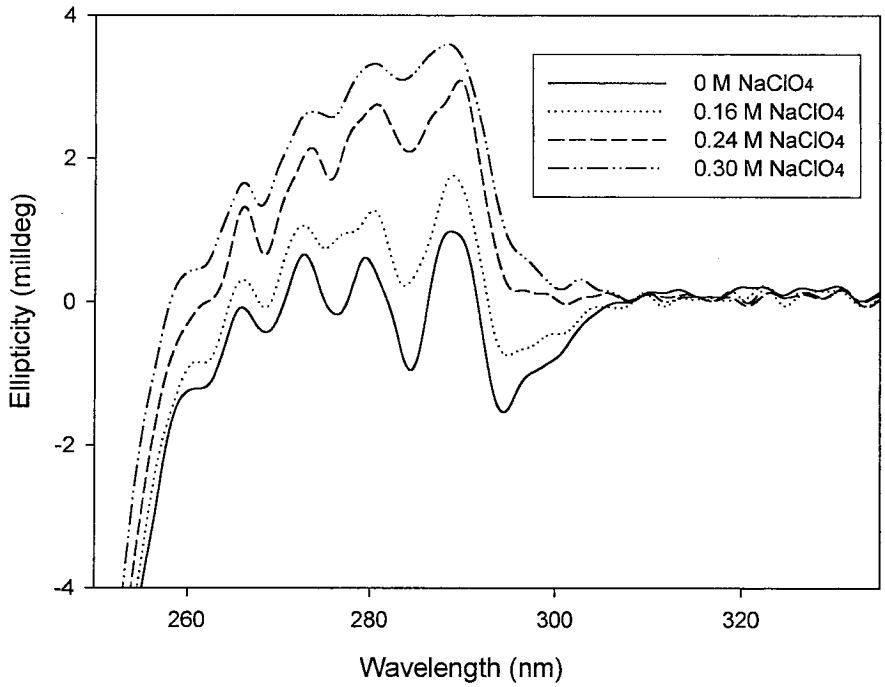

(B)

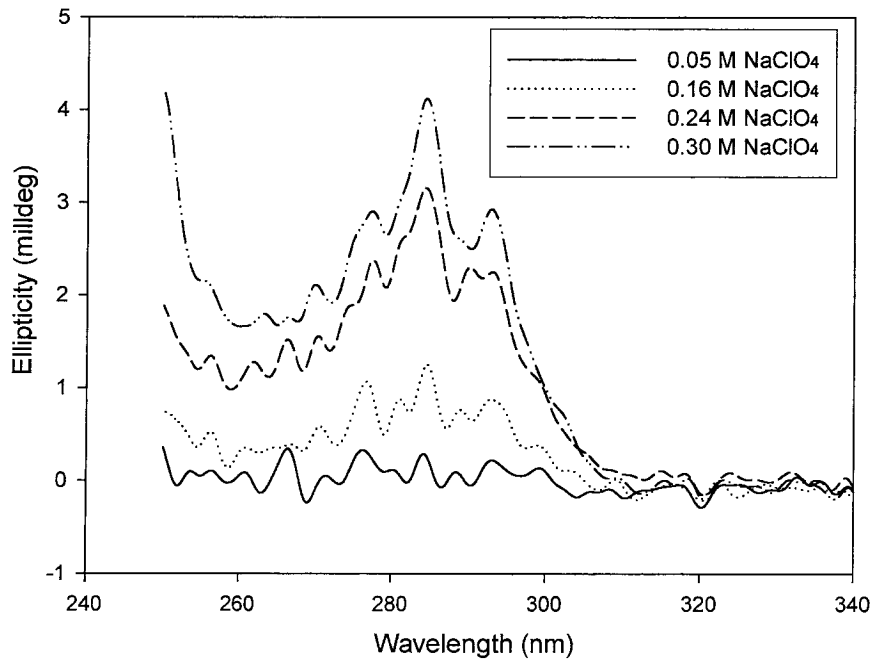

Figure 26: (A) Near UV-CD spectra changes of WT enolase as a function of [$NaClO_4$] (B) Subtracting near UV-CD spectra of WT in 0 M $NaClO_4$ from these of WT in varying [$NaClO_4$]. Protein concentration was 1 mg/ml in buffer A with varying concentration of $NaClO_4$ and NaOAc.

enolase in experiments. Thus, the fractions of monomer were calculated by comparing the CD signal intensity at 284nm of protein samples incubated at different [$NaClO_4$] with that of protein sample incubated at the highest [$NaClO_4$].

3.4.2 Dissociation of WT and two mutant yeast enolases with $NaClO_4$

3.4.2.1 Dissociation curves of WT and calculation the dissociation constant

Effects of varying concentrations of $NaClO_4$ on the enzyme activity, 4^{th} derivative UV and near UV-CD spectra are shown in Figure 24, Figure 25 and Figure 26. As can be seen in these figures, increasing [$NaClO_4$] results in the progressive decrease in R, increase in CD signal at 284 nm and loss of enzyme activity. Thus, these probes were utilized to monitor $NaClO_4$ dissociation effect on yeast enolase in the following studies.

At each $NaClO_4$ concentration, the fraction of dimeric enolase, as monitored by different probes, was calculated as described in section 3.4.1. Dissociation curves monitored by enzyme activity and by spectral changes for the wild type yeast enolase are illustrated in Figure 24 and Figure 27(A), respectively. From the fraction of dimeric and monomeric enolase at each [$NaClO_4$], dissociation constants (K_d) were calculated according to the description in section 2.2.19. A linear relationship was obtained between K_d and [$NaClO_4$], as monitored by different probes, see Figure 27(B). By extrapolation of these lines to 0 M $NaClO_4$, the K_d for the wild type yeast enolase was established to be within the range of 13.8-52 nM from different probes, which is fairly consistent with the

(A)

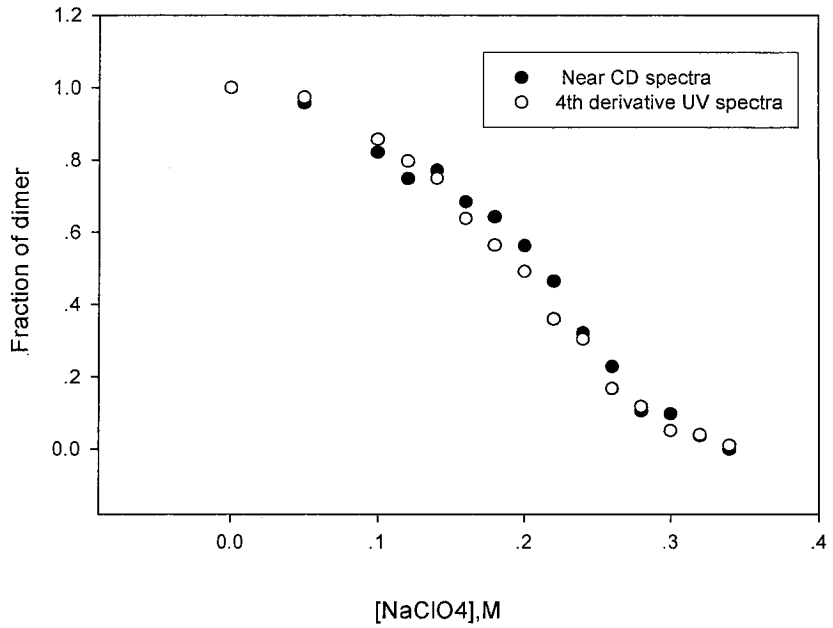

(B)

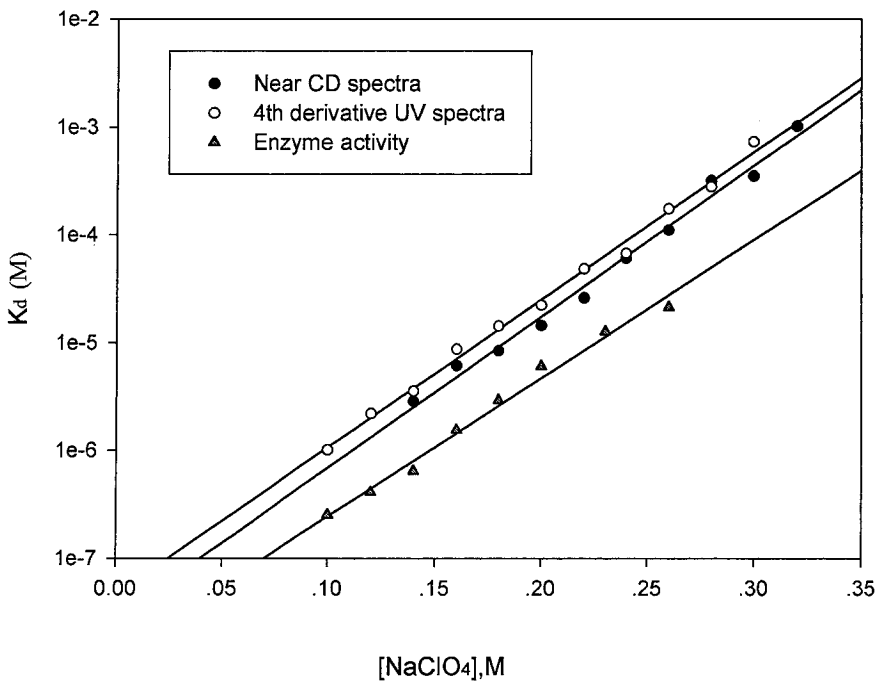

Figure 27: (A) Comparison 4th derivative UV and near UV-CD spectra as probes to detect WT enolase dissociation as a function of [$NaClO_4$] (B) Determining the K_d of WT enolase monitored by different probes. Protein concentration was 1 mg/ml in buffer A with varying concentrations of $NaClO_4$ and NaOAc.

value of 15 nM previously reported for the native yeast enolase (Kornblatt *et al.*, 1995). Based on the relationship of between K_d and ΔG, the conformation stability (ΔG_0) was

also established. The slope of the graph of ΔG versus the concentration of $NaClO_4$, m, is about 71-75 $kJ.mol^{-1}.M^{-1}$ for the wild type obtained by different probes. All the thermodynamic constants established for the wild type are summarized in Table 12. It is obvious that the results obtained from three probes are in good agreement.

3.4.2.2 $NaClO_4$ dissociation of wild type yeast enolase directly confirmed by AUC

The effect of $NaClO_4$ upon enolase has been confirmed by above three probes, as $NaClO_4$ causes spectral changes in 4^{th} derivative UV and near UV-CD spectra, as well as loss enzyme activity. All these changes detected in present study are consistent with Kornblatt's unpublished data about dissociation of yeast enolase with $NaClO_4$. However, these probes could not by themselves, supply us with direct and definitive evidence that these variations in spectra and loss of enzyme activity are owing to dissociation. Therefore, AUC was employed to monitor the sedimentation behavior of wild type incubated at several concentrations of $NaClO_4$, because AUC is a good probe to detect dissociation of enolase and quaternary structure changes in the protein. All experimental data were analyzed using dc/dt^+ software (version 1.14) as described in section 3.3.3. A fully dimeric wild type yeast enolase has a $S_{20,w}$ of 5.482 ±0.03, which was established by performing a concentration dependence study of $S_{20,w}$ in the range of 0.1-2.5 mg/ml (data not shown). A completely dissociated native yeast enolase (monomeric enolase) was earlier determined to have a $S_{20,w}$ of 3.38 ±0.04 by Dr. Kornblatt (personal communication). The fraction of monomer at different of [$NaClO_4$] was calculated

according to the following equation (Padovani, 2003), and are summarized in Table 11.

$$f_{monomeric} = [(S_{20,w(dimeric)} - S_{20,w(sample)})] / [(S_{20,w(dimeric)} - S_{20,w(monomeric)})]$$

As can be seen in Table 11, the $NaClO_4$ dissociation effect on the wild type is directly substantiated by the decrease in $S_{20,w}$; there is a good correlation between the dissociation determined by AUC with that determined by activity and CD spectral changes.

[Protein] uM	[$NaClO_4$] (M)	$S_{20,w}$ (S)	*fm* determined by AUC	*fm* determined by [a]	
				CD spectra	Activity
10.6	0.18	4.863	29.5%	35.7%	-
	0.22	4.430	50.5%	53.5%	-
	0.26	4.026	69.2%	77.2%	-
1.06	0.14	4.756	34.5%	-	32.1%
	0.18	4.207	60.6%	-	55.3%
	0.22	3.837	78.3%	-	79.0%

Table 11: Dissociation of WT yeast enolase with $NaClO_4$ directly confirmed by AUC. Data were analyzed with the dc/dt$^+$ software (version 1.14). [a]: These values were from the discrete points in corresponding dissociation curves. Protein was prepared in buffer A plus different [$NaClO_4$], incubated at 15 °C for overnight. With respect to the AUC data, absorbance scans for [protein] at 1.06 uM and 10.6 uM were monitored at 230 nm and 280 nm, respectively

3.4.2.3 Dissociation curves of G37A and G41A and calculation the dissociation constant

G37A and G41A mutants were incubated in buffer A containing varying $NaClO_4$ and NaOAc, as described in section 2.2.15. The dissociation curves for G37A and G41A monitored by 4^{th} derivative UV and near UV-CD spectra are illustrated in Figure 28(A) and Figure 29(A), respectively. It is apparent that the two mutants are more readily dissociated than wild type, since the two mutants require about 0.2 M $NaClO_4$ to be completely dissociated, whereas 0.3 M $NaClO_4$ is needed to fully dissociate the wild type, when all proteins concentration are 1 mg/ml (10.6 μM). The dissociation constant was also calculated for each mutant using the same method as for determining the dissociation constant for the wild type. K_d values as a function of [$NaClO_4$] are shown in Figure 28(B) and Figure 29(B) for G37A and G41A, respectively. In order to determine whether the dissociation of the two mutants within the range of [$NaClO_4$] used includes loss of some secondary structure, peptide bond CD spectra of each mutant incubated at the highest [$NaClO_4$] and without $NaClO_4$ were performed. No loss of secondary structure was observed (data not shown).

(A)

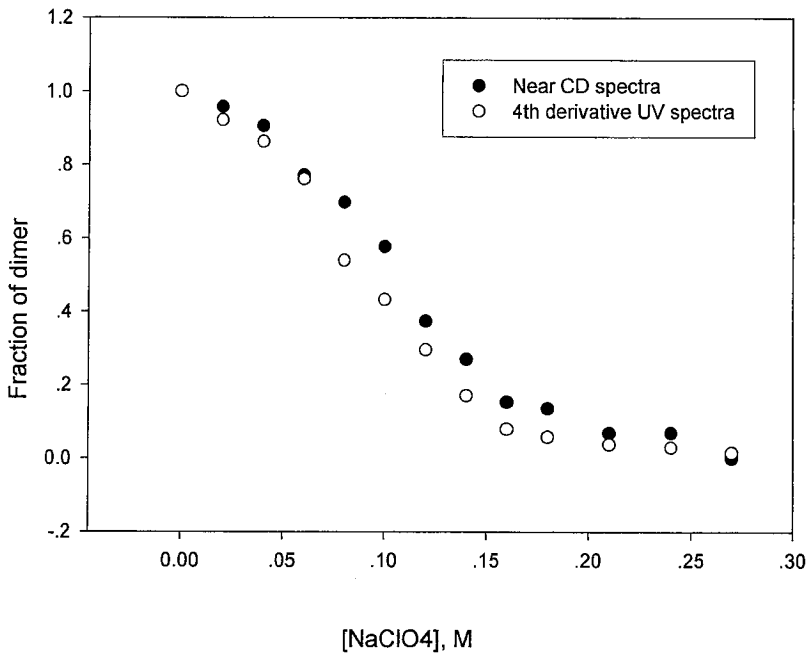

(B)

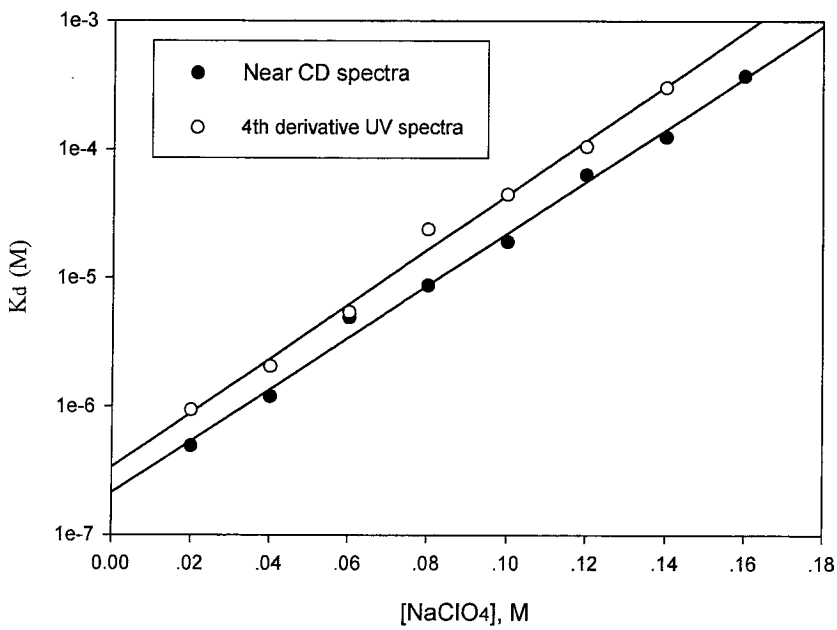

Figure 28: (A) Comparison of 4th derivative UV and near UV-CD spectra as probes to detect G37A mutant dissociation as a function of [$NaClO_4$] (B) Determining the K_d of G37A mutant monitored by 4th derivative UV and near UV-CD spectra. Protein concentration was 1 mg/ml prepared in buffer A with varying concentration of $NaClO_4$ and NaOAc.

(A)

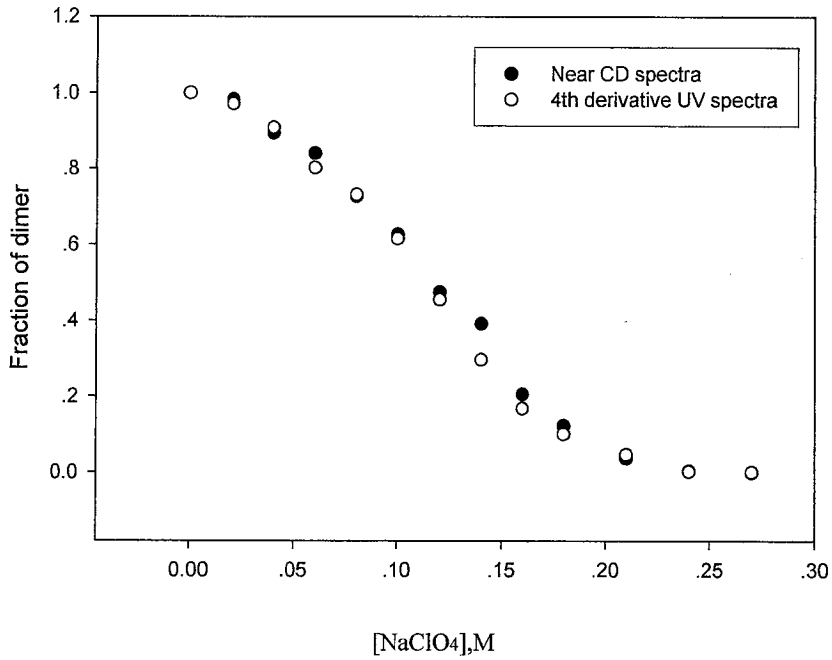

(B)

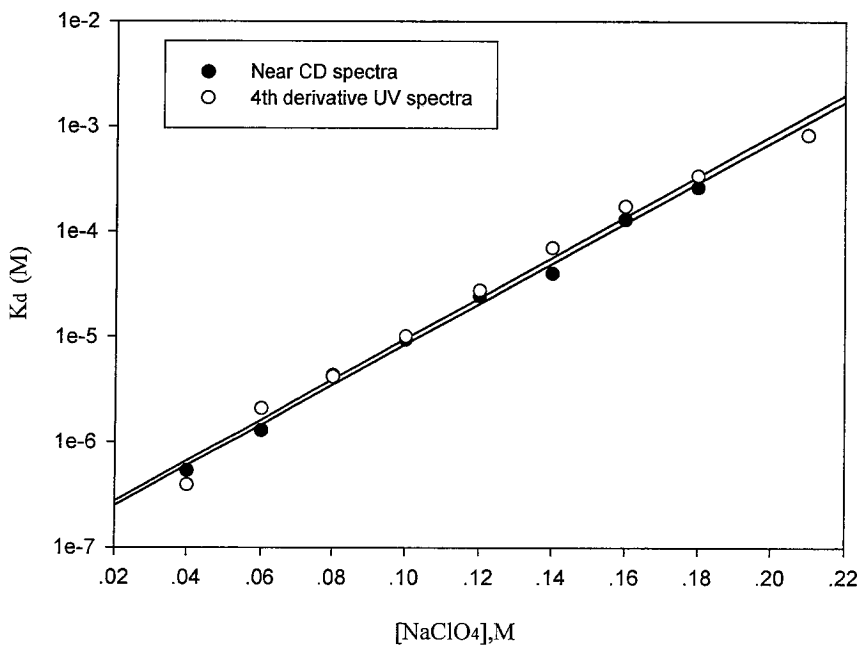

Figure 29: (A) Comparison of the 4th derivative UV and near UV-CD spectra as probes to detect G41A mutant dissociation as a function of [$NaClO_4$] (B) Determining the K_d of G41A mutant monitored by 4th derivative UV and near UV-CD spectra. Protein concentration was 1 mg/ml prepared in buffer A with varying concentration of $NaClO_4$ and NaOAc.

Unlike the conditions used to detect the dissociation of the two mutants monitored by spectral probes, there were differences when monitoring dissociation by enzyme activity. (1) Based on kinetic studies (see section 3.5.1), the concentration of Mg^{2+} used in the assaying system was 50 mM for G37A and 100 mM for G41A. It should be noted that the addition of excess Mg^{2+} may shift the equilibrium in favor of the dimeric state, since there have been reports that divalent cations had a stabilization effect on the enolase dimerization (Kornblatt *et al.*, 1998; Brewer and Weber., 1968; Kornblatt *et al.*, 2004). (2) Protein concentrations used in the final incubations were also varied for three enzymes: 0.1 mg/ml for wild type and G37A, 0.5 mg/ml for G41A. (3) The amount of each enzyme used in the assay was different. These varying factors would make the enzyme activity assay, as a probe, lacking uniformity to detect the dissociation of three enzymes. Thus, compared with the spectra probes, activity is not a good probe to compare the three enzyme's dissociation.

Even though presence of the above varying factors that will probably affect the experiment results, the fraction of dimeric enolase and K_d monitored by enzyme activity were determined for each mutant using the same method as described in section 3.4.1.1. The dissociation curves monitored by activity were compared with that of the wild type, as indicated in Figure 30. It is apparent that the dissociation curves of the two mutants are sharper than the wild type, especially when G37A is at the same protein concentration as the wild type.

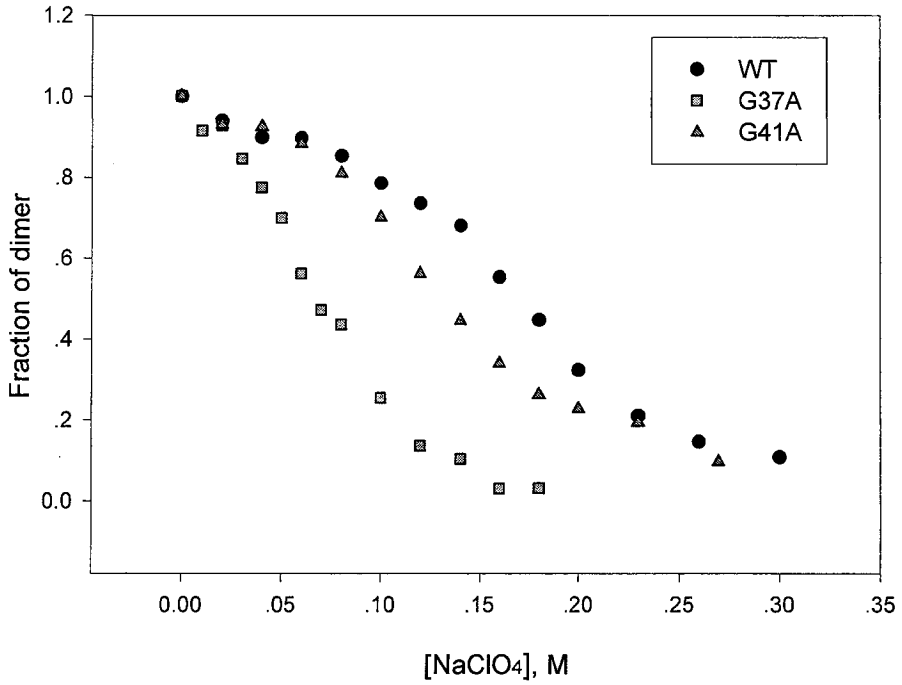

Figure 30: Comparison of $NaClO_4$ dissociation of G37A and G41A with WT monitored by enzyme activity. Protein concentrations for the incubation in $NaClO_4$ were 1.06 μM for WT and G37A, 5.3μM for G41A. Final protein concentrations in the assay for enzyme activity were 8.5 nM for wild type, 53 nM for G37A and 106 nM for G41A. Data from duplicate experiments were averaged.

The values for the thermodynamic constants for dissociation of G37A and G41A monitored by different probes are summarized in Table 12. It is obvious that with the exception of m, nearly all values obtained from three probes for two mutants are in reasonable agreements. The dissociation constants for the two mutants fall within the same range: 92-178 nM for G37A and 94-137 nM for G41A. Thus, compared to the values of 13.8-52 nM for the wild type, the K_d for two mutants have been raised by less than 1 order of magnitude, and the elevation extent is similar for two mutants. This suggests that subunit interactions are slightly weakened in G37A and G41A mutant due to a single mutation in the active site loop, and hinge sites Gly37 and Gly41 seem to play

an identical function in adjusting subunit interactions.

Protein	Method used	K_d (M)	ΔG_0 (kJ/mol)	m(kJ mol^{-1} M^{-1})
Wild type	Enzyme activity	1.38×10^{-8} ±0.02	43.3±2.5	70.6±0.8
	4^{th} derivative UV	5.20×10^{-8}±0.03	40.2±0.2	73.7±0.4
	Near UV-CD	3.20×10^{-8} ±0.05	41.2±1.9	75.1±1.1
G37A	Enzyme activity	9.20×10^{-8}±0.29	38.8±1.2	106.8±3.4
	4^{th} derivative UV	1.78×10^{-7}±0.50	37.2±0.7	119.6±0.8
	Near UV-CD	1.02×10^{-7} ±0.02	38.5±0.9	116.8±0.7
G41A	Enzyme activity	9.40×10^{-8} ± 0.38	38.7±1.6	81.4±3.3
	4^{th} derivative UV	1.37×10^{-7}±0.004	37.8±0.1	105.6±0.6
	Near UV-CD	1.04×10^{-7}±0.006	38.5±0.3	105.6±3.1

Table 12: Summary for the thermodynamic constants for dissociation of WT and two mutants. Protein concentration is 10.6 μM when using 4^{th} derivative UV and near UV-CD spectra as the probes. Activity assay was performed using 8.5 nM for wild type, 53 nM and 106 nM for G37A and G41A respectively. Data from two duplicate experiments were averaged. m is the slope of the graph of ΔG as a function of [$NaClO_4$].

3.5 Steady state kinetic studies

3.5.1 Kinetic studies on the effects of Mg^{2+} and Mn^{2+}concentration on enzyme activity

In order for enolase catalysis to occur, binding of two moles of metal ion and one mole of 2-PGA per active site is necessary. It is well known that Mg^{2+} is the natural cofactor of enolase, producing the highest activity (Wold and Ballou, 1957; Brewer, 1985). Mn^{2+} was originally confirmed as the third activating divalent cation (Wold and Ballou, 1957), but recently it was shown to be the second activating divalent cation in the rank of activating metal ions (Poyner *et al.*, 2002). Both Mg^{2+} and Mn^{2+} have been widely used in many mechanistic studies and crystal structures of yeast enolases. Therefore, detailed kinetic studies of the effects of Mg^{2+} and Mn^{2+} concentration upon the enzyme activity were investigated among wild type and the two mutants. These data were reasonably well fit to a Michaelis-Menten equation when no inhibition was observed at high concentration of divalent cations, or to either of the equations as described in section 2.2.23 when inhibition was observed. The fits to most of the kinetic data were usually within 10% deviation, but the fit to the kinetic data was above 10% deviation when the $[Mn^{2+}]$ effect on the wild type activity was investigated. Kinetic parameters are summarized in Table 13.

The effects of Mg^{2+} concentration on the wild type and two mutant activities were examined in the assay system containing 0.5 mM 2-PGA, and results are shown in Figure

31. A noticeable difference between wild type and two mutants was observed. The activity of wild type yeast enolase was inhibited by Mg^{2+} concentration above 1 mM, which agrees well with previous studies on yeast enolase (Wold and Ballou, 1957; Faller *et al.*, 1977). Strikingly, the activities of G37A and G41A were stimulated by [Mg^{2+}] far higher than 1 mM, and even when the Mg^{2+} concentration was increased to more than 100 mM, 100 times of the normally used Mg^{2+} concentration in standard assay conditions, there was no observable inhibition on enzyme activity.

As can be seen in Table 13, the most remarkable difference between wild type and two mutants is the K_m for Mg^{2+}, which was elevated in the two mutants by about 3 orders of magnitude relative to wild type. The values of k_{cat} for wild type and two mutants were calculated according to the equation as shown in section 2.2.23. Under the activity assay condition we used, the k_{cat} for wild type yeast enolase was 68.4 s^{-1} at 25 °C and pH 7.1; this is comparable to the value of Poyner *et al.* (2002) of 84 s^{-1}, but clearly lower than the value of Faller *et al.* (1977) of 280 s^{-1} at 25 °C and at pH 7.5. This is probably due to the differences in the following aspects: (1) the source of yeast enolase; (2) the molecular weight of protein used; (3) the kinetic analysis used.

Compared with the k_{cat} of wild type, both mutant enolases demonstrate a lower rate of catalysis, with the k_{cat} of 11.5 s^{-1} and 7.2 s^{-1} for G37A and G41A respectively. Furthermore, both G37A and G41A also display greatly lowered catalytic efficiency, as expressed by the 4 orders reduced k_{cat}/K_m relative to that of wild type. This decreased enzyme activity and greatly lowered catalytic efficiency in two mutants probably directly

results from the weaker binding of the second divalent cation and other effects induced by the mutation (see Discussion).

The effect of Mn^{2+} concentration on the wild type and two mutant activities is indicated in Figure 32, and the corresponding kinetic parameters are also outlined in Table 13. Here, we have mentioned above that the deviation in kinetic parameters is above 10% when kinetic assays were carried out on the wild type by varying [Mn^{2+}]. Even though several independent experiments have been performed, we were still unable to obtain a set of data that could be well fit to either of the equations used. However, though the fit is not good, the obtained K_m for Mn^{2+} is 3.4 μM and is comparable to the literature reported values of 2.77 μM for native yeast enolase (Poyner *et al.*, 2002). Results of kinetic assay with Mn^{2+} as the activating divalent cation confirm that two mutants all possess increased K_m's, decreased k_{cat}'s and loss of inhibition by higher Mn^{2+} relative to those of the wild type. But the most surprising observation about the two mutants when assayed with Mn^{2+} is the less noticeably augmented K_m for Mn^{2+} compared with Mg^{2+} as the activating divalent cation.

The results we obtained for G37A and G41A mutants from yeast enolase are somewhat different from the kinetic studies on the same mutants from ββ-enolase investigated by Kornblatt. That study confirmed that G37A mutant has lower activity than the wild type when assayed with Mg^{2+}, but more activity than wild type with other divalent cations, such as Mn^{2+}, Zn^{2+} and Co^{2+}; G41A was more active than wild type only when assayed with Co^{2+} (Kornblatt, 2005). At higher concentration of divalent cations,

inhibition was decreased or absent (Kornblatt, 2005), similar to our results.

In summary, kinetic studies on the two mutants provide us with strong evidence that the movement of the active site loop seems crucial for catalysis to occur in yeast enolase. The absence of inhibition at concentration of high divalent cations in the two mutants suggests that the inhibitory binding site has been distorted. These issues will be further explained in the Discussion section.

Figure 31: Kinetic studies of the dependence of enzyme activity on [Mg^{2+}]. (A) wild type (B) G37A (C) G41A. Initial velocities were measured in buffer B with 0.5 mM 2-PGA by varying of [Mg^{2+}]. All assays were performed in duplicate. The reactions were initiated by adding wild type (1.29 μg), G37A (7.23 μg) and G41A (13.22 μg) enzyme.

(A)

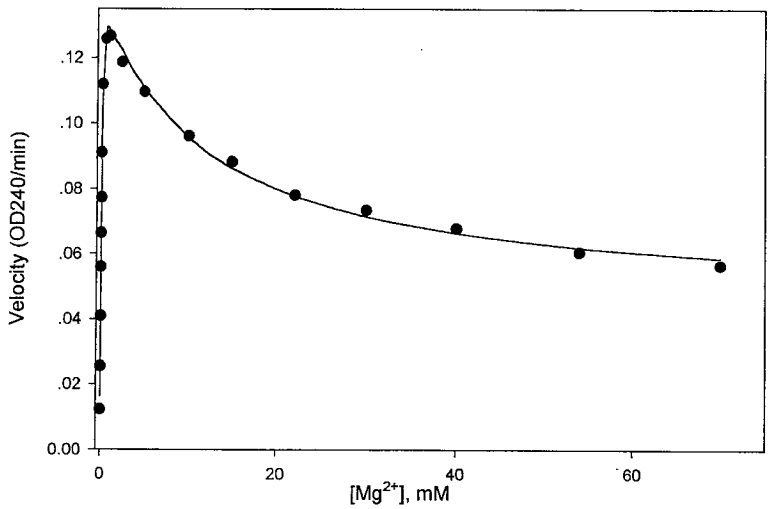
Velocity (OD240/min)
.12
.10
.08
.06
.04
.02
0.00
0
20
40
60
[Mg2+], mM

(B)

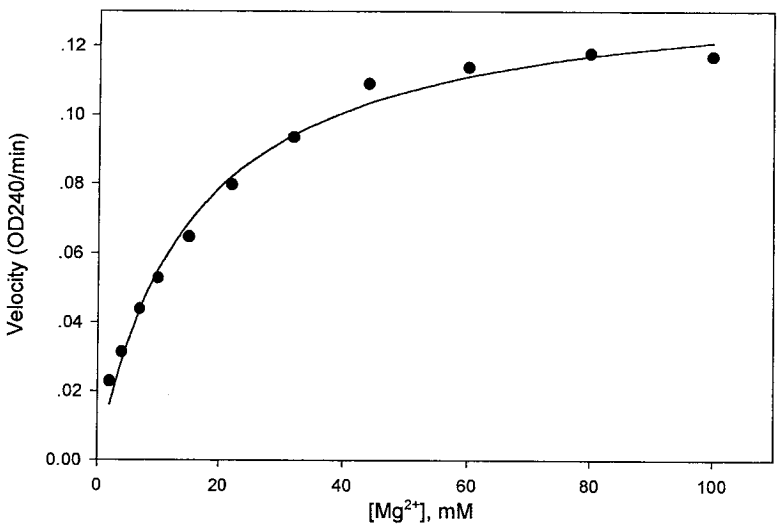
Velocity (OD240/min)
.12
.10
.08
.06
.04
.02
0.00
0
20
40
60
80
100
[Mg2+], mM

(C)

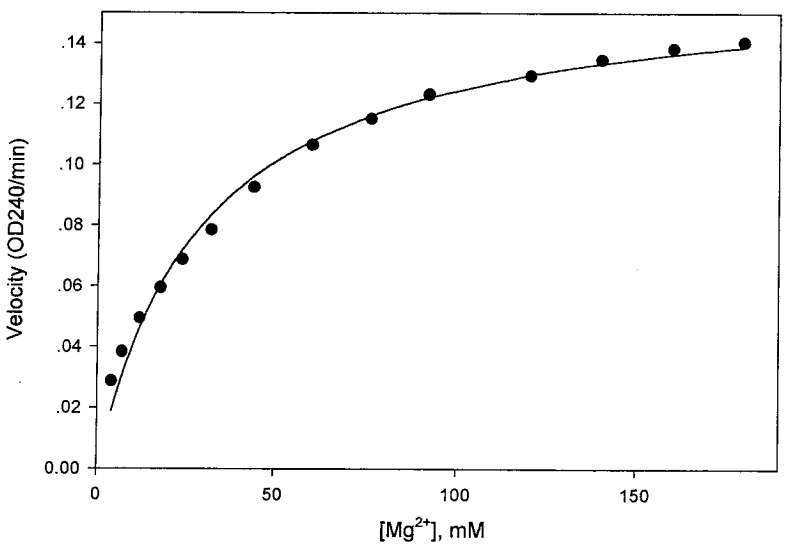
Velocity (OD240/min)
.14
.12
.10
.08
.06
.04
.02
0.00
0
50
100
150
[Mg2+], mM

Figure 32: Kinetic studies of the dependence of enzyme activity on [Mn^{2+}]. (A) wild type (B) G37A (C) G41A. Initial velocities were measured in buffer B with 0.5 mM 2-PGA by varying [Mn^{2+}]. All assays were performed in duplicate. The reactions were initiated by adding wild type (1.84 μg), G37A (11.0 μg) and G41A (23.9 μg) enzyme.

(A)

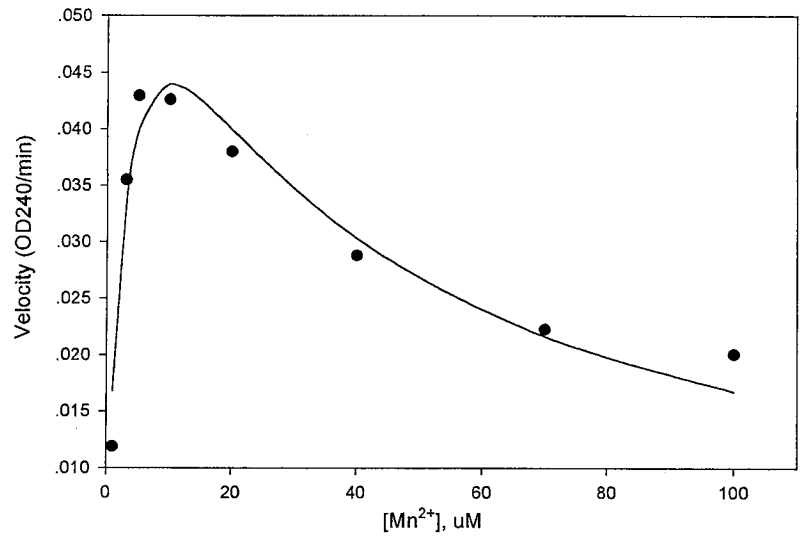
.050
.045
.040
.035
.030
.025
.020
.015
.010
Velocity (OD240/min)
0
20
40
60
80
100
[Mn2+], uM

(B)

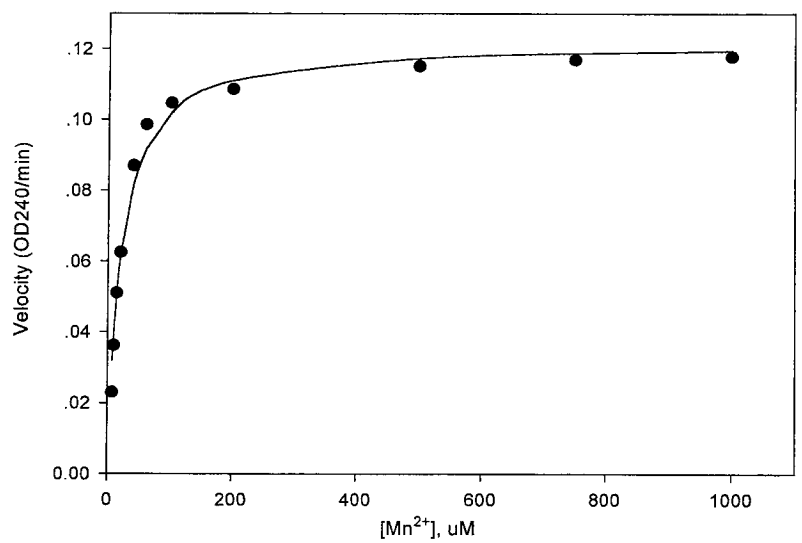
.12
.10
.08
.06
.04
.02
0.00
Velocity (OD240/min)
0
200
400
600
800
1000
[Mn2+], uM

(C)

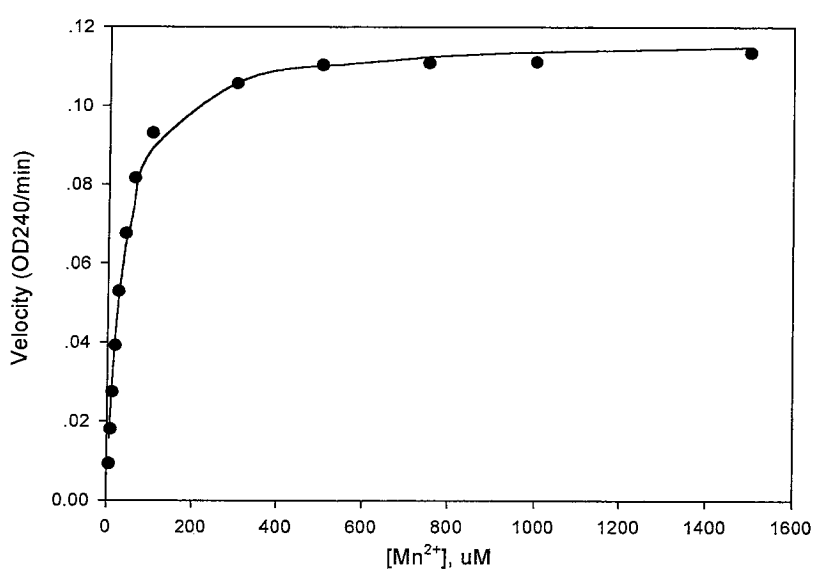
.12
.10
.08
.06
.04
.02
0.00
Velocity (OD240/min)
0
200
400
600
800
1000
1200
1400
1600
[Mn2+], uM

Me^{2+}	Enzyme	k_{cat} (s^{-1})	K_m (μM)	K_i (μM)	k_{cat}/K_m (s^{-1} μM^{-1})
Mg^{2+}	WT	68.4±1.3	37.7±2.2	11350±1923 [a]	1.81
	G37A	11.5±0.3	15346±1372	No inhibition [c]	0.00076
	G41A	7.2±0.2	29339±2753	No inhibition [c]	0.00024
Mn^{2+}	WT	24.1±4.4	3.4±1.1	29.9±10.3 [b]	7.20
	G37A	6.9±0.1	20.7±2.3	No inhibition [c]	0.33
	G41A	3.0±0.1	32.4±2.3	No inhibition [c]	0.09

Table 13: Kinetic parameters for the activation of WT and two mutants by $Mg^{2+}$and Mn^{2+}. ENZFITTER (Biosoft, 2004) was employed to analyze all the kinetic data. [a]: Kinetic data were fit to modified substrate inhibition equation; [b]: Kinetic data was fit to substrate inhibition equation, as described in section 2.2.23, when inhibition was observed by high concentration of divalent cations. [c]: Kinetic data was well fit to the Michaelis-Menten equation when no inhibition was observed by varying the divalent cations concentration;

3.5.2 Kinetic studies on the effects of 2-PGA concentration on enzymes activity

Kinetic studies on the effect of 2-PGA concentration on enzyme activity were examined in the assay system containing fixed Mg^{2+} concentration. However, the Mg^{2+} concentration used for assaying each of the 3 enzymes was different. There is inhibition of enzyme activity above 1 mM Mg^{2+} for wild type, whereas for the two mutants the 1000 fold increased K_m for Mg^{2+} probably means weak binding of Mg^{2+}. Therefore, based on the kinetic studies on enzyme activities as a function of Mg^{2+} concentration, 1 mM, 50

mM and 100 mM Mg^{2+} were finally maintained in wild type, G37A and G41A assay systems to estimate the K_m values for 2-PGA, respectively. These amounts of Mg^{2+} were nearly at saturating levels for the 3 enzymes. The adjustment of Mg^{2+} concentration in the mutant assay system was mainly based on preliminary experiment results (data not shown), though there are reports that K_m values for 2-PGA are decreased by increasing Mg^{2+} concentration (Faller *et al.*, 1977). Nevertheless, preliminary experiments confirmed that if using 1 mM Mg^{2+} in the assay system to determine the K_m values of mutants, it was impossible to obtain a set of data that could be fit to the Michaelis-Menten equation.

Under these assay conditions, the initial velocity values were obtained over a range of 17-700 μM 2-PGA at pH 7.1 for the 3 enzymes, and the data were fit to a Michaelis-Menten equation. These experimental results are displayed in Figure 33. As can be seen in Table 14, the K_m values for 2-PGA are 25.4 μM, 39.0 μM, 47.3 μM for wild type, G37A and G41A respectively. These values are clearly below the concentration (0.5 mM 2-PGA) used in other experiments (such as the kinetic studies on the effects of divalent cation concentrations on enzyme activity). The apparent substrate K_m values for recombinant wild type is in good agreement with literature values of 30 μM (Faller *et al.*, 1977) and 32 μM (Brewer *et al.*, 1998) under almost similar measurement conditions. Moreover, experiment results demonstrate, with G37A and G41A, the K_m values for 2-PGA are not significantly different from that of the wild type, and the two mutants display depressed rate of catalysis compared with that of the wild

type. However, the reduced activity in G37A and G41A couldn't be ascribed to changing in K_m for substrate 2-PGA, since the K_m for 2-PGA isn't significantly altered due to the Gly37 and Gly41 mutation to Ala in the active site loop.

Enzyme	k_{cat} (s^{-1})	K_m (μM)	k_{cat}/K_m (s^{-1} μM^{-1})
Wild type	62.4±0.6	25.4±1.1	2.46
G37A	12.9±0.2	39.0±2.1	0.33
G41A	7.4±0.1	47.3±2.7	0.16

Table 14: Kinetic parameters for activation of WT and two mutants by 2-PGA. Kinetic data were well fit to the Michaelis-Menten equation using ENZFITTER (Biosoft, 2004).

Figure 33: Kinetic studies of the dependence of enzyme activity on [2-PGA]. (A) wild type (B) G37A (C) G41A. Initial velocities were measured in buffer B with 1 mM Mg^{2+} for WT, 50 mM and 100 mM Mg^{2+} for G37A and G41A respectively by varying of [2-PGA]. All assays were performed in duplicate. The reactions were initiated by adding wild type (0.78 μg), G37A (5.53 μg) and G41A (4.34 μg) enzyme.

(A)

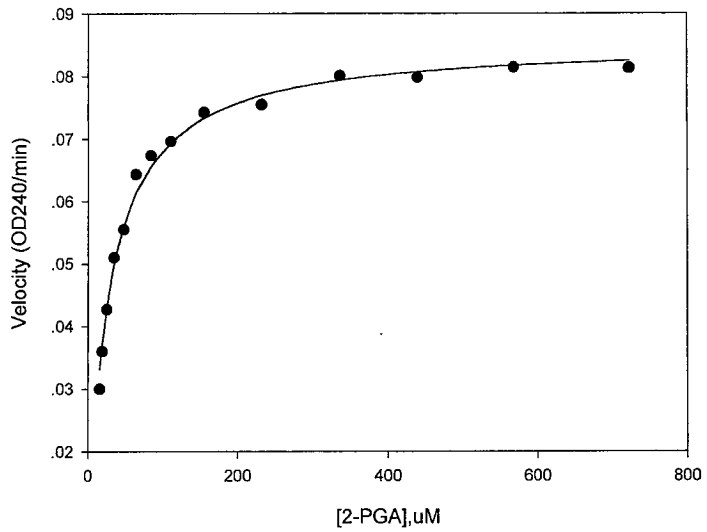
.09
.08
.07
.06
.05
.04
.03
.02
Velocity (OD240/min)
0
200
400
600
800
[2-PGA],uM

(B)

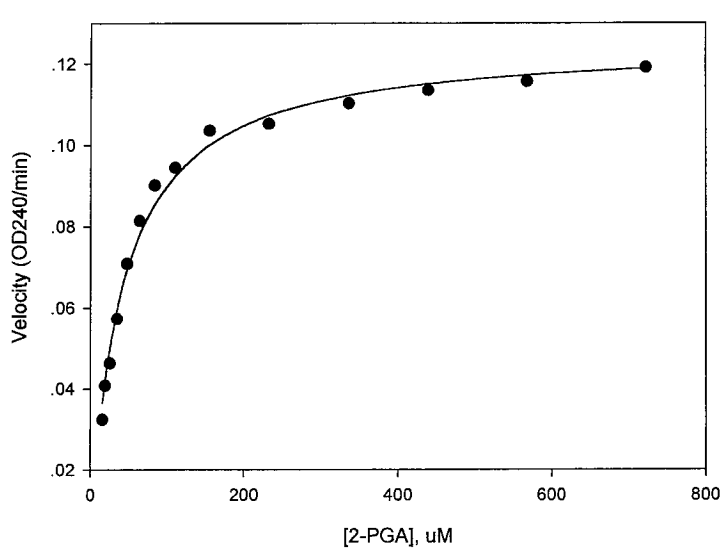
.12
.10
.08
.06
.04
.02
Velocity (OD240/min)
0
200
400
600
800
[2-PGA], uM

(C)

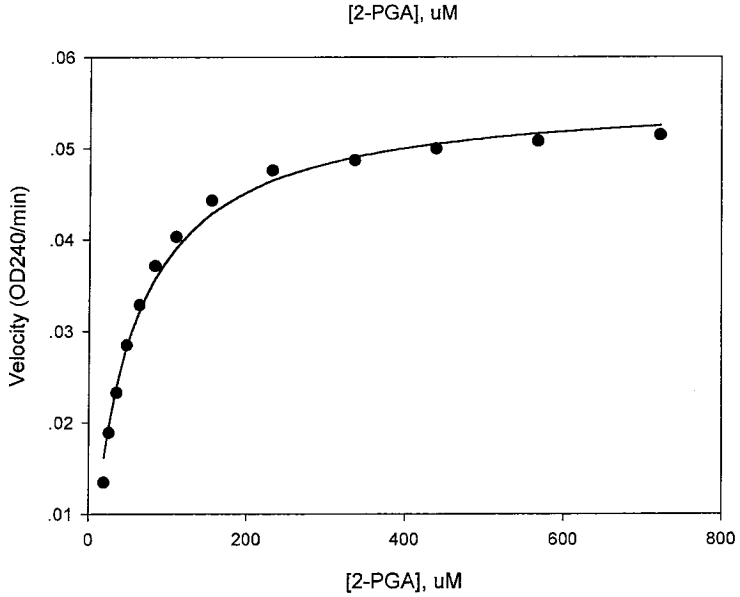
.06
.05
.04
.03
.02
.01
Velocity (OD240/min)
0
200
400
600
800
[2-PGA], uM

4 Discussion

4.1 Purification and structural characterization of the G37A and G41A mutants

G37A and G41A mutant yeast enolase were successfully obtained through site-directed mutagenesis. DNA sequencing results confirmed that the desired mutations had been introduced, and no other unwanted mutations were present in G37A and G41A. The recombinant mutant proteins were expressed properly. Mutant proteins were also effectively purified using the same method as purification of the wild type. The yields of protein are exceedingly high. In general, about 350 mg from 4 liters of culture are obtained for two mutants. The two mutant proteins finally obtained are also highly pure and a further purification step was not necessary.

During the purification, the behaviors of two mutants showed a little difference with the wild type, in that there were two activity peaks present in the elution profile from the Q-Sepharose column (Figure 14). Thus, SDS-PAGE and mass spectra were employed to determine the position of true mutant activity peak (Figure 15, Figure 16). Although the results of SDS-PAGE provided the clue that the first activity peak is most likely to be that of mutant yeast enolase, the definitive evidence was not obtained until from mass spectrometry. Based on the results of SDS-PAGE and mass spectra, we concluded that the first activity peak in the Q-Sepharose elution profile was the true mutant activity peak, and the later peak is attributed to the *E. coli* enolase activity peak. In fact, this part of activity is also present in all the wild type purification steps, but

compared with the high activity of the wild type yeast enolase, it only accounts for a small fraction of the total activities. Thus, during purification of the wild type protein, it is not visible in the elution profile from Q-Sepharose column. However, due to the reduced activities of the two mutants, this part of activity accounts for a relatively large fraction of the total activities, and thus is readily observed in the mutant's elution profile. The later activity peak is considered as the *E. coli* enolase activity peak, which is not only consistent with the previously reports that *E. coli* enolase binds tighter to anion exchange column (Spring and Wold, 1971), but also comparable to the result of a control experiment of purification *E. coli* enolase.

G37A and G41A were characterized structurally in order to substantiate the impacts of the replacement of Gly by Ala residues on the protein. The results of structural characterization revealed the two mutants demonstrated similar secondary and tertiary structure relative to wild type, as indicated by the far UV-CD and 4^{th} derivative UV as well as near UV-CD spectra (Figure 19, Figure 20, Figure 21). Though the near UV-CD spectra demonstrated that there was a slight increase in intensity in the aromatic region for G37A, the AUC experiments provided definitive evidence that two mutants were not appreciably dissociated under the measurement condition and were correctly folded dimer. Therefore, the slightly increased CD signal in aromatic region in G37A was attributed to conformational variation induced by mutation, especially in loop regions, where some aromatic residues are located, and apparently these aromatic residues become more mobile in G37A than in wild type and G41A.

4.2 Subunit dissociation with $NaClO_4$

All the dissociation experiments were carried out using $NaClO_4$, which has also been widely utilized to dissociate mammalian enolase (Trepanier *et al.*, 1990; Kornblatt *et al.*, 1996; Kornblatt *et al.*, 2002). Its destabilization effect on protein structure was discussed in section 1.6.

Figure 34: Distribution of the tyrosine and tryptophan residues in the crystal structure of yeast enolase (PDB: 1ONE). Tyrosine and tryptophan residues are labeled in red and green ball and stick, respectively. Solid blue ribbon indicates the whole loop (Pro35-Gly60), in which the hinge sites Gly37 and Gly41 are shown in red color.

In yeast enolase, there are 9 tyrosine and 5 tryptophan residues, and their distribution in the crystal structure of yeast enolase is shown in Figure 34. Three tyrosine residues

(Tyr6, Tyr11, Tyr130) (Kornblatt *et al.*, 1995) and Trp56 are near the dimer interface in yeast enolase; about half of the tryptophan and tyrosine residues are located on the mobile loops (Kornblatt *et al.*, 1998). The distribution of these aromatic residues make them a good probe to detect the dissociation of enolase, thus they all have the possibility of contribution to the 4th derivative UV and /or near UV-CD spectral changes induced by $NaClO_4$ dissociation.

4.2.1 Interpretation of the spectral changes as a function of dissociation of yeast enolase

The 4th derivative UV spectrum changes as a function of increasing [$NaClO_4$] leading to a decrease in R, which provides some information about the changes that happen during $NaClO_4$ dissociation of yeast enolase. As shown in Figure 25, the values of R determined for wild type yeast enolase at 0 M and 0.3 M $NaClO_4$ are about 0.8 and 0.5, respectively. The apparent decrease in R signifies that polarity of the environment of aromatic residues decreases as the yeast enolase is dissociated. However, the decrease in R as a result of dissociation of yeast enolase is in fact contrary to the changes observed as the majority of proteins are denatured (Ragone *et al.*, 1984). In the present studies, the observable changes in R were mainly interpreted as the environmental polarity changing about tyrosine residues. This is due to the following reasons. Firstly, through simulation the 4th derivative UV spectra of wild type yeast enolase in 0.3 M [$NaClO_4$] and 0 M $NaClO_4$ using standard spectra of tyrosine and tryptophan in different solvents (personal

communication with Dr. Kornblatt), the simulation results indicate that changes in R are due to changes in the environment of tyrosine residues. Secondly, it should be noted that 4 of the 9 tyrosine residues in the monomer are buried and 2 tyrosine residues (Tyr6 and Tyr11), as indicated in Figure 34, are located near a cleft between the subunits interface. The crystal structure of yeast enolase (Stec and Lebioda, 1990) indicates that there are 353 rigid waters; some of these rigid waters in the cleft make the immediate environment of Tyr6 and Tyr11 residues uncommonly polar in dimeric enolase (Kornblatt *et al.*, 1995). When dimeric yeast enolase dissociates into monomer, the environment of 2 tyrosine residues becomes less polar, which is consistent with literature reports (Kornblatt *et al.*, 1995). Therefore, dissociation of yeast enolase is accompanied by a less polar environment of tyrosine residues, which is directly indicated in the decrease in R in the 4^{th} derivative UV spectra (Figure 25). The decrease in R observed in 4^{th} derivative UV spectra with the increasing $NaClO_4$ has also been formerly reported by Kornblatt *et al.* using the hydrostatic pressure as dissociation force (Kornblatt *et al.*, 1998; Kornblatt *et al.*, 2004). However, the trend of environment polarity changing upon dissociation yeast enolase is oppose to what was observed for dissociation of ββ-enolase (Kornblatt *et al.*, 1996), in which the environment becomes more polar after dissociation. Therefore, the spectral changes induced by dissociation of yeast enolase should be different from that of dissociation of ββ-enolase.

Near UV-CD spectra can provide information about the protein tertiary structure due to aromatic residue absorption in the aromatic region. Each of three aromatic amino

acids (Phenylalanine, Tyrosine, Tryptophan) possesses characteristic absorption bands, which are sensitive to the tertiary environment changes of the protein (Strickland, 1974). Dissociation of yeast enolase results in a more positive spectrum in the aromatic region and the induced ellipticity of these aromatic residues significantly increased upon dissociation (Figure 26), which agrees well with previously reported spectral changes as a function of dissociation (Kornblatt *et al.*, 1998). Generally, CD signal intensity changes in aromatic region reflect either the mobility changes of the aromatic amino acids, or changes in the extent of the aromatic residue interactions with other groups (Strickland, 1974). However, as regards to yeast enolase dissociated by $NaClO_4$, we suggest that increased intensity of near UV-CD spectra induced by dissociation was mainly due to Trp56 environment changes, as well as the variations in loop conformations. First of all, the crystal structure of yeast enolase has indicated that Trp56 is a part of the whole loop of Pro35-Gly60 (including the active site loop), and positioned near the subunit interface (Stec and Lebioda, 1990), so the dissociation must have more effect on its environment than on other aromatic residues. Secondly, by subtracting the near UV-CD spectrum of wild type protein incubated at different [$NaClO_4$] from that of the protein incubated at 0 M $NaClO_4$, the corresponding difference spectra are shown in Figure 35. It is apparent that these difference CD spectra at high [$NaClO_4$] look like the standard near UV-CD spectrum of tryptophan residues in water (Strickland, 1974). Thus, the increased intensity of the near UV-CD spectra upon dissociation was mainly ascribed to loss of the CD signal from tryptophan residues. Thirdly, previous CD spectra study has shown that there

were striking difference in the near UV-CD spectra of the Mg^{2+}-enolase, apoenolase and dissociated enolase (Kornblatt *et al.*, 1998). These difference were suggested to reflect that the mobile loops possess different conformations in three forms of yeast enolase, considering that about half of the tryptophan and tyrosine residues are located on the mobile loops (Kornblatt *et al.*, 1998). To sum up, these changes observed in the near near UV-CD spectra upon dissociation reflect that the aromatic residues become more mobile in monomeric enolase than in dimeric enolase, especially for the residue of Trp56.

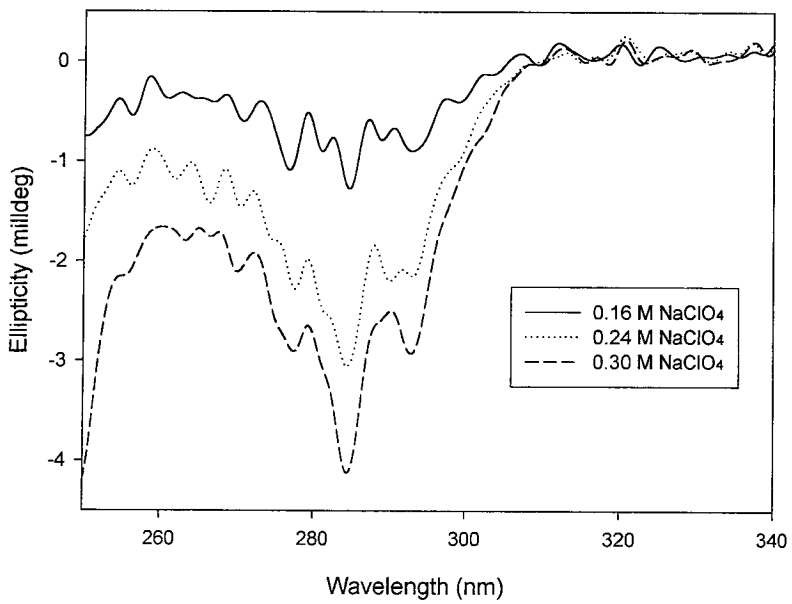

Figure 35: Subtracting near UV-CD spectra of WT in 0.16 M, 0.24 M and 0.30 M $NaClO_4$ from that of WT in 0 M $NaClO_4$. Protein concentration was 1 mg/ml in buffer A with varying concentration of $NaClO_4$ and NaOAc.

4.2.2 Dissociation studies on wild type and the two mutants

$NaClO_4$ has been widely employed to study mammalian enolase dissociation monitored by enzyme activity and 2^{nd} derivative UV or 4^{th} derivative UV spectra. These

changes were previously interpreted by assuming that the dimeric enolase was dissociated into monomeric enolase by $NaClO_4$ (Kornblatt *et al.*, 1996). The activity and spectral changes were indeed observed in the present studies (Figure 24, Figure 25, Figure 26), but the conclusive evidence for dissociation by $NaClO_4$ were from AUC experiments. AUC experiments clearly demonstrate the dissociation determined by AUC matched the inactivation, as well as the observable spectral changes (Table 11). For that reason, we conclude that the $NaClO_4$ is dissociating yeast enolase, the monomers produced are inactive and with altered spectral characteristics.

In order to compare the dimer stabilities, the dissociation of wild type and two mutants with $NaClO_4$ were carried out and monitored by enzyme activity, 4^{th} derivative UV and near UV-CD spectra (Figure 27, Figure 28, Figure 29, Figure 30). Several probes of dissociation were employed in order to determine whether the changes observed in loss of activity, 4^{th} derivative UV and near UV-CD spectral variation correspond to the same process or to several different processes. The experimental results show that the dissociation of wild type and two mutants are not related to loss of secondary structure or sample aggregation within the [$NaClO_4$] used. The enolase dimer dissociation to monomer was the only change detected. The K_d estimated using three different probes are in reasonable agreement for the 3 proteins (Table 12).

4.2.3 Impact on subunit interactions of the mutation in the active site loop

It is apparent that although the mutation sites in the active site loop are far away

from the subunit interface, the mutation in the two hinge sites leads to weakened subunit interactions, as seen by the higher K_d. The only common feature is the mutation that has adverse effect on the active site loop conformation. How can the altered conformation of active site loop affect the subunit interactions? As we know, the active site loop (loop 1) is the most mobile part of the whole loop (Pro35-Gly60), so the mutation in the active site loop must have the direct effect on the conformation of the whole loop, in which the backbone N of Trp56 in one subunit forms a hydrogen bond with the carboxyl oxygen of Glu188 in the other subunit across the subunit interface (Figure 6) (Stec and Lebioda, 1990). Given that the replacement of Gly by Ala in two hinge sites in the active site loop has changed the dimer stability only by 3-5 kJ/mole, the change in ΔG_0 is small. Hence, we interpret the most likely for the weakened subunit interactions is that the hydrogen bond between Trp56 and Glu188 is slightly weakened in the two mutants.

Aside from the increase in K_d for two mutants, the other characteristic that should be emphasized is the increased m for the two mutants relative to the wild type. During the protein denaturation studies, m reflects the level of protein surface area exposure to solvent upon unfolding (Stephen, 1997). In enolase dissociation studies, it has been interpreted as having the same meaning as for unfolding a protein (Lin and Kornblatt, 2000; Kornblatt *et al.*, 2002). Kornblatt *et al.* (2002) made a suggestion that "with the dissociation of wild type enolase, changes in the exposed surface area occur due to exposure of the surface that was buried at dimer interface and changes in the conformations of some of the loops". Therefore, based on this suggestion, an increase in

m may mean that change in exposed surface is larger when two mutants dissociate than when the wild type dissociates. Since there was no loss of secondary structure observed in two mutants when they were incubated at the highest concentration of $NaClO_4$, the increased exposure region in the two mutants is most possibly in the subunit interface and /or in these loop regions. However, the G37A mutant has a slightly higher increase in m than G41A, which seems consistent with earlier observation that the near UV-CD spectrum of G37A shows a larger variation than that of the G41A. Another issue we should note is the m values determined for each mutant from the enzyme activity, which is somewhat smaller than that determined by spectra probes. To some extent, this may be a reflection of adding excess Mg^{2+} effect upon the experiment results.

All in all, the impact of mutation in the active site loop is extended to the subunit interface through the active site loop movement, and indirectly reduces the subunit interactions by slightly weakening the hydrogen bonding between Trp56 and Glu188. At the same time, the mutation in the active site loop also results in increase in the exposure surface in two mutants. If only considering the changes in K_d and m values induced by mutation, it seems that the hinge sites at Gly37 and Gly41 play the identical function in adjusting the active site loop involved in subunit interactions.

4.3 Steady state kinetic studies

During enolase catalysis, the loop movement is a significant and remarkable characteristic. The movement of the active site loop (loop 1) has been suggested to

perform a crucial protection or stabilization function on the carbanion intermediate (Wedekind *et al.*, 1994), formed during enolase catalysis (Stubbe and Abeles, 1980). The loop movement and essential function have been described in detail in section 1.3. In enolase, the specific movements of these loops were evidently related to metal ions and substrate binding (Lebioda and Stec, 1991; Kornblatt *et al.*, 1996). The importance of residue Ser39 located in loop 1 has formerly been substantiated by its direct coordination with metal II (Wedekind *et al.*, 1994). The crucial function of Ser39 in fixing the closed conformation of loop 1 has also been established by mutating Ser39 to Ala. This mutant shows 4 orders of magnitude of reduced activity relative to the wild type (Brewer *et al.*, 1998; Poyner *et al.*, 2002). The crystal structure of S39A yeast enolase-Mg^{2+}-PhAH complex (Poyner *et al.*, 2002) reveals that in the S39A mutant protein: loop 1 lacks the ability to close completely on the second Me^{2+}; the ligand to the second Me^{2+} was changed to two water molecules rather than the carbonyl and hydroxyl oxygens of Ser39; loop 2 is moved away from the active site, so that the ring of His159 located in loop 2 is outside hydrogen bonding distance of the PhAH.

The smaller residues Gly37 and Gly41 in the vicinity of Ser39 in loop 1 probably provide Ser39 with enough space to rotate into a position to correctly coordinate with metal II or favor the maximum movement of the loop 1 (Wedekind *et al.*, 1994). In the present study, the smaller disturbance on the movement of loop 1 was carried out by substituting a larger residue, Ala, for a smaller residue, Gly, at two hinge positions 37 and 41 in loop 1, in the hope of reducing the enzyme activity. This hypothesis was

corroborated by the following kinetic studies on three enzymes (section 3.5), which demonstrated that G37A and G41A were distinctly different from the wild type in the following aspects (Figure 31, Figure 32, Table 13, Table 14): (1) K_m increased by 3 orders of magnitude for Mg^{2+}, and by 6-10 fold for Mn^{2+}; (2) a lower rate of catalysis, as seen by the reduced k_{cat} for 2-PGA, Mg^{2+} and Mn^{2+}; (3) no inhibition was observed at high concentration of divalent cations; (4) 4 orders of magnitude lowered catalytic efficiency, as indicated by the expression of k_{cat}/K_m when assayed with Mg^{2+}. The results, we obtained for G37A and G41A from yeast enolase, are somewhat different from the results of kinetic studies on the same mutants from ββ-enolase (Kornblatt, 2005), which have been described in detail in section 3.5.1. However, the two same mutants from ββ-enolase show increase in K_m for cations and lower k_{cat} when assayed with Mg^{2+}, as well as absence or decrease of inhibition at high concentration of cations (Kornblatt, 2005), all of which are similar to our results.

With regard to the G37A and G41A mutants from yeast enolase, the lower rate of catalysis was not caused by the loss of affinity for substrate, nor by the observable secondary or tertiary structure changes. The values of K_m for 2-PGA with two mutants are similar to the value for native yeast enolase, and the mutation at Gly37 and Gly41 didn't lead to overall structure changes in G37A and G41A enolases (Figure 19, Figure 20, Figure 21). What are the real reasons that cause the lower rate of catalysis in two mutants?

4.3.1 Significantly increased K_m for Mg^{2+} in two mutants

Although the K_m for divalent cation may not supply a direct measurement of the enzyme binding affinity for metal ion, it can serve as a relative indication of the affinity for metal ion in enolase. Detailed kinetic and binding studies on divalent cation have been previously carried out in yeast enolase by Lee and Nowak (1992), and they concluded that the values of K_m for divalent cations always falls midway between the values for the dissociation constants for site I and II. Hanlon and Westhead also showed that the K_m for divalent cations was similar to the dissociation constants at the second binding sites (Hanlon and Westhead, 1969b; Hanlon and Westhead, 1969a). Thus, we have good reason to believe that the significantly increased K_m for divalent cations in two mutants may imply a weaker binding affinity for the second divalent cation, though the dissociation constants K_d only could be finally established through binding studies. Therefore, the 3 orders of magnitude increased K_m for Mg^{2+} strongly suggests weaker catalytic Mg^{2+} binding affinity in G37A and G41A mutants, and probably reflects that the favorable chelate effect from coordination of the carbonyl and hydroxyl oxygens of Ser39 to catalytic Mg^{2+} is badly disrupted. Generally, the binding of the catalytic Mg^{2+} directly affects the pKα of proton at carbon-2 of 2-PGA, which favors the first step of the reaction catalyzed by enolase (Hilal *et al.*, 1995). Thus, it appears that the weak interactions between Ser39 and catalytic Mg^{2+} in the two mutants may disfavor the first step of the reaction, which, to some extent, directly results in the lower rate of catalysis in two

mutants. Given that both the major catalytic base-acid pair K345/E211 and the crucial catalytic Mg^{2+} binding ligand Ser39 are all still present in the two mutants, the most likely reason causing the weak interactions between Ser39 and Mg^{2+} is the impeded movement of loop 1.

As the Ser39 correct coordination with catalytic Mg^{2+} plays a key role in fixing the closed conformation in loop 1 (Poyner *et al.*, 2002), the apparently impaired coordination with the catalytic Mg^{2+} may, in turn, reflect that loop 1 in G37A and G41A mutants is most likely unable to close upon the second Me^{2+}, assuming an incomplete closure conformation, analogous to loop 1 in S39A mutant. The closure of the loop in most enzymes is an important issue that affects enzyme activities (Lolis and Petsko, 1990; Pompliano *et al.*, 1990; Ramakrishnan and Qasba, 2001; Zgiby *et al.*, 2002). In enolase, the closure of loop 1 has been postulated to exclude solvent water, and lessen the dielectric constant in the active site (Brewer *et al.*, 1998), which would finally obtain a significant augmentation in catalytic rate by strengthening these electrostatic interactions between two Me^{2+}, substrate and these charged residues in the active site. Thus, an incompletely closed loop 1 is probably another reason that leads to the lower rate catalysis and the 4 orders of magnitude reduced catalytic efficiency in two mutants.

4.3.2 Loss of inhibition by higher divalent cations in two mutants

With regard to the inhibition of native enolase by excess Me^{2+}, it has been interpreted as product inhibition, thus catalytic Me^{2+} must depart from the

enzyme-Me^{2+}-PGA/PEP complex before dissociation of PEP (Poyner *et al.*, 2001). However, this interpretation does not explain both the noticeable stimulation of activity and the loss of inhibition by that higher Me^{2+} observed in two mutants (Figure 31, Figure 32), as also emphasized by Brewer *et al.*'s (2003) study on the H159A, H159N and H159F mutant enolases from yeast. The presence of the inhibitory binding site has been suggested and confirmed through the binding studies (Faller *et al.*, 1977; Lee and Nowak, 1992; Vinarov and Nowak, 1999), and recently further established by the crystal structure of *T. brucei* enolase (da Silva Giotto *et al.*, 2003). Thus, it seems that the presence a third inhibitory binding site is the best and most reasonable hypothesis up to date, and the presence of the inhibitory binding site in enolase is also widely accepted by most investigators (Faller *et al.*, 1977; Elliott and Brewer, 1980; Brewer and Ellis, 1983; Lee and Nowak, 1992; Brewer *et al.*, 2003; Kornblatt, 2005).

The crystal structure of *T. brucei* enolase-$(Zn^{2+})_2$-complex (da Silva Giotto *et al.*, 2003) has substantiated that with Me^{2+} bound at the inhibitory site: (1) loop 1 adopts an intermediate conformation between the "open" and "closed" form, which is like but differs from the "incompletely closed" substrate-single Me^{2+}-complex of yeast enolase; (2) the transition of loop 2 from "open" to "closed" conformation is impossible; (3) the side chain of His156 (His159 in yeast enolase) located on loop 2, was one of the ligands at the inhibitory site. Therefore, the loss of inhibition at higher $[Mg^{2+}]$ and $[Mn^{2+}]$ in the two mutants must mean that the inhibitory binding site has been distorted in G37A and G41A mutants. As G37A and G41A show some similar kinetic properties to the S39A

mutant, such as the reduced affinity for the second Me^{2+} and loss of inhibition at higher $[Mg^{2+}]$ and $[Mn^{2+}]$ (Poyner *et al.*, 2002), it is reasonable to suggest that loop 2 in G37A and G41A mutants is probably altered in the same manner as in S39A mutant, simultaneously causing changes in the precise position of His159. If that is the case, the position changes of His159 can provide us with a good interpretation to the loss of inhibition at higher $[Mg^{2+}]$ and $[Mn^{2+}]$ in two mutants. Aside from being an inhibitory binding ligand, His159 is also in contact with the phosphoryl oxygens of the substrate (Duquerroy *et al.*, 1995). Though its role in enzyme catalysis was not finally determined, the mutation of His159 to Ala leads to a 4 orders of magnitude lower rate of catalysis (Vinarov and Nowak, 1999). Hence, the small disturbance on loop 1 in two mutants is most likely causing the alteration in the conformation of loop 2, as also confirmed by investigation of the same mutants from ββ-enolase (Kornblatt, 2005). Therefore, it seems that the movement of loop 1 has a long range interaction, it is not only necessary for enzyme to approach active site upon divalent cation binding, but it may also affect the precise conformation of loop 2, especially around His159. Results from the kinetic studies apparently support the suggestion that loop movement is coordinated in enolase examined by the MD simulations (Gunasekaran *et al.*, 2003).

Indeed, the contact among three important loops has already been noted in the crystal structure of the asymmetric dimer of Enolase-PGA/PEP complex (Zhang *et al.*, 1997). The strong interactions between loop 1 and loop 2 have previously been confirmed through the MD simulations (Gunasekaran *et al.*, 2003). They found, during simulation,

the presence of remarkable hydrogen bonding, between ε-NH_2 of Gln167 and the backbone oxygen of Thr40, between His159 $N^{\delta 1}$ and Thr40 $O^{\gamma 1}$ and between Ala38 O and His159 $N^{\delta 1}$, is the major contribution to the strong interactions between loop 1 and loop 2. Through the loop-loop interactions, loop 2 is likely to play the function of decreasing the energy barrier for the loop 1 to overcome (Gunasekaran *et al.*, 2003). The QM/MM analysis of the enolase active site also emphasized the crucial role of some residues located on loops, such as Ala38 (loop 1), His159 and Gln167 (both in loop 2), all of which favorably contribute to lowering the energy barrier for proton abstraction (Liu, 2000). Therefore, it can be imagined that these strong hydrogen bonding interactions between two loops probably have been reduced in G37A and G41A mutants owing to the steric effects of replacement of the smaller residue, Gly, by the larger residue, Ala, near these hydrogen bonds. The weakened interactions between loop 1 and loop 2 must lead to a higher energy barrier for the first step of the reaction catalyzed by enolase. For that reason, we suggest the lower rate of catalysis of the two mutants seems not to just stem from the immediate environment changing of Ser39, and incompletely closed loop 1, but also from the micro environment alteration in loop 2, especially around His159, as well as from the weakened interactions between loop 1 and loop 2.

4.3.3 Other observations from kinetic studies

Though G37A and G41A showed similar kinetic behaviors, such as both activities stimulated by higher Mg^{2+} and Mn^{2+}, increased K_m's and decreased k_{cat}, it seems that the

Gly mutation to Ala at position 41 has a slightly bigger effect than the same mutation at position 37. The G41A mutation demonstrated a lowered k_{cat} value and much increased K_m for divalent cations compared to the G37A. Thus, the hinge site at position 41 probably plays a more crucial function than the hinge site at position 37 for the enzyme activity to occur.

4.4 Proposal from the subunit dissociation and kinetic studies

Based on the results of subunit dissociation and kinetic studies on two mutants and wild type, we propose that the small disturbance in loop 1 not only causes the altered conformation of loop 1, but also leads to altered conformation of loop 2. As the two mutants demonstrate slightly weakened subunit interactions and distinctly different kinetic profile from the wild type, it seems that the precise loop conformation is indispensable for the subunit interactions and the correct active site structure and further substantiates that "disrupting the forces that maintain the conformation of the loops would weaken subunit interactions and disrupt the active site structure" (Kornblatt *et al.*, 1996).

5 Conclusions

(1) Purified G37A and G41A mutant proteins are folded properly, and the mutation has no significant effect on the ternary and quaternary structure of the two mutants.

(2) Thermal denaturation confirmed that G37A and G41A are less stable than wild type, and denaturation is a two state mechanism.

(3) The replacement of Gly by Ala at position 37 and 41 in the active site loop weakens subunit interactions and the two hinges sites play the identical function in adjusting subunit interactions

(4) Higher Mg^{2+} concentration can significantly stimulate G37A and G41A mutant's specific activity, respectively.

(5) The replacement of Gly by Ala at position 37 and 41 doesn't have a large effect on the values of K_m for substrate 2-PGA.

(6) The replacement of Gly by Ala at position 37 and 41 has significant effect on the values of K_m for divalent cations. The affinity of two mutants for the second divalent cation is greatly reduced relative to the wild type.

(7) The replacement of Gly by Ala at position 37 and 41 has resulted in lower rate of catalysis of enzyme.

(8) The loss of inhibition at high concentration of divalent cations implies that the mutation of Gly to Ala at position 37 and 41 in loop 1 affect the precise conformation of loop 2. The hinge site at position 41 plays a more crucial function than the hinge

site at position 37 for the enzyme activity to occur.

(9) The active site loop movement is not only essential for correctly positioning Ser 39 for coordination of the catalytic metal ion, but also plays some crucial function in maintaining the proper linkage with other loops. In turn, these precise loop conformations are crucial in maintaining the correct active site structure and proper subunit interactions.

(10) Disturbing the correct loop conformation would not only impair the stability of the enolase dimer, but would break the active site structure as well. Thus, the precise loop conformation is major factor that affect the enzyme activity and subunit interactions in enolase.

6 Future works

We don't yet have any direct measure of catalytic divalent cation binding, though the K_m for Mg^{2+} obtained here suggests that the interaction of catalytic divalent cation with the enzyme is weaker than with the wild type. Further experiments are necessary to determine the dissociation constant in quantitative manner. Titrating 3 apo-proteins (WT, G37A and G41A) using Mg^{2+} in the presence of saturating stronger inhibitor PhAH can be monitored by fluorescence intensity changes in the hope of determining the catalytic Mg^{2+} binding constant.

In order to further address the question as about the crucial role of the active site loop upon the activity, the primary KIE's should be measured. Since the dehydration of 2-PGA to form PEP catalyzed by enolase requires the breakage of a C-H bond from C-2 of the substrate2-PGA, KIE's on the rate of dehydration of 2-PGA can be measured by direct comparison of initial velocity with saturating [2-^{1}H]-PGA and [2-^{2}H]-2-PGA with varying the concentration of divalent cations. G37A and G41A mutant from ββ-enolase (Kornblatt, 2005) exhibit increased KIE's relative to the wild type when assayed with all 4 divalent cations, but show large KIE's only when assayed with Mg^{2+}. S39A mutant from yeast enolase (Poyner *et al.*, 2002) also demonstrated substantial KIE's with all of the divalent cations tested, but native yeast enolase only exhibits KIE's when assayed with Mg^{2+} and Mn^{2+}. Observation of these KIE's indicates proton elimination from C-2 of 2-PGA has become the rate limiting step in these mutants with the Me^{2+} assayed.

Moreover, there are reports that in the presence of Mg^{2+}, proton elimination is only partially rate limiting in native yeast enolase (Shen and Westhead, 1973; Anderson *et al.*, 1994). Therefore, it is feasible to investigate the presence or absence of KIE's in two mutants when assayed with different divalent cations. If two mutants show some KIE's, it probably also suggests that proton elimination from C-2 of 2-PGA has become the rate limiting step in two mutants. However, the reason making this step the rate limiting step is not due to proton abstraction itself. Given that the main catalytic base-acid pair K345/E211 and the crucial metal II binding ligand Ser39 are all still present in two mutants, the most likely reason is the impeded movement of active site loop effect on the reaction.

Finally, limited proteolysis has provided a very useful analytical tool to study the conformational changes in proteins. In native state, the protease selectively cleaves the peptide bond of residues exposed to solvent or protein protruded regions which have a flexible loop or coiled structure (Ramasamy *et al.*, 2003). In order to investigate whether these mutation in the active site loop affect the relative mobility of the active site loop, and whether these mutations contribute to relatively more open state of the active site loop, limited proteolysis experiment should be carried out in wild type and two mutants if possible .

7 References

Anderson, S.R., Anderson, V.E. and Knowles, J.R.: Primary and secondary kinetic isotope effects as probes of the mechanism of yeast enolase. Biochemistry 33 (1994) 10545-55.

Arakawa, T. and Timasheff, S.N.: Preferential interactions of proteins with salts in concentrated solutions. Biochemistry 21 (1982) 6545-52.

Asuncion, M., Blankenfeldt, W., Barlow, J.N., Gani, D. and Naismith, J.H.: The structure of 3-methylaspartase from *Clostridium tetanomorphum* functions via the common enolase chemical step. J Biol Chem 277 (2002) 8306-11.

Babbitt, P.C., Hasson, M.S., Wedekind, J.E., Palmer, D.R., Barrett, W.C., Reed, G.H., Rayment, I., Ringe, D., Kenyon, G.L. and Gerlt, J.A.: The enolase superfamily: a general strategy for enzyme-catalyzed abstraction of the α-protons of carboxylic acids. Biochemistry 35 (1996) 16489-501.

Brewer, J.M.: The interaction of potassium chloride and acetate with yeast enolase. Arch Biochem Biophys 134 (1969) 59-66.

Brewer, J.M.: Yeast enolase: mechanism of activation by metal ions. CRC Crit Rev Biochem 11 (1981) 209-54.

Brewer, J.M.: Specifity and mechanism of action of metal ions in yeast enolase. FEBS Lett 182 (1985) 8-14.

Brewer, J.M., Carreira, L.A., Collins, K.M., Duvall, M.C., Cohen, C. and DerVartanian, D.V.: Studies of activating and nonactivating metal ion binding to yeast enolase. J Inorg Biochem 19 (1983) 255-67.

Brewer, J.M. and Collins, K.M.: Studies of the role of catalytic and conformational metals in producing enzymatic activity in yeast enolase. J Inorg Biochem 13 (1980) 151-64.

Brewer, J.M. and Ellis, P.D.: ^{31}P-NMR studies of the effect of various metals on substrate binding to yeast enolase. J Inorg Biochem 18 (1983) 71-82.

Brewer, J.M., Glover, C.V., Holland, M.J. and Lebioda, L.: Significance of the enzymatic properties of yeast S39A enolase to the catalytic mechanism. Biochim Biophys Acta 1383 (1998) 351-5.

Brewer, J.M., Glover, C.V., Holland, M.J. and Lebioda, L.: Enzymatic function of loop movement in enolase: preparation and some properties of H159N, H159A, H159F, and N207A enolases. J Protein Chem 22 (2003) 353-61.

Brewer, J.M. and Wampler, J.E.: A differential scanning calorimetric study of the effects of metal ions, substrate/product, substrate analogues and chaotropic anions on the thermal denaturation of yeast enolase 1. Int J Biol Macromol 28 (2001) 213-8.

Brewer, J.M. and Weber, G.: The effect of magnesium on some physical properties of yeast enolase. J Biol Chem 241 (1966) 2550-7.

Brewer, J.M. and Weber, G.: The reversible dissocation of yeast enolase. Proc Natl Acad

Sci U S A 59 (1968) 216-23.
Brown, C.K., Kuhlman, P.L., Mattingly, S., Slates, K., Calie, P.J. and Farrar, W.W.: A model of the quaternary structure of enolases, based on structural and evolutionary analysis of the octameric enolase from *Bacillus subtilis*. J Protein Chem 17 (1998) 855-66.
Brown, T.A.: Molecular Biology LabFax. Academic Press Inc and Bios Scientific Publishers Ltd, (1991) 290-1 .
Chai, G., Brewer, J.M., Lovelace, L.L., Aoki, T., Minor, W. and Lebioda, L.: Expression, purification and the 1.8 Å resolution crystal structure of human neuron specific enolase. J Mol Biol 341 (2004) 1015-21.
Chin, C.C.: The primary structure of rabbit muscle enolase. J Protein Chem 9 (1990) 427-32.
Chin, C.C., Brewer, J.M., Eckard, E. and Wold, F.: The amino acid sequence of yeast enolase. Preparation and characterization of peptides produced by chemical and enzymatic fragmentation. J Biol Chem 256 (1981a) 1370-6.
Chin, C.C., Brewer, J.M. and Wold, F.: The amino acid sequence of yeast enolase. J Biol Chem 256 (1981b) 1377-84.
Cohn, M., Pearson, J.E., O'Connell, E.L. and Rose, I.A.: Nuclear magnetic resonance assignment of the vinyl hydrogens of phosphoenolpyruvate. Stereochemistry of the enolase reaction. J Am Chem Soc 92 (1970) 4095-8.
Collins, K.D. and Washabaugh, M.W.: The Hofmeister effect and the behaviour of water at interfaces. Q Rev Biophys 18 (1985) 323-422.
Collins, K.M. and Brewer, J.M.: Circular dichroism (CD) studies on yeast enolase: activation by divalent cations. J Inorg Biochem 17 (1982) 15-28.
da Silva Giotto, M.T., Hannaert, V., Vertommen, D., de, A.S.N.M.V., Rider, M.H., Michels, P.A., Garratt, R.C. and Rigden, D.J.: The crystal structure of *Trypanosoma brucei* enolase: visualisation of the inhibitory metal binding site III and potential as target for selective, irreversible inhibition. J Mol Biol 331 (2003) 653-65.
Dinovo, E.C., & Boyer, R.H: Isotopic probes of the enolase reaction mechansm. J.Biol.Chem 246 (1971) 4586-93.
Duquerroy, S., Camus, C. and Janin, J.: X-ray structure and catalytic mechanism of lobster enolase. Biochemistry 34 (1995) 12513-23.
Ehinger, S., Schubert, W.D., Bergmann, S., Hammerschmidt, S. and Heinz, D.W.: Plasmin(ogen)-binding α-enolase from *Streptococcus pneumoniae*: crystal structure and evaluation of plasmin(ogen)-binding sites. J Mol Biol 343 (2004) 997-1005.
Elliott, J.I. and Brewer, J.M.: Binding of inhibitory metals to yeast enolase. J Inorg Biochem 12 (1980) 323-34.
Engel, P.C.: Enzyme LabFax. Bios Scientific publisher, Oxford, UK &Academic Press, San Diego, USA (1996).

Faller, L.D., Baroudy, B.M., Johnson, A.M. and Ewall, R.X.: Magnesium ion requirements for yeast enolase activity. Biochemistry 16 (1977) 3864-9.

Faller, L.D. and Johnson, A.M.: Calorimetric studies of the role of magnesium ions in yeast enolase catalysis. Proc Natl Acad Sci U S A 71 (1974) 1083-7.

Gerlt, J.A., Babbitt, P.C. and Rayment, I.: Divergent evolution in the enolase superfamily: the interplay of mechanism and specificity. Arch Biochem Biophys 433 (2005) 59-70.

Good, L.N., R . N: Plasmid mini-preparations from culture streak. Benchmark, Bio Techiniques (1997) 404-6.

Gulick, A.M., Hubbard, B.K., Gerlt, J.A. and Rayment, I.: Evolution of enzymatic activities in the enolase superfamily: crystallographic and mutagenesis studies of the reaction catalyzed by D-glucarate dehydratase from *Escherichia coli.* Biochemistry 39 (2000) 4590-602.

Gunasekaran, K., Ma, B. and Nussinov, R.: Triggering loops and enzyme function: identification of loops that trigger and modulate movements. J Mol Biol 332 (2003) 143-59.

Hall, D.R., Leonard, G.A., Reed, C.D., Watt, C.I., Berry, A. and Hunter, W.N.: The crystal structure of *Escherichia coli* class II fructose-1, 6-bisphosphate aldolase in complex with phosphoglycolohydroxamate reveals details of mechanism and specificity. J Mol Biol 287 (1999) 383-94.

Hanlon, D.P. and Westhead, E.W.: Equilibrium measurements of the interaction of yeast enolase with activating metal ions. Biochemistry 8 (1969a) 4247-55.

Hanlon, D.P. and Westhead, E.W.: Kinetic studies on the activation of yeast enolase by divalent cations. Biochemistry 8 (1969b) 4255-60.

Hasson, M.S., Schlichting, I., Moulai, J., Taylor, K., Barrett, W., Kenyon, G.L., Babbitt, P.C., Gerlt, J.A., Petsko, G.A. and Ringe, D.: Evolution of an enzyme active site: the structure of a new crystal form of muconate lactonizing enzyme compared with mandelate racemase and enolase. Proc Natl Acad Sci U S A 95 (1998) 10396-401.

Helin, S., Kahn, P.C., Guha, B.L., Mallows, D.G. and Goldman, A.: The refined X-ray structure of muconate lactonizing enzyme from *Pseudomonas putida* PRS2000 at 1.85 Å resolution. J Mol Biol 254 (1995) 918-41.

Hilal, S.H., Brewer, J.M., Lebioda, L. and Carreira, L.A.: Calculated effects of the chemical environment of 2-phospho-D-glycerate on the pKa of its carbon-2 and correlations with the proposed mechanism of action of enolase. Biochem Biophys Res Commun 211 (1995) 607-13.

Holland, M.J., Holland, J.P., Thill, G.P. and Jackson, K.A.: The primary structures of two yeast enolase genes. Homology between the 5' noncoding flanking regions of yeast enolase and glyceraldehyde-3-phosphate dehydrogenase genes. J Biol Chem 256 (1981) 1385-95.

Holleman, W.H.: The use of absorption optics to measure dissociation of yeast enolase

into enzymatically active monomers. Biochim Biophys Acta 327 (1973) 176-85.
Hosaka, T., Meguro, T., Yamato, I. and Shirakihara, Y.: Crystal structure of *Enterococcus hirae* enolase at 2.8 Å resolution. J Biochem (Tokyo) 133 (2003) 817-23.
Huang, P., Dong, A: Thermal,chemical and chemothermal denaturation of yeast enolase. Spectroscopy 17 (2003) 453-67.
Janin, J., Miller, S. and Chothia, C.: Surface, subunit interfaces and interior of oligomeric proteins. J Mol Biol 204 (1988) 155-64.
Jensen, W.A, Armstrong, J.M, Giorgio, J.D and Hearn, M.T.W.: Stability studies on maize leaf phosphoenolpyruvate carboxylase: the effect of salts. Biochemistry 34 (1995) 472-80.

Kaufmann, M. and Bartholmes, P.: Purification, characterization and inhibition by fluoride of enolase from *Streptococcus mutans* DSM 320523. Caries Res 26 (1992) 110-6.
Keresztes-Nagy, S. and Orman, R.: Dissociation of yeast enolase into active monomers. Biochemistry 10 (1971) 2506-8.
Kornblatt, J. and Hui Bon Hoa, G.: The pressure-induced, reversible inactivation of mouse brain enolases. Eur J Biochem 128 (1982) 577-81.
Kornblatt, J.A., Kornblatt, M.J. and Hoa, G.H.: Second derivative spectroscopy of enolase at high hydrostatic pressure: an approach to the study of macromolecular interactions. Biochemistry 34 (1995) 1218-23.
Kornblatt, M.J.: Mechanism of rabbit muscle enolase: identification of the rate-limiting steps and the site of Li^+ inhibition. Arch Biochem Biophys 330 (1996) 12-18.
Kornblatt, M.J.: Changing the metal ion selectivity of rabbit muscle enolase by mutagenesis: effects of the G37A and G41A mutations. Biochim Biophys Acta 1748 (2005) 20-5.
Kornblatt, M.J., Al-Ghanim, A. and Kornblatt, J.A.: The effects of sodium perchlorate on rabbit muscle enolase--Spectral characterization of the monomer. Eur J Biochem 236 (1996) 78-84.
Kornblatt, M.J. and Klugerman, A.: Characterization of the enolase isozymes of rabbit brain: kinetic differences between mammalian and yeast enolases. Biochem Cell Biol 67 (1989) 103-7.
Kornblatt, M.J., Kornblatt, J.A. and Hui Bon Hoa, G.: The role of water in the dissociation of enolase, a dimeric enzyme. Arch Biochem Biophys 306 (1993) 495-500.
Kornblatt, M.J., Lange, R. and Balny, C.: Can monomers of yeast enolase have enzymatic activity? Eur J Biochem 251 (1998) 775-80.
Kornblatt, M.J., Lange, R. and Balny, C.: Use of hydrostatic pressure to produce "native" monomers of yeast enolase. Eur J Biochem 271 (2004) 3897-904.
Kornblatt, M.J. and Musil, R.: The inhibition of yeast enolase by Li^+ and Na^+. Arch

Biochem Biophys 277 (1990) 301-5.
Kornblatt, M.J., Zheng, S.X., Lamande, N. and Lazar, M.: Cloning, expression and mutagenesis of a subunit contact of rabbit muscle-specific (ββ) enolase. Biochim Biophys Acta 1597 (2002) 311-9.
Kreiq, P.M., D: Large scale isolation of plasmid DNA from *E.coli.*, 1991.
Kuhnel, K. and Luisi, B.F.: Crystal structure of the *Escherichia coli* RNA degradosome component enolase. J Mol Biol 313 (2001) 583-92.
Laemmli, U.K.: Cleavage of structural proteins during the assembly of the head of bacteriophage T4. Nature 227 (1970) 680-5.
Lange, R., Frank,J., Saldana, J.L&Balny, C: Fouth derivative UV-spectroscopy of proeins under high pressure.I Factors affecting the fourth derivative spectrum of the aromatic amino acids. Eur. Biophys. J 24 (1996) 277-83.
Larsen, T.M., Wedekind, J.E., Rayment, I. and Reed, G.H.: A carboxylate oxygen of the substrate bridges the magnesium ions at the active site of enolase: structure of the yeast enzyme complexed with the equilibrium mixture of 2-phosphoglycerate and phosphoenolpyruvate at 1.8 Å resolution. Biochemistry 35 (1996) 4349-58.
Lebioda, L., Hatada, M.H., Tulinsky, A. and Mavridis, I.M.: Comparison of the folding of 2-keto-3-deoxy-6-phosphogluconate aldolase, triosephosphate isomerase and pyruvate kinase. Implications in molecular evolution. J Mol Biol 162 (1982) 445-58.
Lebioda, L. and Stec, B.: Mechanism of enolase: the crystal structure of enolase-Mg^{2+}-2-phosphoglycerate/phosphoenolpyruvate complex at 2.2-Å resolution. Biochemistry 30 (1991) 2817-22.
Lebioda, L., Stec, B. and Brewer, J.M.: The structure of yeast enolase at 2.25-Å resolution. An 8-fold β+α-barrel with a novel ββαα$(\beta\alpha)_6$ topology. J Biol Chem 264 (1989) 3685-93.
Lee, B.H. and Nowak, T.: Influence of pH on the Mn^{2+} activation of and binding to yeast enolase: a functional study. Biochemistry 31 (1992) 2165-71.
Levy, C.W., Buckley, P.A., Sedelnikova, S., Kato, Y., Asano, Y., Rice, D.W. and Baker, P.J.: Insights into enzyme evolution revealed by the structure of methylaspartate ammonia lyase. Structure (Camb) 10 (2002) 105-13.
Lin, T. and Kornblatt, M.J.: The binding of Na^+ to apo-enolase permits the binding of substrate. Biochim Biophys Acta 1476 (2000) 279-86.
Liu, H.Y., Zhang, Y.K and Yang, W.T: How is the active site of enolase organized to catalyze two different reaction steps? J Am Chem Soc 122 (2000) 6560-70.
Lolis, E., Alber, T., Davenport, R.C., Rose, D., Hartman, F.C. and Petsko, G.A.: Structure of yeast triosephosphate isomerase at 1.9-Å resolution. Biochemistry 29 (1990) 6609-18.
Lolis, E. and Petsko, G.A.: Crystallographic analysis of the complex between triosephosphate isomerase and 2-phosphoglycolate at 2.5-Å resolution: implications for catalysis. Biochemistry 29 (1990) 6619-25.

Maniatis, T., Sambrook, J., and Fritsch, E.F.: In Molecular Cloning: a laboratory manual. Cold spring harbor laboratory press, N.Y. USA (1989).

McAlister, L. and Holland, M.J.: Targeted deletion of a yeast enolase structural gene. Identification and isolation of yeast enolase isozymes. J Biol Chem 257 (1982) 7181-8.

Murphy, J.B., Kies, M .W: Note on spectrophotometric determination of proteins in dilute solution. Biochim Biophys Acta 45 (1960) 382-4.

Neidhart, D.J., Howell, P.L., Petsko, G.A., Powers, V.M., Li, R.S., Kenyon, G.L. and Gerlt, J.A.: Mechanism of the reaction catalyzed by mandelate racemase. 2. Crystal structure of mandelate racemase at 2.5-Å resolution: identification of the active site and possible catalytic residues. Biochemistry 30 (1991) 9264-73.

Padovani, A.: Characterization of subunit interactions versus catalysis in yeast enolase, Chemistry and Biochemistry. Concordia Univesity, Montreal (2003).

Paladini, A.A., Jr. and Weber, G.: Pressure-induced reversible dissociation of enolase. Biochemistry 20 (1981) 2587-93.

Pompliano, D.L., Peyman, A. and Knowles, J.R.: Stabilization of a reaction intermediate as a catalytic device: definition of the functional role of the flexible loop in triosephosphate isomerase. Biochemistry 29 (1990) 3186-94.

Poyner, R.R., Cleland, W.W. and Reed, G.H.: Role of metal ions in catalysis by enolase: an ordered kinetic mechanism for a single substrate enzyme. Biochemistry 40 (2001) 8009-17.

Poyner, R.R., Larsen, T.M., Wong, S.W. and Reed, G.H.: Functional and structural changes due to a serine to alanine mutation in the active-site flap of enolase. Arch Biochem Biophys 401 (2002) 155-63.

Poyner, R.R., Laughlin, L.T., Sowa, G.A. and Reed, G.H.: Toward identification of acid/base catalysts in the active site of enolase: comparison of the properties of K345A, E168Q, and E211Q variants. Biochemistry 35 (1996) 1692-9.

Ralston.G: Introduction to analytical ultracentrifugation, for Beckman Instrument Inc (1993).

Ramakrishnan, B. and Qasba, P.K.: Crystal structure of lactose synthase reveals a large conformational change in its catalytic component, the β1,4-galactosyltransferase-I. J Mol Biol 310 (2001) 205-18.

Ramasamy, V., Ramakrishnan, B., Boeggeman, E. and Qasba, P.K.: The role of tryptophan 314 in the conformational changes of β1,4-galactosyltransferase-I. J Mol Biol 331 (2003) 1065-76.

Ragone, R., Colonna, G., Balestrieri, C., Servillo, L., and Irace, G.: Determination of tyrosine exposure in proteins by second-derivative spectroscopy. Biochemistry 23 (1984) 1871-5.

Rozovsky, S., Jogl, G., Tong, L. and McDermott, A.E.: Solution-state NMR investigations of triosephosphate isomerase active site loop motion: ligand release in relation to active site loop dynamics. J Mol Biol 310 (2001) 271-80.

Rozovsky, S. and McDermott, A.E.: The time scale of the catalytic loop motion in triosephosphate isomerase. J Mol Biol 310 (2001) 259-70.

Sampson, N.S. and Knowles, J.R.: Segmental motion in catalysis: investigation of a hydrogen bond critical for loop closure in the reaction of triosephosphate isomerase. Biochemistry 31 (1992a) 8488-94.

Sampson, N.S. and Knowles, J.R.: Segmental movement: definition of the structural requirements for loop closure in catalysis by triosephosphate isomerase. Biochemistry 31 (1992b) 8482-7.

Schurig, H., Rutkat, K., Rachel, R. and Jaenicke, R.: Octameric enolase from the hyperthermophilic bacterium *Thermotoga maritima*: purification, characterization, and image processing. Protein Sci 4 (1995) 228-36.

Shen, T.Y. and Westhead, E.W.: Divalent cation and pH dependent primary isotope effects in the enolase reaction. Biochemistry 12 (1973) 3333-7.

Sims, P.A., Larsen, T.M., Poyner, R.R., Cleland, W.W. and Reed, G.H.: Reverse protonation is the key to general acid-base catalysis in enolase. Biochemistry 42 (2003) 8298-306.

Singh, R.P. and Setlow, P.: Enolase from spores and cells of *Bacillus megaterium*: two-step purification of the enzyme and some of its properties. J Bacteriol 134 (1978) 353-5.

Sinha, U. and Brewer, J.M.: Cu(II) activates yeast enolase. J Inorg Biochem 22 (1984) 175-7.

Spring, T.G. and Wold, F.: The purification and characterization of *Escherichia coli* enolase. J Biol Chem 246 (1971) 6797-802.

Stec, B. and Lebioda, L.: Refined structure of yeast apo-enolase at 2.25 Å resolution. J Mol Biol 211 (1990) 235-48.

Stephen, E.H.: Protein engineering: a practical method, second edition ed. Oxford Uniersity press (1997).

Strickland, E.H.: Aromatic contributions to circular dichroism spectra of proteins. CRC Crit Rev Biochem 2 (1974) 113-75.

Stubbe, J. and Abeles, R.H.: Mechanism of action of enolase: effect of the β-hydroxy group on the rate of dissociation of the α-carbon-hydrogen bond. Biochemistry 19 (1980) 5505-12.

Trepanier, D., Wong, C. and Kornblatt, M.J.: The salt-induced dissociation and inactivation of a mammalian enolase: evidence for the formation of active monomers. Arch Biochem Biophys 283 (1990) 271-7.

Vinarov, D.A. and Nowak, T.: pH dependence of the reaction catalyzed by yeast Mg^{2+}-enolase. Biochemistry 37 (1998) 15238-46.

Vinarov, D.A. and Nowak, T.: Role of His159 in yeast enolase catalysis. Biochemistry 38 (1999) 12138-49.

Warburg, O.C., W.: Isolation and crystallization of enolase. Biochem.Z 310 (1942) 384-421.

Wedekind, J.E., Poyner, R.R., Reed, G.H. and Rayment, I.: Chelation of serine 39 to Mg^{2+} latches a gate at the active site of enolase: structure of the bis(Mg^{2+}) complex of yeast enolase and the intermediate analog phosphonoacetohydroxamate at 2.1-Å resolution. Biochemistry 33 (1994) 9333-42.

Wedekind, J.E., Reed, G.H. and Rayment, I.: Octahedral coordination at the high-affinity metal site in enolase: crystallographic analysis of the MgII--enzyme complex from yeast at 1.9 Å resolution. Biochemistry 34 (1995) 4325-30.

Wold, F.: Enolase, in The Enzyme,(Boyer, P. D.,Ed.), 3rd ed., Vol. 5, Academic Press, New York(1971) 499-538.

Wold, F. and Ballou, C.E.: Studies on the enzyme enolase. II. Kinetic studies. J Biol Chem 227 (1957) 313-28.

Zgiby, S., Plater, A.R., Bates, M.A., Thomson, G.J. and Berry, A.: A functional role for a flexible loop containing Glu182 in the class II fructose-1,6-bisphosphate aldolase from *Escherichia coli*. J Mol Biol 315 (2002) 131-40.

Zhang, E., Brewer, J.M., Minor, W., Carreira, L.A. and Lebioda, L.: Mechanism of enolase: the crystal structure of asymmetric dimer enolase-2-phospho-D-glycerate/enolase-phosphoenolpyruvate at 2.0 Å resolution. Biochemistry 36 (1997) 12526-34.